Title
Mechanisms of Homeostatic Control of Neuronal Intrinsic Excitability

Author
Kulik, Yelena

Publication Date
2019

Peer reviewed|Thesis/dissertation

Mechanisms of Homeostatic Control of Neuronal Intrinsic Excitability

by
Yelena Kulik

DISSERTATION
Submitted in partial satisfaction of the requirements for degree of
DOCTOR OF PHILOSOPHY

in

Neuroscience

in the

GRADUATE DIVISION
of the
UNIVERSITY OF CALIFORNIA, SAN FRANCISCO

Approved:

DocuSigned by:
Lily Jan
394456D87457494...

Lily Jan

Chair

DocuSigned by:
Anatol Kreitzer
DocuSigned by:

Anatol Kreitzer

DocuSigned by:
Mark von Zastrow
DocuSigned by:

Mark von Zastrow

DocuSigned by:
Kevin Bender
DocuSigned by:

Kevin Bender

DocuSigned by:
Graeme Davis
CAABDC3DF89F4A3...

Graeme Davis

Committee Members

DEDICATION

This dissertation is dedicated to my family, whose love, sacrifice, and immeasurable support made my life and opportunities possible. This work would not have been possible without them.

CONTRIBUTIONS

Chapter 1 was reprinted with permission from the following publication:

> Kulik, Y., Jones, R., Moughamian, A. J., Whippen, J. & Davis, G. W. Dual separable feedback systems govern firing rate homeostasis. *Elife* **8**, doi:10.7554/eLife.45717 (2019).

Figure	**Contributions**
Figure 2.1	R.J. - image, Shal RNAi IK_A and FI; Y.K. - $Shal^{W362F}$ generation, $Shal^{W362F}$ IK_A and FI
Figure 2.3	Y.K.
Figure 2.4	Y.K. - IK_{DR}; R.J. - IK_{Ca}, IN_{Ap}, I_{ca}
Figure 2.5	R.J.
Figure 2.6	R.J.
Figure 2.7	R.J.
Figure 2.8	R.J.
Figure 2.9	Y.K. - IK_{DR} Shal;Kr RNAi and Kr RNAi, IK_{Ca} Kr RNAi; R.J. - IK_{Ca} I_{Ca}, IK_A Shal;Kr RNAi
Figure 2.10	Y.K.
Figure 2.11	Y.K. - IK_{DR}, IK_{Ca}, AP waveform, $Shal^{W362F}$ qPCR; J.W. - $Shal^{495}$ qPCR; A.M. - negative geotaxis assay, presynaptic homeostatic potentiation

Yelena Kulik (Y.K.), Ryan Jones (R.J.), Armen Moughamian (A.M.), Jenna Whippen (J.W.)

Chapter 2 was written by Yelena Kulik. This manuscript is currently in revision.

Contributions: Yelena Kulik performed all experiments, with collaboration from Özgür Genç for collection of RNA-sequencing data.

ACKNOWLEDGEMENTS

With gratitude:

To the UCSF Neuroscience Graduate Program: I cannot imagine a better place to have received scientific training. The program directors, Roger Nicoll and Anatol Kretizer, and the program administrators, Pat Vietch and Lucita Nacionales, fostered a supportive environment. Thank you for giving me the opportunity to pursue this PhD among such a wonderful community of scientists.

To my thesis advisor: Dr. Graeme Davis, a leader in the field of homeostatic plasticity. I am exceptionally thankful for the training I received in the Davis lab. Grae's enthusiasm, knowledge of the field, and ability to see the bigger picture has shaped my approach to science and the ultimate outcomes of my dissertation research. This work would not exist without his support.

To my thesis committee: Drs. Lily Jan, Anatol Kreitzer, Mark Van Zastrow, Kevin Bender, and Graeme Davis, who have given me much constructive feedback, suggestions, and encouragement as I developed my thesis project. In particular, I thank Kevin Bender for his expertise in patch clamp electrophysiology and his open-door policy for seeking advice.

To the Davis Lab: Nathan Harris, Kevin Ford, Mike Gaviño, Alyssa Johnson, Ting Ting Wang, Özgür Genç, Armen Moughamian, Peter Chipman, Brian Orr, Jenna Whippen, Cody Locke, Ling Chen, Kenton Hokanson, Ashley Smart, Amy Tong, Jennifer Ortega, Giulia Zunino, Isaac Solomon, Javier Bernardo Garcia, Ryan Jones, Richard Fetter, Anna Hauswirth and Gamaliel Ruiz, who have made the lab a welcoming environment and who have taught, motivated, and inspired me. I would especially like to thank Ryan Jones, my co-author on the 2019 eLIFE paper "Dual separable feedback systems govern firing rate homeostasis". Ryan trained me in patch clamp electrophysiology, giving me the solid theoretical and technical foundation that was

necessary to develop my doctoral research. Ryan continues to be a mentor to me. He is always willing to offer helpful advice in my research, career, and life.

To my classmates: Anna Hauswirth, Christopher Zimmerman, Yiming Chen, Alexandra Clemente, Yuan-Hung Lin, Lynn Wang, Claire Tang, Ryan Morrill, Rachel Care, Jenna Whippen, Racheli Wercberger, Jason Chung, Jiggy Athilingham, Ally Girasole, Faten Sayed, John King, Jermyn See. It has been an honor to go through the graduate school journey alongside you.

To my friends: Jennifer Ortega, Natasha Zimin, Eirene Markenscoff-Papadimitriou, Christopher Zimmerman, Ashley Oliphant, Kate Terry, Brian Orr, David Lieb, Daniel Estandian, John Hattori, Rachel Care, Claire Tang, Alexandra Clemente, Margaret Cunniff, Alex Borkin, Jeff Mahler, Pete Chipman, Nathan Harris, Irina Khaimovich, Alex Segal, Jeff Fenchel, Jenna Whippen, Yiming Chen, and many, many more. Thank you for making me laugh and for providing me with meaning outside of the lab.

To my partner: Nikolas Steinberg, who is a rock.

To my family: My parents, Tatiana and Dmitri Kulik, brought me into this world and taught me notice its beauty. My father is a scholar at heart and one of the most curious and intelligent people I know. When I was having trouble in graduate school, my father would tell me: “To do science is horrible, but not to do science is even worse.” My mother would remind me not to take anything too seriously. My grandmother Galina Datsenko inspires me with her resilience and her lifelong passion for chemistry. Her battle with Parkinson’s Disease makes our work in neuroscience all the more meaningful. My grandmother Dina Kulik ensured I made it to adulthood and then continued to look after me from afar. In the most challenging times, I have always had reminders from her that I am loved and valued. My grandfather Igor Kulik taught me to approach the world with humor and introduced me to much of the music that provided the

soundtrack to the last six years. Igor sadly passed away before I embarked on my graduate studies. I wish he could have seen how far our lineage has come.

Mechanisms of Homeostatic Control of Neuronal Intrinsic Excitability

Yelena Kulik

ABSTRACT

A neuron's identity and function are dictated by its electrophysiological signature. The firing pattern of a neuron emerges from the particular combination of ion channels in its membrane. A neuron can "tune" the combination of ionic conductances that it expresses to return back to its target excitability when faced with changing conditions. While this phenomenon of firing rate homeostasis (FRH) is well-established, the mechanisms underlying it have remained mysterious. A prevalent theory proposes that firing rates are maintained through regulatory feedback relying on the detection and stabilization of a single variable, calcium. Within the framework of this theory, all perturbations with equivalent effects on neuronal activity should invoke the same homeostatic response. In a direct test of this hypothesis, we compared two independent experimental manipulations to the Shal potassium ion channel. While we observed FRH following either a conductance-blocking mutation or complete elimination of the Shal protein, the compensating currents and the molecular mechanisms underlying the homeostatic response differed between the two conditions. Neurons lacking the Shal protein enacted transcriptional upregulation of the ion channels *slo*, *Shab*, and *Shaker*, in part through the transcription factor Krüppel. In contrast, neurons with a non-conducting Shal channel compensated through non-transcriptional modification of a different set of conductances. We propose that neurons have multiple, separable homeostatic signaling systems, including proteostatic and activity-sensitive feedback systems. We then further expand on the mechanisms of FRH to include a role for the Notch signaling system. This canonical pathway for neural development is reactivated following loss of Shal and is necessary for stabilization of firing rates. We propose a model in which the loss of the transcription factor Nerfin-1 de-

represses *Notch*, and Notch cleavage by Presenilin followed by cooperation of NICD with Su(H) results in transcriptional rebalancing of ion channels. These findings have implications for the pathophysiology of human channelopathies and Alzheimer's disease.

Table of Contents

Table of Figures

1. Introduction

1.1 Firing properties of Neurons

A central question of neuroscience is how information is represented and stably maintained in the brain. Neuronal time-averaged spiking rates have long been thought to encode information in the nervous system. Information transfer is constrained by each neuron's finite range of firing rates, bounded by zero and some maximum rate of spiking that is determined by the duration of the action potential and refractory period. Neurons can be clustered into subtypes based on similar electrophysiological properties[1-6]. A given cell establishes its particular firing pattern during development and maintains those properties throughout the lifetime of the neuron, presumably in order to perform its function within a given circuit.

The diversity of firing patterns across the various neuronal subtypes is staggering[2,4-10]. These differences arise from differences in morphology and ion channel expression patterns[2,4-12]. Ion channels are multimeric protein complexes that span the cellular membrane, opening and closing with distinct time- and voltage-sensitivity to selectively pass certain ions from one side of the membrane to the other[13,14]. When ion channels open, conductance increases, and the movement of charged ions constitutes an electric current that forms the basis to all electrical events in the brain. Multiple ionic conductances interact to give rise to the activity pattern typical of the neuronal subtype. Since the foundational work of Hodgkin and Huxley describing the ionic mechanisms underlying the action potential[15] and subsequent identification, cloning and characterization of the now hundreds of different species of ion channels[16,17], many studies have been devoted to uncovering how different combinations of channels contribute to the particular electrophysiological properties of various types of cells[2,12,18,19].

Theoretical work has demonstrated that similar neuronal activity patterns can be produced from many combinations of ionic conductances[18,20-27]. Computational modeling of

neurons with known biophysical properties has been used to test how particular ionic currents can shape a cell's electrophysiological behavior. For example, in one of the most large-scale studies, a population of ~600,000 four-compartment models of the lateral pyloric (LP) neuron of the stomatogastric ganglion of the crab *Cancer borealis* was generated[18]. Eleven different conductances, representing different species of ion channels, were distributed into the compartments at random. The behavior of each model was assessed, including measurements of spontaneous and evoked firing rates. Surprisingly, 1300 models matched the known electrophysiological properties of the biological LP neuron, rather than presenting a single possible solution. The differences in underlying parameters can be substantial. Ion channel densities as large as an order of magnitude apart can give rise to nearly identical model neuron behavior[21]. Such studies suggest that there are many possible ways that a particular functional subtype of neuron could be established through the expression or function of different ion channels, and that real neurons may tolerate large changes in the densities of ion channels on their membranes while maintaining normal firing rates.

Experimental studies have supported the idea that similar firing patterns can be produced from different combinations of ion channels. While an identified neuron can have similar electrical behavior across animals, the measured voltage-gated ion channel densities can vary substantially from animal to animal[26-30]. Foundational work in *Cancer borealis* has demonstrated high variability in ion channel gene expression and current density in single identified neuron subtypes both across animals and across neurons of a given cell type within an animal [26,27]. Channel expression levels have been found to vary between 3- to 5-fold [26,27]. Some studies have found that this variability is constrained by patterns of correlated currents or channel expression [26,27,31-35], suggesting that certain ion channels may be co-regulated. These correlations have been proposed to preserve normal neuronal function in spite of the large cell-to-cell variability in channel expression. However, other studies have not detected fixed ratios of conductances, suggesting that these correlations are not required for the maintenance of an

electrophysiological phenotype[36,37]. Together, such observations have given rise to the idea that, while the characteristic firing pattern for a particular neuron is fixed, the ion channels underlying it may not be. It is possible that the target firing pattern for a neuronal subtype is genetically encoded, and the ion channels expressed by the neuron are tunable to achieve the normal firing pattern.

1.2 Ion Channel Compensation

1.2.1 Compensation following ion channel loss

The diversity of channels that can underlie a particular neuronal activity pattern is most evident in cases of compensation for loss of an ion channel subtype. For example, overexpression [38] or deletion [39,40] of the A-type potassium current mediated by Shal/Kv4.2 triggers the upregulation of a subset of other ionic conductances. The precision of the compensatory response is remarkable, resulting in firing properties that are virtually indistinguishable between wild-type and Kv4.2 mutant cells. Channel compensation for disrupted Kv4 homologs has been documented in the worm [41], fly [42,43], crab [29,38], and rodent [39,40], suggesting either evolutionary conservation or a remarkable example of convergence. This phenomenon is not limited to potassium channels. Upregulation of sodium channels has been observed in response to overexpression of the leak channel Kir2.1 [44], and changes in potassium, leak, sodium, and calcium channels have been shown to compensate for sodium channel loss [30,45,46]. These studies show that neurons are equipped with compensatory response mechanisms to ion channel loss that involve changes in other channel subtypes.

In identifying the response of a cell to the loss of one subtype of channel, is important to distinguish between degenerate ion channel function and active compensatory mechanisms. Ion channels often share overlapping roles in their contributions to shaping neuronal electrophysiological properties, so one set of channels can compensate for the loss of

another[30,47,48]. Because multiple voltage-dependent currents have complicated interactions, acutely removing one ionic current can alter the voltage across the neuronal membrane in ways that cause other ionic currents to immediately change[30,49]. A comparison of acute and chronic perturbations to an ion channel subtype reveals the existence of distinct mechanisms driving compensatory conductance remodeling over longer periods of time. For example, Cerebellar Purkinje neuron burst firing persists in the presence of half-blocking concentrations of the sodium channel blocker tetrodotoxin because waveform changes from the reduced sodium current result in decreases in potassium currents[30]. In contrast, long-term reductions in sodium current density in $Na_v1.6$ mutant Purkinje neurons preserve burst firing through an upregulation of calcium current[30]. The difference between the response to acute and chronic changes in one ionic current suggests that neurons may be equipped with both immediate compensation and long-term feedback mechanisms that maintain normal neuronal firing following perturbation.

If a neuron can appropriately function after loss of a fundamental conductance, why does the conductance exist to begin with? Degeneracy of ion channel function allows neurons to be robust to environmental perturbations or natural fluctuations of ion channel gene expression within some range. However, outside of this range, an ion channel may be essential to the maintenance of normal firing properties, as demonstrated by the effects of acute pharmacological block of the channel[47,49-52]. In some cases, even small changes in particular conductances can have dramatic effects on the firing properties of neurons[53]. In conditions of chronic ion channel loss, compensatory mechanisms may not precisely restore all electrophysiological properties of the neuron. For example, while $Na_v1.6$ mutant retinal ganglion cells exhibit channel compensation by Nav1.1 and Nav1.2, the neurons still have firing rates different from wild-type[46]. The channel compensation response and severity of the phenotype vary by cell subtype[46]. Lastly, mutations in ion channels are known to cause disease states such as epilepsy, which is characterized by abnormal neural activity[54,55]. Therefore, there may be limits to compensation for loss of an ion channel.

1.2.2 Compensation following perturbations to activity

Plasticity of intrinsic excitability through modulation of ionic conductances occurs in response to other perturbations that alter the normal electrical functioning of the cell. Intrinsic excitability is the electrical excitability of a neuron, determined by channel and receptor abundance and distribution. Classic work in the lobster stomatogastric ganglion demonstrated that neurons can change expression of ionic conductances to compensate for the loss of synaptic drive [56,57]. Ionic current densities can reversibly change in response to prolonged stimulation mimicking normal activity [37]. Similarly, lack of evoked synaptic transmission reversibly increases intrinsic excitability [58], while increased levels of synaptic excitation reduce intrinsic excitability of *Drosophila* motoneurons through tuning of ionic currents [59]. Intrinsic excitability is inversely correlated with synaptic input across different fly genetic backgrounds [60]. In a rodent model, chronically depriving cultured cortical pyramidal neurons of activity with TTX leads to increases in intrinsic excitability due to ion channel rebalancing [61]. These reports and others gave rise to the idea that neurons are capable of homeostatic plasticity and can be described by control theory.

1.3 Homeostasis

1.3.1 Homeostatic Control

Homeostatic control can maintain the output of a system stable despite changing inputs. Examples of homeostatic control can be found throughout biological systems, such as the maintenance of blood glucose level by insulin secretion, control of body temperature, and maintenance of extracellular salt balance. Homeostatic regulation from the level of single cells to the level of organs contributes to the maintenance of overall stable function of the body. The extent to which various cellular processes are under homeostatic control, however, is not well understood.

In engineering and mathematics, control theory describes how the behavior of dynamical systems with inputs is modified by feedback. In any control system, there is a variable that is

being controlled. The goal of the system is to maintain the output of some component, y, as close as possible to a goal value, x. Usually, the value of x is fixed and represents a set point. In an ideal system, the actual value of the control variable is always equal to the target value (y=x). To implement, a controller issues a command that generates an output y as close as possible to the target x. An effector enacts the changes that are necessary to return to the set point. Often, an error signal encodes how close the actual outcome is to the target (y-x), which can be used to modify the system, and equals zero in an ideal system.

Modified feedback control theory can be applied to biological systems to create a model for how homeostasis could be achieved. In such a model, a biological variable is kept stable. The level at which the variable is held constant is referred to as the set point. Molecular machinery that transforms input to the system into information that can be used by the rest of the system is represented by a sensor. When the input and set point differ, an error signal is triggered. This error signal changes the activity of effector molecules that modify the output, restoring homeostasis. This model can be used to make predictions about potential homeostatic processes that are hypothesized to maintain certain properties of neurons constant.

1.3.2 Phenomenology of Firing Rate Homeostasis

Neurons are hypothesized to have an excitability set point[57,62,63]. There are many documented examples of cells, when faced with a perturbation that alters normal firing patterns, returning to baseline levels of excitability or activity over time[29,30,38-40,44]. For example, cerebellar Purkinje neurons cease firing after acute pharmacological block of the sodium current[47]. However, Purkinje neurons with a genetic deletion of the sodium channel maintain burst firing due to compensatory changes in calcium currents[30]. This is evidence that compensatory mechanisms are engaged in the chronic presence of a perturbation. The system of control that allows neurons to maintain stable firing patterns and to compensate for channel and receptor disruption is often referred to as Firing Rate Homeostasis (FRH).

FRH is commonly thought to be activity-dependent[37,57]. Evidence for activity-dependent FRH can be drawn from recent *in vivo* studies demonstrating rat visual cortical neurons recovering normal firing rates after an initial depression of activity during chronic monocular visual deprivation [64,65]. Because intracellular calcium concentration correlates with neuronal activity, integrated calcium signal over time has long been proposed to serve as a proxy for activity, triggering ion channel re-balancing after disruption of normal firing [36,37,63,66,67]. In such a homeostatic signaling system, calcium is the controlled variable, and calcium sensors are used to track the intracellular calcium concentration. This theory is backed by experimental evidence that calcium channel blockers and calcium chelators prevent perturbations of neuronal activity and ion channels from leading to conductance rebalancing [34,37,56,68]. However, the theory that FRH occurs solely through calcium signaling has never been directly tested.

An alternate hypothesis is that FRH may be activity-independent. Evidence for activity-independent ion channel compensation has been found in response to channel over-expression [38]. Injection of the Kv4 homolog *Shal* RNA into neurons causes an increase in Shal-mediated potassium current and a concomitant increase in the hyperpolarization-activated inward current (I_h), allowing the neuron to maintain normal firing properties[29,38]. However, injection of nonfunctional mutated *Shal* RNA also triggers an increase in I_h, despite no changes to the Shal-mediated current, suggesting activity-independent coupling between *Shal* mRNA or protein and I_h[29,38]. This data is consistent with observations of ion channel co-regulation in individual neurons from wild-type organisms [26,27,31-34]. Whether FRH induced by ion channel gene mutations is activity-independent remains unknown.

1.3.2 Mechanisms of Firing Rate Homeostasis

In spite of the many documented examples of FRH, research on the underlying molecular mechanisms are lacking. Molecular sensors of activity and channel expression have yet to be identified. However, a few studies are worthy of note. The sodium channel *paralytic* (*para*) mRNA abundance changes bidirectionally when synaptic input is reduced and when

synaptic release is enhanced in *Drosophila* motoneurons [60]. Blocking synaptic neurotransmitter release by pan-neuronal expression of tetanus toxin light chain (TeTx-A) or by using a null allele of *n-synaptobrevin* results in increased *para* expression[60]. Increasing synaptic release by elevating cAMP by using an allele of *dunce* or by pan-neuronal expression of *rutabaga*.results in decreased *para* expression[60]. The translational repressor Pumilio binds *para* mRNA and regulates its expression, as *para* mRNA increases in a loss-of-function *pumilio (pum)* background and decreases in the background of *pum* overexpression[60,69]. Accordingly, the *pum* mutant has increased membrane excitability, and overexpression of *pum* causes decreased membrane excitability[60]. Pumilio is differentially expressed in the different synaptic activity backgrounds[60]. As the strongest evidence that Pumilio is a homeostatic effector molecule, Pumilio is necessary for the change in *para* expression under conditions of altered synaptic drive due to the overexpression of *rutabaga*[60,69].

Mechanisms of FRH may be evolutionarily conserved. The role of Pumilio in regulating sodium current is similar in mammals[70]. Chronically activity depriving or enhancing cultured rat visual cortical pyramidal neurons by pharmacologically blocking excitatory or inhibitory synapses causes bidirectional changes in Pumilio-2 expression, $Na_V1.6$ expression, and sodium current [70]. Pumilio-2 directly binds $Na_V1.6$ transcript, alters its expression and regulates intrinsic excitability [70]. Thus, although the fly and rat diverged over 60 million years ago, a common molecular mechanism for regulating intrinsic excitability has been maintained.

1.4 Developmental Signaling Pathways

Drosophila melanogaster is, perhaps, the best understood model system for investigating development. Thanks to a century of genetic discoveries in *Drosophila*, many subfields of developmental biology were established. Early findings from mutagenesis screening efforts in *Drosophila* established that distinct genes were responsible for specific aspects of embryonic development. Subsequently, many of these genes were found to be evolutionarily

conserved in vertebrates, and to be of importance to human development and disease. Below, I outline a few of these genes, which I later demonstrate to be key regulators of Firing Rate Homeostasis in mature neurons.

1.4.1 Notch signaling

The Notch signaling pathway was first discovered in *Drosophila*[71-74]. Mutations in *Notch* were initially reported to cause a notch in the wings of *Drosophila*, and later documented to affect embryonic development[74]. Some of the most well-characterized functions of Notch are those pertaining to neurogenesis[75]. Mutations in *Notch* cause an enlarged embryonic CNS due to differentiation of hypoderm into neuroblasts, described as a 'neurogenic' phenotype. Notch signaling has since been found to participate in different stages of development, even within a single tissue, with differing outcomes[76]. Notch initially determines the number of cells to acquire neural potential, and later controls whether the progeny will adopt neural or glial fates[76]. In a process termed lateral inhibition, direct cell-cell interaction mediated by the ligand Delta on one cell and the Notch receptor on a second allows a cell to signal to its immediate neighbors to inhibit them from adopting its own fate[77]. While a group of cells may begin as roughly equivalent, activation of Notch in one cell inhibits production of the ligand, resulting in reduced inhibition onto the neighboring cell that allows this second cell to produce more ligand, forcing the first cell to produce even less. This feedback process allows populations of cells to influence each other and spatio-temporally organize themselves into different developmental pathways through the amplification of small initial differences.

Cellular context is crucial in determining the end result of Notch signaling[78]. While Notch is typically thought of as an inhibitor of neural differentiation, it has also been shown to promote neural fates in mouse embryonic stem cells[79]. The importance of Notch signaling also extends beyond the nervous system, affecting heart, blood cell, skin, and bone development[74,77,78]. More recently, some roles of Notch in post-developmental functions have been found, such as in the formation of alcohol cue preference in adult *Drosophila*[80]. As the list of processes known to be

mediated by Notch grows, it is increasingly important to understand the molecular details of how Notch functions in different contexts.

The Notch signaling pathway has been extensively mapped. Unlike many molecular signaling systems, Notch signals directly from the plasma membrane to the nucleus, with no intermediates[76,78]. Canonically, ligand-mediated activation induces multiple proteolytic cleavages in the membrane-localized Notch receptor[76,78]. The first is catalyzed by the ADAM family of metalloproteases and second by γ-secretase, an enzyme complex composed containing Presenilin, Nicasatrin, PEN2, and APH1[76,78]. This second cleavage event releases the Notch intracellular domain (NICD). NICD travels to the nucleus and cooperates with DNA-binding protein Suppressor of Hairless (CSL/CBF1/LAG-1/RBP-J) and co-activator Mastermind (Mam/MAML1) to induce the transcription of target genes[76,78]. Additional transcription factors are recruited to this complex, while co-repressors are released. The end result is changes in gene expression relevant to the developmental or physiological process.

Our understanding of the Notch signaling pathway is important because it is evolutionarily conserved[81]. The *Drosophila* genome encodes a single Notch receptor and two ligands, Delta and Serrate. The mammalian genome contains four *Notch* paralogues (Notch1-4) and encodes multiple ligands in the Delta-like and Jagged families. The general principles of this simple paradigm are conserved across species, and core components of the Notch pathway that were discovered in *Drosophila* have been shown to have conserved roles in vertebrates[81]. Because of its contributions to so many fundamental processes, it is perhaps unsurprising that disruptions of the Notch signaling pathway have been linked to many human disorders. For example, mutations in the *NOTCH3* gene cause cerebral autosomal dominant arteriopathy with subcortical infarcts and leukoencephalopathy (CADASIL), a devastating neurological disorder [82]. Mutations in *PSEN1* (encoding Presenilin-1) cause familial Alzheimer's disease [83]. For these reasons, *Drosophila* continues to be an important model system for investigating ways in which

Notch signaling is regulated and contributes to neural development and function, with relevance to human health.

1.4.2 Differentiation factors

Much of the foundational work detailing features of neurogenesis was conducted in *Drosophila*. Type I neuroblasts, the major neural stem cells in the central nervous system of *Drosophila,* divide asymmetrically to restore the stem cell pool and to generate the ganglion mother cell, which then divides symmetrically to produce neurons or glia[84]. Cell fate determinants are sequestered into the ganglion mother cell at every cell division in order to promote its differentiation, and disruption of this process can cause the formation of tumors[85-88].

Nerfin-1 is among the few transcription factors that have been found to maintain neuronal cell fate in *Drosophila.* Loss of this protein causes terminally differentiated neurons to dedifferentiate back to a neuroblast-like fate[89-92]. Dedifferentiation is the reversal of differentiation, during which cells lose their identity[93]. Dedifferentiation is thought to happen through changes to chromatin architecture and gene expression, suggesting that transcriptional regulators are required to actively maintain cellular differentiated state[92]. Nerfin-1 has previously been reported to maintain the neuronal differentiated state by promoting expression of neuronal genes and repressing genes associated with proliferation and stemness[89]. In particular, Nerfin-1 maintains neuronal cell fate by regulating the expression and activity of the Notch signaling pathway [92]. Nerfin-1 directly binds to *Notch, Serrate, Delta, mastermind, Su(H),* and other Notch pathway gene loci [92]. In Nerfin-1 mutants, Notch signaling is ‘de-repressed’, and Notch pathway components are transcriptionally upregulated [92]. Whether the regulation of Notch signaling by Nerfin-1 is important in other contexts is yet to be explored.

1.4.3 Gap genes

Genetic screens for regulators of embryonic development in *Drosophila* have identified so-called ‘gap genes’. The *Drosophila* embryo is made up of serially repeated units, or body segments, along the anterior-posterior axis that are morphologically distinct. Mutations in gap

genes result in the elimination of large contiguous areas of the normal cuticular pattern (a ‘gap’ in the body plan)[94]. Gap genes encode transcription factors which regulate the expression of ‘pair-rule’ genes. Mutations in pair-rule genes result in the loss of one region of every alternate segment. Their expression depends on the varying concentrations of gap gene protein products. One of the first gap genes discovered was named *Krüppel*, meaning ‘cripple’ in German, after the mutant phenotype of severe body malformation[94]. The human homologs of *Krüppel* are the *Krüppel*-like family of transcription factors (KLFs), of which there are over a dozen. KLFs have been documented to play roles in blood cell differentiation, adipocyte differentiation, heart development, and tumor suppression, among other functions [95-97]. Most notably, KLF4 belongs to the set of Yamanaka factors, whose over-expression in differentiated cells can induce pluripotency[98].

Krüppel was recently demonstrated to regulate ion channel gene expression[43]. *Krüppel* expression is normally high during embryonic development, but virtually absent in third-instar *Drosophila* larvae[43]. Surprisingly, *Krüppel* transcript and protein are highly increased in larvae lacking the voltage-gated ion channel Shal[43]. Driving overexpression of *Krüppel* is sufficient to alter the expression of several ion channels, making it compelling as a candidate controller of FRH[43]. However, *Krüppel* has never previously been tested for direct involvement in stabilization of neuronal firing properties.

1.5 Open Questions

While there are many known examples of FRH following the loss of an ion channel, how this occurs is not well-understood. It is still unknown whether this process is triggered by changes in neuronal activity, or whether neurons respond to changes in ion channel protein abundance. In the first part of this thesis, I address this question directly. I compare the effects of two different experimental perturbations, removing the Shal ion channel protein and chronically blocking the conductance Shal. Because these perturbations are functionally equivalent, they are predicted to trigger a compensatory response through identical

mechanisms if FRH is activity-dependent. However, I find that eliminating the protein or blocking the conductance induce different types of self-corrective homeostatic signaling. On the basis of this data, I discuss a new model that incorporates at least two separable regulatory systems that are linked to channel loss, one that is activity-dependent and another that is proteostatic.

In the second part of this thesis, I propose how a cell could enact this form of self-restorative plasticity. I describe the first molecular signaling pathway that selectively controls neuronal firing rates following the loss of an ion channel. I demonstrate that downregulation of Nerfin-1 and expression of the Notch signaling pathway is required for maintenance of firing rates at wild-type levels after loss of Shal. The work described here represents a significant progress towards gaining a molecular grasp on mechanisms controlling ion channel rebalancing during FRH.

2. Dual Separable Feedback Systems Govern Firing Rate Homeostasis

Introduction

Firing Rate Homeostasis (FRH) is a form of homeostatic control that stabilizes spike rate and information coding when neurons are confronted by pharmacological, genetic or environmental perturbation [63,99]. FRH has been widely documented within invertebrate neurons[56,69,70] and neural circuits[100] as well as the vertebrate spinal cord[101], cortical pyramidal neurons[102] and cardiomyocytes[39,103,104]. In many of these examples, the genetic deletion of an ion channel is used to induce a homeostatic response. The mechanisms of FRH correct for the loss of the ion channel and precisely restore neuronal firing properties to normal, wild type levels[29,30,38,40,42,43,46,68-70,102]. To date, little is understood about the underlying molecular mechanisms[43,60,105,106].

FRH induced by an ion channel gene deletion is truly remarkable. The corrective response is not limited to the de novo expression of an ion channel gene with properties that are identical to the deleted channel, as might be expected for more generalized forms genetic compensation[107]. Instead, the existing repertoire of channels expressed by a neuron can be 'rebalanced' to correct for the deletion of an ion channel[30,40,42,43,46,69,70,102]. How is it possible to precisely correct for the absence of an essential voltage-gated ion channel? The complexity of the problem seems immense given that many channel types functionally cooperate to achieve the cell-type specific voltage trajectory of an action potential.

Theoretical work argues that different mixtures of ion channels can achieve similar firing properties in a neuron[62,63,108,109]. These observations have led to a pervasive and intuitively attractive theory that a single physiological variable, calcium, is detected and stabilized through regulatory feedback control of ion channel gene expression[63]. Yet, many questions remain unanswered. There are powerful cell biological constraints on ion channel transcription, translation, trafficking and localization in vivo[102,110]. How do these constraints impact the

expression of FRH? Is calcium the only intracellular variable that is sensed and controlled by homeostatic feedback? There remain few direct tests of this hypothesis[105]. Why are homeostatic signaling systems seemingly unable to counteract disease-relevant ion channel mutations, including those that have been linked to risk for diseases such as epilepsy and autism[111,112]?

Here, we take advantage of the molecular and genetic power of *Drosophila* to explore FRH in a single, genetically identified neuron subtype. Specifically, we compare two different conditions that each eliminate the Shal/Kv4 ion channel conductance and, therefore, are expected to have identical effects on neuronal excitability. We demonstrate robust FRH following elimination of the Shal protein and, independently, by eliminating the Shal conductance using a pore blocking mutation that is knocked-in to the endogenous Shal locus. Thus, consistent with current theory, FRH can be induced by molecularly distinct perturbations to a single ion channel gene. However, we find that these two different perturbations induce different homeostatic responses, arguing for perturbation-specific effects downstream of a single ion channel gene.

Taken together, our data contribute to a revised understanding of FRH in several ways. First, altered activity cannot be the sole determinant of FRH. Two functionally identical manipulations that eliminate the Shal conductance, each predicted to have identical effects on neuronal excitability, lead to molecularly distinct homeostatic responses. Second, homeostatic signaling systems are sensitive to the type of mutation that affects an ion channel gene. This could have implications for understanding why FRH appears to fail in the context of human disease caused by ion channel mutations, including epilepsy, migraine, autism and ataxia. Finally, our data speak to experimental and theoretical studies arguing that the entire repertoire of ion channels encoded in the genome is accessible to the mechanisms of homeostatic feedback, with a very large combinatorial solution space[62,63]. Our data are consistent with the

existence of separable proteostatic and activity-dependent homeostatic signaling systems, potentially acting in concert to achieve cell-type-specific and perturbation-specific FRH.

Results

We first established a system to assess firing rate homeostasis following the elimination of the somatic A-type potassium channel encoded by the *Shal* gene, which contributes to the A-type potassium current (IK_A). To do so, we took advantage of the *GAL4-UAS* expression system for gene specific knockdown in *Drosophila melanogaster*. The *GAL4* line *MN1-GAL4* (previously referred to as *MN1-Ib-GAL4*[113]) expresses selectively in a pair of segmentally repeated motoneurons that form synapses onto muscle 1 of the dorsal body wall (Figure 2.1A). We combined *MN1-GAL4* with a previously described *UAS-Shal-RNAi* that was shown to completely eliminate Shal protein when driven pan-neuronally[43]. Consistent with the previously documented effectiveness of the *Shal-RNAi* transgene, we found a dramatic reduction in somatically measured IK_A when *Shal-RNAi* was driven by *MN1-GAL4* (Figure 2.1B). In wild type MN1, IK_A activated at approximately -30 mV and reached an average current density of 20 pA/pF at +40 mV. By contrast, no substantial current was present in MN1 expressing *Shal-RNAi* until +20 mV, and voltage steps above +20 mV revealed only a small outward current with IK_A characteristics. Importantly, prior characterization of a Shal protein null mutation demonstrated the same current-voltage trajectory, including the same observed +50mV shift in voltage activation[42]. In that prior study, the remaining, voltage-shifted, outward current was determined to reflect the homeostatic up-regulation of the Shaker channel, which resides in the electrotonically distant axonal membranes. This conclusion was independently confirmed in an additional, prior study[43]. Given these data, we conclude that *Shal-RNAi* effectively eliminated the relevant somatic IK_A that would participate in action potential repolarization.

Cell autonomous induction of firing rate homeostasis

To test for the cell autonomous induction of FRH, we compared the effects of acute pharmacological block of IK_A using 4-aminopyridine (4-AP, 2.5 mM) with chronic IK_A knockdown caused by *Shal-RNAi* expressed specifically in MN1 (Figure 2.1C-F). We demonstrate that application of 4-AP caused a significant increase in MN1 firing rate compared to wild type across all current steps greater than 50 pA (Figure 2.1C & D; WT +4-AP, orange traces). At current steps above 150 pA, depolarization block was routinely observed, limiting the maximal firing rate that could be quantified (Figure 2.1C, arrowhead). Depolarization block was never observed in wild type. By contrast, Shal knockdown in MN1, eliminating somatic IK_A (Figure 2.1B), did not result in a significant change in firing rate. Furthermore, depolarization block was never observed, just as in wild type (Figure 2.1C & D). Notably, 4-AP does not alter firing rate when applied to motoneurons lacking the Shal conductance, demonstrating the specificity of 4-AP at the concentration used in these experiments (see below). The differential effect of acute 4-AP versus chronic Shal knockdown can be taken as evidence for homeostatic, compensatory signaling that we define, here, as FRH. Based on this argument, we provide evidence that FRH can be induced and expressed in a single neuron.

Homeostatic preservation of action potential waveform

To further investigate the precision of FRH, we examined the effects of 4-AP and Shal knockdown on action potential waveforms. Acute application of 4-AP caused a significant reduction in the after-hyperpolarization amplitude with no significant effect on amplitude or half-width (AHP, AP amp. and AP HW, respectively; Figure 2.1E & F; see Figure 2.2 for how these measurements are made). By contrast, no significant changes were observed when somatic IK_A was eliminated selectively in MN1. We note that while 4-AP is a well-described IK_A channel blocker[114], it lacks complete specificity[115]. We can rule out a major contribution of Shaker to the 4-AP effect because Shaker channels are localized at an electrotonically distant site in the axon and presynaptic terminal[116] (Figure 2.1B). Furthermore, the half-maximal effect of 4-AP on IK_A in

other systems (1-2 mM) is considered to have reasonable specificity and this concentration of 4-AP has quantitatively similar effects in *Drosophila*[116,117]. Regardless, it is remarkable that action potential repolarization and neuronal firing rate are statistically identical to wild type following the elimination of the Shal-mediated somato-dendritic IK_A current. Thus, we demonstrate conservation of action potential waveform despite the absence of a primary fast potassium channel conductance (IK_A).

Firing rate homeostasis induced by persistent elimination of the Shal conductance

We next asked whether FRH is induced when the Shal conductance is eliminated by a pore-blocking mutation. We used 'scarless' CRISPR-Cas9 gene editing technology[118] (Figure 2.1G) to engineer a point mutation in the *Shal* locus that renders the Shal channel non-conducting. This point mutation is a single amino acid substitution in the channel pore (W362F), a highly conserved mutation demonstrated to function as a pore-blocking mutation in systems as diverse as mammalian heterologous cells and cultured *Drosophila* embryonic neurons[119,120]. We note that, both in vitro and in vivo, overexpression of this pore-blocked channel traffics to the plasma membrane[119,120]. Here, we demonstrate that motoneurons in the homozygous $Shal^{W362F}$ mutant lack somatically recorded IK_A (Figure 2.1H). Next, we demonstrate the existence of robust FRH in $Shal^{W362F}$, and it is just as precise as that observed when Shal was eliminated using *UAS-Shal-RNAi* expressed in MN1 (Figure 2.1I). In contrast to wild-type motoneurons, bath application of 4-AP did not increase firing rates in $Shal^{W362F}$ mutant neurons (Figure 2.3). Thus, FRH can be induced by the loss of Shal channel function as well as loss of Shal protein.

Shal knockdown induces FRH by compensatory changes in IK_{Ca} and IK_{DR}

We hypothesized, based on work in *Drosophila* and other systems, that FRH is achieved by compensatory changes in ion channel gene expression[40,43,62]. Therefore, we assessed ionic conductances predicted to have a major role in controlling firing rate and action potential waveform including: the fast activating and inactivating potassium current IK_A, the delayed

rectifier potassium current (IK_{DR}), the calcium-activated potassium current (IK_{Ca}), the voltage-gated sodium current (I_{Na}) and the voltage-gated calcium current (I_{Ca}). We found a significant enhancement of IK_{DR} and IK_{Ca}, but no change in sodium or calcium currents in MN1 lacking Shal compared to wild type (Figure 2.4A, B, C & D, respectively). It was challenging to properly assess the total fast somatic sodium currents using standard voltage step protocols typically used in dissociated cells due to the inability to adequately maintain voltage control of the axon initial segment where action potentials are initiated. Therefore, we utilized a voltage-step protocol designed to isolate persistent sodium currents as a proxy for the total sodium current density[121,122]. Although sodium spikes occasionally escaped voltage clamp (Figure 2.4C, traces), we were able to accurately measure persistent sodium current in both wild type and *Shal-RNAi* and found no significant change compared to wild type MN1.

The largest compensatory conductance change that we observed following Shal knockdown was the enhancement of IK_{Ca}. To verify that our measurements were specific to calcium-dependent potassium currents, we performed the same protocol in the slowpoke (*slo*) mutant background, which eliminates the *Drosophila* BK channel ortholog[123-126]. The IK_{Ca} current was virtually eliminated in the *slo* mutant (Figure 2.4B, gray line). We previously demonstrated that both BK and SK channel transcripts are increased in the *Shal*^{495} null mutant background[43]. While we cannot rule out a contribution of SK channels, we propose that the elevated IK_{Ca} in the *Shal-RNAi* background is primarily due to an increase in Slo-dependent IK_{Ca} (see also below). We also observed a significant change in the delayed rectifier current (IK_{DR}) in MN1 expressing *Shal-RNAi* (Figure 2.4A). This effect parallels similar changes in IK_{DR} in Kv4.2 knockout cardiac myocytes[39] and pyramidal neurons in mice[40]. The IK_{DR} current can be encoded by four genes in *Drosophila* including: *Shab*, *Shaw*, *Shawl* and *KCNQ*. Pharmacological tools to dissect the function of each individual gene do not exist. However, the drug XE991 is a potent and selective inhibitor of KCNQ channels in both mammals and *Drosophila*[127,128]. Application of XE991

(10μM) diminished IK_{DR} in wild type MN1, but there was no differential effect following *Shal-RNAi* (data not shown).

The Krüppel transcription factor is essential for FRH following loss of Shal

We previously demonstrated that expression of the Krüppel (Kr) transcription factor is induced by genetic depletion or pharmacological inhibition of the Shal channel[43]. Kr expression is virtually absent in the wild type third instar CNS, but becomes highly expressed following loss of Shal[43]. Furthermore, over-expression of Kr in post-mitotic neurons is sufficient to drive changes in ion channel gene expression[43]. However, the role of Kr has never been studied at the level of somatic firing rates, nor has ion channel function been addressed. Therefore, it remains unknown whether Kr actually participates in the mechanisms of FRH. More specifically, it remains unclear to what extent Kr-dependent control of ion channel transcription influences the remodeling of ionic conductances during FRH. Indeed, we have previously documented that ion channel gene expression changes following loss of Shal[43], but causal links to changes in ionic conductances have yet to be established. Finally, it remains unknown if the effects of Kr can be cell autonomous, or whether it acts through intercellular signaling intermediates.

If Kr is required for homeostatic plasticity, then loss of Kr in the Shal background should enhance firing rates, similar to what we observed with acute pharmacological block of IK_A (Figure 2.1D). We quantified firing rates in MN1 in four conditions: 1) wild type, 2) *Kr-RNAi,* 3) *Shal-RNAi*, and 4) co-expression of *Shal-RNAi* and *Kr-RNAi*. Firing rates are equivalent when comparing wild type and *MN1-GAL4>Shal-RNAi* animals (Figure 2.5A). Firing rates are also unchanged when comparing wild type and *MN1-GAL4>Kr-RNAi* animals (Figure 2.5B). This is an important control, demonstrating that post mitotic knockdown of Kr, a master regulator of cell fate in the embryo, has no baseline effect. However, when Kr and Shal are simultaneously knocked down in MN1, firing rates were significantly decreased compared to wild type at all current steps above 25 pA (Figure 2.6A & B). These data are consistent with the conclusion that

induction of Kr expression following loss of Shal is required for FRH. It was surprising, however, that firing rates were depressed compared to wild type, rather than enhanced, as predicted.

Kr controls the homeostatic regulation of action potential waveform

In the *Shal-RNAi* condition, action potential (AP) waveforms are indistinguishable from wild type, arguing for preservation of AP waveform during FRH (Figure 2.6C, D & E). We found that *Kr-RNAi* has no effect on AP waveform. However, when Shal and Kr were simultaneously knocked down in MN1, AP waveforms were significantly altered (Figure 2.6C & D). Specifically, the after-hyperpolarization amplitude was significantly smaller and AP half-width duration was significantly increased compared to wild type. These effects on AP waveform can be clearly observed when representative APs are overlaid (Figure 2.6C) and in phase-plane plots of representative action potentials (Figure 2.6E). The phase-plane plots were generated for five sequential APs from individual representative recordings from each genotype, selected as matching the average properties presented in Figure 2.6D. In particular, we note the reduced rate of repolarization in double *Shal-RNAi, Kr-RNAi* (Figure 2.6E, arrowhead). Thus, Kr participates in homeostatic control of both action potential waveform and firing rates following loss of Shal.

MN1 cell identity is maintained following post-mitotic Kr knockdown

It is well established that Kr is a master regulator of cell fate determination in neurons[129] and other cell types[130]. But, the action of Kr in post-mitotic neurons is not understood. To confirm that we have not grossly altered cell fate, we examined MN1 morphology and passive-electric properties comparing *MN1-GAL4>UAS-GFP* (wild type) to the three genotypes analyzed throughout this paper: knockdown of Kr, knockdown of Shal, and simultaneous knockdown of both Kr and Shal. There was no change in MN1 cell number or gross morphology in the CNS (Figure 2.7A, B, C & D). We further measured somatic diameter and the width of the proximal dendrite as features that contribute to the passive electrical properties of these cells. No significant differences were observed (Figure 2.7E & F). Finally, we quantified cell capacitance

and input resistance (Figure 2.7G & H). We found a decrease in input resistance for both *Kr-RNAi* and combined *Shal-RNAi, Kr-RNAi*. Although, the double *Shal-RNAi, Kr-RNAi* condition has an effect on input resistance, this cannot account for the difference in AP waveform or firing rates since *Kr-RNAi* alone matches wild type for both measures.

Increased firing rate variance is associated impaired FRH

The observation that firing rates are decreased in the combined *Shal-RNAi, Kr-RNAi* condition could be due to MN1 acquiring a new firing rate set point or it could be due to the loss of homeostatic control. We reason that if a new set point is established, then the cell would target the new set point firing rate accurately, and the variance of firing rate would be equivalent to that observed in wild type controls. By contrast, if FRH is disrupted by loss of Kr, then we expect to observe an increase in firing rate variability. We compared the F-I curves of individual MN1 neurons within each genotype (Figure 2.8A). It is clear that there was increased variability across cells in the double *Shal-RNAi, Kr-RNAi* condition compared to wild type and each individual knockdown alone. We quantified cell-to-cell variability across all current injections using the coefficient of variation (Figure 2.8B). The double *Shal-RNAi, Kr-RNAi* condition had the highest variability of all four genotypes, an effect that is not additive for current steps above 100pA. These data are consistent with the hypothesis that Kr is essential for firing rate homeostasis, rather than revealing a new homeostatic set point. However, we acknowledge that the molecular basis for a homeostatic set point, in any system, has yet to be defined. Finally, it is worth noting that no individual cell ever fired at rates exceeding wild type as we observe following application of 4-AP (Figure 2.1D), indicating that the loss of firing rate homeostasis is not without some remaining constraint on firing frequencies in vivo.

Kr selectively controls the homeostatic enhancement of IKCa

We next addressed the ionic conductances that are controlled by Kr. In principle, loss of Kr could specifically impair the homeostatic rebalancing of ion channel expression, or it could simply de-regulate gene expression and, thereby, non-specifically alter firing rates. We have

shown that the two most prominent changes following loss of Shal are increases in IKCa and IK_{DR} (Figure 2.4A & B). Here we demonstrate that the increase in IKCa following loss of Shal was completely blocked by simultaneous Kr knockdown (Figure 2.9C). Importantly, Kr knockdown had no effect on baseline IKCa (Figure 2.9D) or on voltage-gated calcium currents in the *Shal-RNAi* background (Figure 2.9E). Thus, Kr is required for the homeostatic enhancement of IKCa. To our knowledge, Kr is the first gene demonstrated to have a selective action for homeostatic changes in channel function, without altering baseline channel activity.

Next, we examined IK_{DR}. We found that IK_{DR} remained elevated in the double *Shal-RNAi, Kr-RNAi* condition (Figure 2.9A), similar to that observed in *Shal-RNAi* alone (Figure 2.4A). This suggests that Kr does not control the homeostatic upregulation of IK_{DR} following loss of Shal. We confirmed that Kr knockdown alone had no effect on baseline IK_{DR} (Figure 2.9B). Finally, as another control, we quantified IK_A in double *Shal-RNAi, Kr-RNAi* neurons and demonstrate that IK_A was knocked down just as efficiently as when *Shal-RNAi* was driven alone (Figure 2.9F). Thus, any effect of the double RNAi is not a consequence of diluting GAL4-mediated expression of our transgenes. Taken together, our data argue that Kr has an activity that is required for the homeostatic rebalancing of IKCa, but not IK_{DR}. Thus, we conclude that loss of Kr participates in a specific facet of FRH induced by loss of Shal.

The BK channel Slo is essential for maintenance of set point firing rates

We reasoned that if the decreased firing rate observed in double *Shal-RNAi, Kr-RNAi* neurons is due to a selective loss of IKCa, then acute pharmacological inhibition of IKCa should also decrease firing rate. We bath applied the selective BK channel inhibitor paxilline (600 nM) to both wild type and *Shal-RNAi* preparations, and observed significantly reduced firing rates in MN1 (Figure 2.10A, B & C). Paxilline reduced maximal firing rates by 34% on average, compared to the 12% reduction due to driving *Kr-RNAi* in the *Shal-RNAi* background. This difference in effect size is consistent with Kr specifically regulating the increase in IKCa

following loss of Shal rather than eliminating IKCa. The effects of paxilline on action potential waveform were also consistent with those seen in the double *Shal-RNAi, Kr-RNAi* condition. We observed decreased AHP amplitude and a larger AP half-width duration (Figure 2.10D & E). These data explain decreased firing rates in the double *Shal-RNAi, Kr-RNAi*. Loss of Slo-dependent AP repolarization leads to the observed broader action potential and shallower AHP, an effect that is predicted to impede recovery of sodium channels from inactivation and thus cause decreased firing rate.

An alternate homeostatic mechanism is induced in pore blocked Shal mutants

We have shown that a pore-blocking, knock-in mutation ($Shal^{W362F}$) induces equally robust FRH when compared to elimination of Shal with expression of *Shal-RNAi*. Thus, we expected to observe identical changes in both IKCA and IK_{DR}. First, we demonstrate upregulation of IK_{DR} in $Shal^{W362F}$ (Figure 2.11A), consistent with this expectation. Furthermore, we found no significant change in IKCa (Figure 2.11B). We confirmed, via quantitative PCR, that *Slo* transcript is upregulated following loss of Shal protein (Figure 2.11E; see Parrish et al., 2014 for initial observation). However, we did not observe a change in *Slo* transcript in the $Shal^{W362F}$ non-conducting mutant (Figure 2.11F). In agreement, we observed a small but statistically significant broadening of the AP waveform in $Shal^{W362F}$ (Figure 2.11C & D). Thus, FRH appears to be differentially achieved in $Shal^{W362F}$ compared to *Shal-RNAi*.

One possibility is that the $Shal^{W362F}$ pore blocking mutation induces a unique homeostatic solution. To assess this possibility, we used quantitative PCR to examine changes in gene expression for *Krüppel*, *Shaker*, *slo*, and *Shab*. The transcripts for all four of these genes are significantly elevated in the shal null mutant ($Shal^{495}$; Parrish et al., 2014). Here, we compare the Shal null mutant ($Shal^{495}$) to $Shal^{W362F}$ since both directly alter the Shal gene locus and do so throughout the nervous system and throughout development. Confirming prior observations using gene expression arrays[43], the transcription all four genes was increased in

the Shal null mutant (Figure 2.11E). However, none of these genes showed altered expression in *Shal*^{W362F} (Figure 2.11F, bottom). We then extended this analysis in *Shal*^{W362F} to include KCNQ, Shaw and Shawl (Figure 2.11F, top). Again, there was no change in the expression of these channels, whereas KCNQ was upregulated in the Shal null[43]. Thus, eliminating Shal using either a null mutation or via expression of *Shal-RNAi* initiates FRH that is achieved by induction of the Krüppel transcription factor followed by Krüppel-dependent enhancement of IKCa current and Krüppel-independent enhancement of IK_{DR} current, as well as increased transcription of several other ion channel genes. By contrast, in the *Shal*^{W362F} mutant, equally robust FRH is achieved by a selective increase in the IK_{DR} current without a change in the expression of major IK_{DR} genes. Thus, it appears that two separable, equally robust, homeostatic solutions are achieved downstream of different mutations in a single ion channel gene.

Solution-specific effects on motor behavior

Wild type, *Shal*^{W362F}, and Shal knockdown animals were individually tested for motor behavior in a negative geotaxis assay (Figure 2.11G, H). Negative geotaxis is a powerful innate behavior that can be used to assess adult *Drosophila* motility and coordination without confounding effect of motivation or learning. All wild type and *Shal*^{W362F} flies climbed up the walls of a glass vial above 10 cm within 10 seconds. No statistically significant differences in average climbing speed were detected, consistent with the idea that FRH enables normal motor behavior. Since the *Shal*^{W362F} mutation is present throughout the CNS, throughout development, we initially compared *Shal*^{W362F} to pan-neuronal Shal knockdown (*elav-Gal4; Shal-RNAi*), expecting similarly robust motor behavior. This was not observed. Instead, pan-neuronal Shal knockdown dramatically altered animal behavior, and every animal that was tested failed to ascend past the 10 cm mark within 30 seconds, the maximal allotted time. The shal null mutation behaves similarly, being unable to climb the walls of a vial (not shown). Control animals (*Shal-RNAi*/+) were no different from wild type. As a further control, we assessed motoneuron-specific Shal knockdown (*OK371-Gal4*). In this experiment, climbing behavior was

wild type, again consistent with the conclusion that FRH, which we demonstrate in motoneurons, is sufficient to restore normal animal behavior. Why is motor behavior differentially affected in pan-neuronal Shal knockdown and Shal null mutants compared to the pan-neuronal effects of the *Shal*^{W362F} mutation? One possibility is that every neuronal cell type is able to engage the form of homeostatic plasticity triggered by the *Shal*^{W362F} mutation, but not every cell type engages FRH equivalently following deletion of the Shal protein. Alternatively, loss of Shal protein triggers a homeostatic response that includes changes in ion channel gene expression, and in some cell types the altered expression of ion channel genes could lead to maladaptive effects on circuit function and animal behavior (see discussion).

Solution-specific effects on presynaptic homeostatic plasticity

We previously demonstrated that FRH, induced by pan-neuronal knockdown of Shal, interferes with the subsequent induction of presynaptic homeostatic plasticity (PHP), assayed at the neuromuscular junction[42]. A current model for this interference effect is that increased Shaker expression, caused by the presence of the protein null *Shal*^{495} mutation or by direct over-expression of a *Shaker* transgene, blocks the expression of PHP that is selectively induced at the NMJ[42,43] (Figure 2.11I & J). Increased levels of Shaker channel, which localizes to the presynaptic terminal at the NMJ (Figure 2.11), prevents ENaC channel-dependent depolarization of the presynaptic plasma membrane, which is necessary to increase presynaptic calcium influx that drives enhanced neurotransmitter release during PHP[43,131,132]. If this model is correct, then FRH induced by the *Shal*^{W362F} mutation should have no effect of the rapid induction of PHP because the mechanisms of FRH in the *Shal*^{W362F} mutation do not include a change in *Shaker* expression. This is precisely what we observe. We induced PHP by incubating the NMJ in a sub-blocking concentration of the glutamate receptor antagonist philanthotoxin-433 (PhTX; 15-20 μM) according to well-established protocols[133]. Decreased mEPSP amplitude was precisely offset by an increase in presynaptic release (quantal content, QC) that restored EPSP amplitudes to pre-PhTx amplitudes in both wild type and *Shal*^{W362F} animals (Figure 2.11K & L).

Thus, unlike in the protein null *Shal*^{495} mutant, synapses in the pore-blocking *Shal*^{W362F} mutant were capable of undergoing PHP. Thus, the differential expression mechanisms of FRH induced by loss of Shal protein versus the *Shal*^{W362F} mutation can have different effects on synaptic transmission and synaptic plasticity.

Discussion

Here we advance our mechanistic understanding of FRH in several ways. First, we demonstrate that FRH can be induced and fully expressed in single, genetically identified neurons. Since changes in the activity of a single motoneuron are unlikely to dramatically alter the behavior of the larvae, these data argue strongly for cell autonomous mechanisms that detect the presence of the ion channel perturbation and induce a corrective, homeostatic response. Second, we demonstrate that FRH functions to preserve the waveform of individual action potentials. This argues for remarkable precision in the homeostatic response. Third, we provide new evidence that the transcription factor Krüppel is essential for FRH, and selectively controls the homeostatic enhancement of IKCA, without altering the baseline ion channel current. Finally, we demonstrate that different mechanisms of FRH are induced depending upon how the Shal current is eliminated, and these differential expression mechanisms can have perturbation-specific effects on animal behavior.

We propose the existence of parallel homeostatic mechanisms, responsive to differential disruption of the Shal gene. We observe different compensatory responses depending upon whether the Shal protein is eliminated or the Shal conductance is eliminated. The following evidence supports the functional equivalence of our manipulations. First, the *Shal*^{W362F} mutation completely eliminates somatically recorded IK_A (Figure 2.1). Second, we demonstrate a dramatic reduction in IK_A when *Shal-RNAi* is driven by *MN1-GAL4* in a single, identified neuron. Notably, the current-voltage relationship observed for *Shal-RNAi* is identical to that previously published for the *Shal*^{495} protein null mutation, being of similar size and voltage trajectory

including a +50mV shift in voltage activation[42]. This remaining, voltage-shifted, IK_A -like conductance is attributed to the compensatory up-regulation of the Shaker channel on axonal membranes[42,43] an effect that does not occur in the *Shal*^{W362F} mutant (Figure 2.11). Thus, it seems reasonable to assume that Shal protein elimination and Shal conductance blockade initially create identical effects on neuronal excitability by eliminating Shal function. Subsequently, these perturbations trigger divergent compensatory responses. But, we acknowledge that we lack direct information about the immediate effects of the two perturbations.

Comparison with prior studies of FRH in *Drosophila*

We define FRH as the restoration of neuronal firing rate in the continued presence of a perturbation. This definition is important because it necessitates that the underlying molecular mechanisms of FRH must have a quantitatively accurate ability to adjust ion channel conductances such that firing rate is precisely restored. Mechanistically, a prior example of FRH involves an evolutionarily conserved regulation of sodium channel translation by the translational repressor Pumilio[60,69]. This work, originally pursued in *Drosophila*, was extended to mouse central neurons where it was shown that Pumilio-dependent bi-directional changes in the sodium current occur in response to altered synaptic transmission, initiated by application of either NBQX or Gabazine[70]. These data highlight the emerging diversity of molecular mechanisms that can be induced and participate in the execution of FRH[105,106].

It is necessary to compare our current results with prior genetic studies of the Shal channel in *Drosophila*. A prior report, examining the effects of partial Shal knockdown in larval motoneurons, observed a trend toward an increase in the sustained potassium current, but concluded no change[134]. However, the small sample size for potassium current measurements in that study (n=3 cells) and the incomplete Shal knockdown that was achieved, likely conspired to prevent documentation of the significant increase in IK_{DR} that we observe (IKCA was not

measured in Schaefer et al., 2010). A second prior study examined over-expression of a pore-blocked Shal transgene in cultured *Drosophila* embryonic neurons, revealing elevated firing rate and a broadened action potential[120]. This was interpreted as evidence against the existence of FRH[120]. However, neuronal precursors were cultured from 5hr embryos[120], prior to establishment of neuronal cell fate and prior to the emergence of IK_A currents in vivo, which occurs ~10 hours later in development[135]. It remains unclear whether these cultured neurons are able to achieve a clear cell identity, which may be a prerequisite for the expression of homeostatic plasticity[99,136]. Another possibility concerns the time-course of FRH, which remains uncertain. Finally, over[64]-expression of the transgene itself might interfere with the mechanisms of FRH[38], emphasizing the importance of the scarless, CRISPR-mediated gene knock-in approach that we have employed.

Distinct homeostatic mechanisms downstream of a single ion channel gene

It is clear from studies in a diversity of systems that FRH can be induced by perturbations that directly alter neuronal activity without genetic or pharmacological disruption of ion channels or neurotransmitter receptors. For example, monocular deprivation induces an immediate depression of neuronal activity in the visual cortex, followed by restoration of normal firing rates[64]. Research on the lobster stomatogastric system ranging from experiments in isolated cell culture[56] to de-centralized ganglia[137] have documented the existence of FRH that is consistent with an activity-dependent mechanism. It is equally clear that FRH can be induced by the deletion of an ion channel gene, including observations in systems as diverse as invertebrate and vertebrate central and peripheral neurons and muscle[30,40,42,43,46,69,70,102]. But, it has remained unknown whether FRH that is induced by changes in neural activity is governed by the same signaling process that respond to ion channel gene mutations. Our current data speak to this gap in knowledge.

We demonstrate that changes in neural activity cannot be solely responsible for FRH. We compare two different conditions that each completely eliminate the Shal ion channel conductance and, therefore, are expected to have identical effects on neuronal excitability. We demonstrate robust FRH in both conditions. However, two separate mechanisms account for FRH. *Shal-RNAi* induces a transcription-dependent homeostatic signaling program. There is enhanced expression of Krüppel and a Krüppel-dependent increase in the expression of the *slo* channel gene and enhanced IKCA current. By contrast, the *Shal*^{W362F} mutant does not induce a change in the expression of *Krüppel*, *slo* or any of five additional ion channel genes. Instead, we observe a change in the IK_{DR} conductance, the origin of which we have yet to identify, but which appears to be independent of a change in ion channel gene transcription.

We propose the existence of two independent homeostatic signaling systems, induced by separate perturbations to the Shal channel gene. First, we propose that *Shal-RNAi* and the *Shal* null mutation trigger a homeostatic response that is sensitive to the absence of the Shal protein. In essence, this might represent an ion channel-specific system that achieves channel proteostasis, a system that might normally be invoked in response to errors in ion channel turnover (Figure 2.12). We speculate that many, if not all ion channels could have such proteostatic signaling systems in place. In support of this idea, the induction of Kr is specific to loss of Shal, not occurring in eight other ion channel mutant backgrounds, each of which is sufficient to alter neural activity, including *eag*, *para*, *Shaker*, *Shab*, *Shawl*, *slo*, *cac* and *hyperkinetic*[43]. Each of these channel mutations is well established to alter neuronal activity[51,138-143]. But, Kr responds only to loss of Shal.

Next, we propose that eliminating the Shal conductance in the *Shal*^{W362F} mutant background induces a separable mechanism of FRH that is independent of ion channel transcription. While the mechanisms of this homeostatic response remain unknown, it is tempting to speculate that this mechanism is activity dependent, consistent with data from other

systems cited above (Figure 2.12). Finally, it remains possible that these homeostatic signaling systems are somehow mechanistically linked (Figure 2.12). If so, this might provide a means to achieve the precision of FRH. For example, changes in ion channel gene expression might achieve a crude re-targeting of set point firing rates, followed by engagement of activity-dependent processes that fine tune the homeostatic response (Figure 2.12). Notably, distinct, interlinked negative feedback signaling has been documented in cell biological systems, suggesting a common motif in cell biological regulation[144].

An interesting prediction of our model is that activity-dependent mechanisms of FRH could be constrained by the action of the channel-specific homeostatic system. For example, loss of Shal induces a Shal-specific gene expression program and activity-dependent homeostatic signaling would be constrained to modulate the Shal-specific response. As such, the homeostatic outcome could be unique for mutations in each different ion channel gene. Given this complexity, it quickly becomes possible to understand experimental observations in non-isogenic animal populations where many different combinations of ion channels are observed to achieve similar firing rates in a given cell[62,63,108,109]. The combined influence of dedicated proteostatic and activity-dependent homeostatic signaling could achieve such complexity, but with an underlying signaling architecture that is different from current theories that focus on a single calcium and activity-dependent feedback processor.

Finally, although we propose the existence of proteostatic feedback induced by the Shal null mutant and pan-neuronal RNAi, other possibilities certainly exist for activity-independent FRH, inclusive of mechanisms that are sensitive to channel mRNA[38]. For example, the transcriptional compensation that we document could be considered a more general form of ‘genetic compensation’[107]. Yet, our data differ in one important respect, when compared to prior reports of genetic compensation. In most examples of genetic compensation, gene knockouts induce compensatory expression of a closely related gene. For example, it was observed that

knockout of ß-actin triggers enhanced expression of other actin genes[107]. The compensatory effects that we observe involve re-organization of the expression profiles for many, unrelated ion channel genes. Somehow, these divergent conductances are precisely adjusted to cover for the complete absence of the somato-dendritic A-type potassium conductance. Thus, we favor a more complex form of genetic compensation based upon homeostatic, negative feedback regulation (Figure 2.12).

Kr-dependent control of IK_{Ca}

How does Kr-dependent control of IK_{Ca} participate in FRH? IK_{Ca} is a rapid, transient potassium current. Therefore, it makes intuitive sense that elevated IK_{Ca} could simply substitute for the loss of the fast, transient IK_A current mediated by Shal. If so, this might be considered an instance of simple genetic compensation[107]. But, if this were the case, then blocking the homeostatic increase in IK_{Ca} should lead to enhanced firing rates. This is not what we observe. Instead, average firing rates decrease when Kr is eliminated in the background of *Shal-RNAi*. Thus, the Kr-dependent potentiation of IK_{Ca} seems to function as a form of positive feedback, accelerating firing rate in order to achieve precise FRH, rather than simply substituting for the loss of Shal. Consistent with this possibility, acute pharmacological inhibition of IK_{Ca} decreases, rather than increases, average firing rate. However, it should also be emphasized that the role of IK_{Ca} channels in any neuron are quite complex, with context specific effects that can either increase or decrease neuronal firing rates[145]. Indeed, it has been argued that BK channels can serve as dynamic range compressors, dampening the activity of hyperexcitable neurons and enhancing the firing of hypoexcitable neurons[145]. This broader interpretation is also consistent with the observed Kr-dependent increase IK_{Ca} during FRH.

In the stomatogastic nervous system of the crab, single cell RT-PCR has documented positive correlations between channel mRNA levels, including transcript levels for IK_{Ca} and Shal[34,146,147]. The molecular mechanisms responsible for the observed correlations remain unknown, but it

seems possible that these correlations reflect a developmental program of channel co-regulation. Upon homeostatic challenge, the steady-state positive correlations are supplanted by homeostatic compensation, notably enhanced IK_{Ca} in the presence of 4-AP. The pressing challenge is to define molecular mechanisms that cause the observed correlations and compensatory changes in ion channel expression during homeostatic plasticity. The Kr-dependent control of IK_{Ca} following loss of Shal is one such mechanism. Clearly, there is additional complexity, as highlighted by the differential response to Shal null and Shal pore blocking mutations and the Pumilio-dependent control of sodium channel translation in flies and mice[60,69,70].

The limits of FRH and implications for disease

Why do ion channel mutations frequently cause disease? If activity-dependent homeostatic signaling is the primary mechanism of FRH, then any ion channel mutation that alters channel function should be detected by changes in neural activity and firing rates restored. One possibility is that FRH is effective for correcting for an initial perturbation, but the persistent engagement of FRH might become deleterious over extended time. Alternatively, each solution could effectively correct firing rates, but have additional maladaptive consequences related to disease pathology. While this remains to be documented in disease, we show that loss of Shal protein throughout the CNS causes deficits in animal behavior that are not observed in animals harboring a pore-blocking channel mutation. Indeed, if one considers that FRH can include altered expression of a BK channel, the potential for maladaptive consequences is high. Altered BK channel function has been repeatedly linked to neurological disease including idiopathic generalized epilepsy[148], non-kinesigenic dyskinesia[149] and Alzheimer's disease[150-152]. Thus, there are potentially deleterious ramifications of altering BK channel expression if a homeostatic signaling process is engaged throughout the complex circuitry of the central nervous system. Although the phenotype of maladaptive compensation that we observe is clear, a block in synaptic homeostasis and impaired animal motility, there is

much to be learned about the underlying cause. Ultimately, defining the rules that govern FRH could open new doors toward disease therapies that address these maladaptive effects of compensatory signaling.

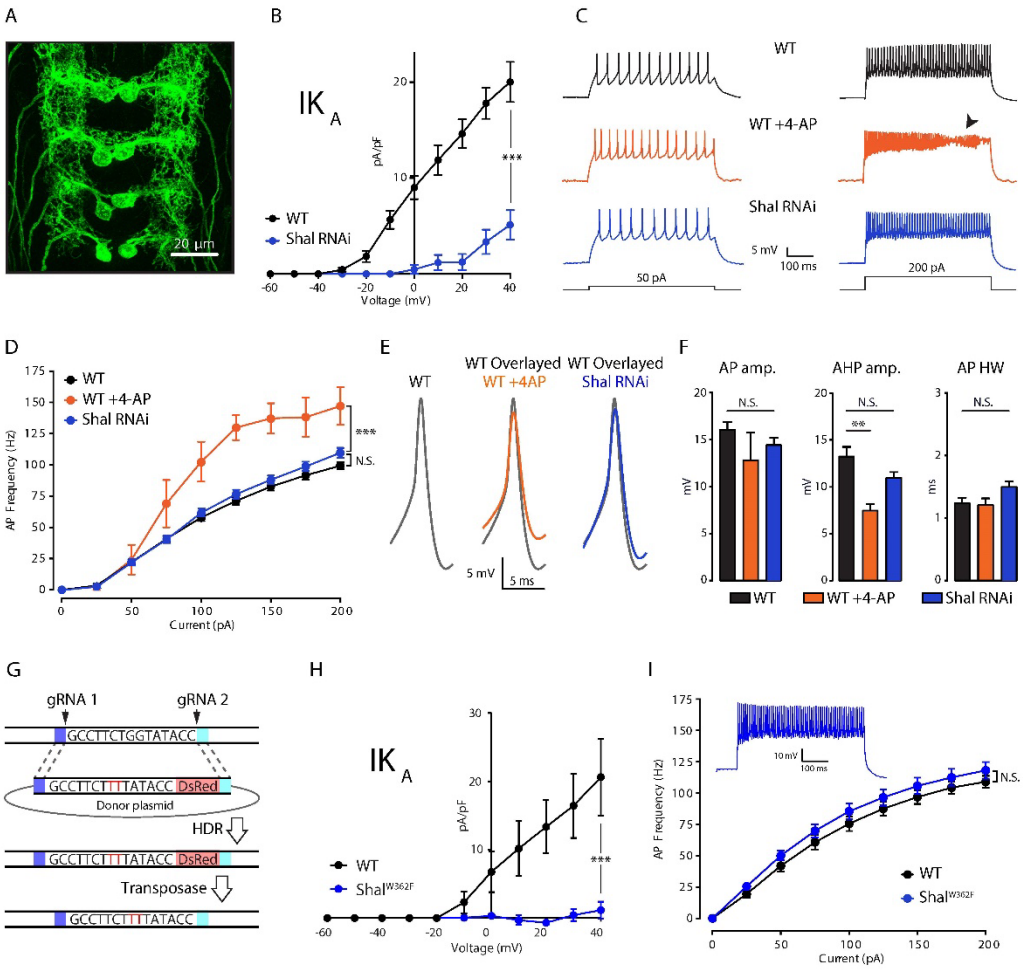

Figure 2. 1 : Firing Rate Homeostasis in *Drosophila* Motoneurons

(A) Confocal max projection of *Drosophila* 3rd instar larval VNC shows selective Gal4 expression in MN1 (*MN1-GAL4 > UAS-CD8:GFP*). **(B)** I-V plots of MN1 IK_A in WT (black, n = 20) and *Shal-RNAi* (blue, n = 10). **(C)** Representative voltage traces from WT (black), WT + 4-AP (orange) and *Shal-RNAi* (blue) at 50 pA (left) and 200 pA (right) current injections. Arrow indicates impaired action potentials due to depolarization block. **(D)** F-I curves of WT (n = 10), WT +4-AP (n = 4) and *Shal-RNAi* (n = 15). **(E)** Example action potential waveforms (left) and overlay (right). **(F)** Quantification of action potential, after-hyperpolarization amplitudes (AP amp. AP AHP amp., respectively) and action potential half-width (AP HW). **(G)** CRISPR strategy for generating a targeted pore-blocking point mutation in Shal. Dark and light blue regions represent 5' and 3' 1kb homology arms designed for recombination of mutated segment from pHD-ScarlessDsRed donor vector into the endogenous Shal gene locus. Selection marker represented in pink. **(H)** Elimination of IK_A across all motoneurons in the *Shal*^{W362F} mutant. WT (black, n=7) and *Shal*^{W362F} (blue, n=13). **(I)** F-I curves of WT (n=19) and *Shal*^{W362F} (n=15). Inset: Representative voltage trace from *Shal*^{W362F} motoneuron at 200pA current injection. Mean ± S.E.M.; *p < 0.05; **p < 0.005; ***p < 0.0005. N.S., not significant; two-way RM-ANOVA with post-hoc tests (I-V plots & F-I curves) or one-way ANOVA with Bonferoni post-hoc tests (AP waveform measurements).

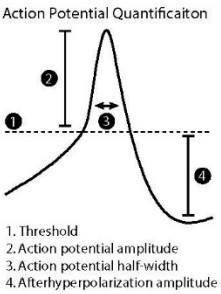

Figure 2. 2: Action Potential Waveform Measurements.

Action potential threshold was the membrane potential at the first inflection point, calculated as 1.5 standard deviations away from the mean second derivative of the AP wave at baseline. Action potential amplitude (AP amp) was the difference in voltage between the threshold and the maximum potential. Action potential half-width (AP HW) was the AP width at half-max amplitude. After-hyperpolarization amplitude (AHP) was the difference in voltage between threshold and the minimum potential after the peak. AP amp, AP HW, and AHP measurements were averaged from all action potentials elicited from a standard current step protocol for each cell.

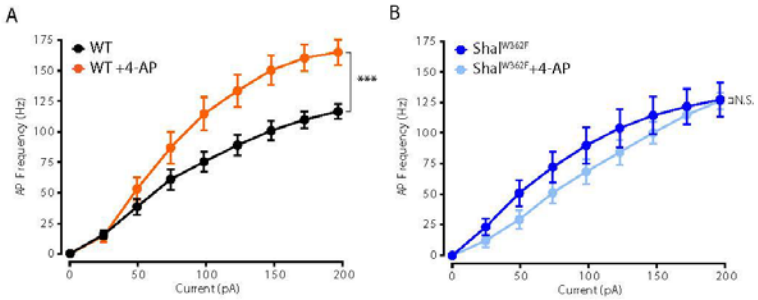

Figure 2. 3 : 4-AP Does Not Increase Firing Rates in *Shal*^{W362F} Motoneurons.

(A) F-I curves of WT (black, n=9) and WT+4-AP (orange, n=9). (B) F-I curves of *Shal*^{W362F} (dark blue, n=5) and *Shal*^{W362F} +4-AP (light blue, n=9). Mean ± S.E.M.; two-way RM-ANOVA and Bonferroni's multiple comparisons test.

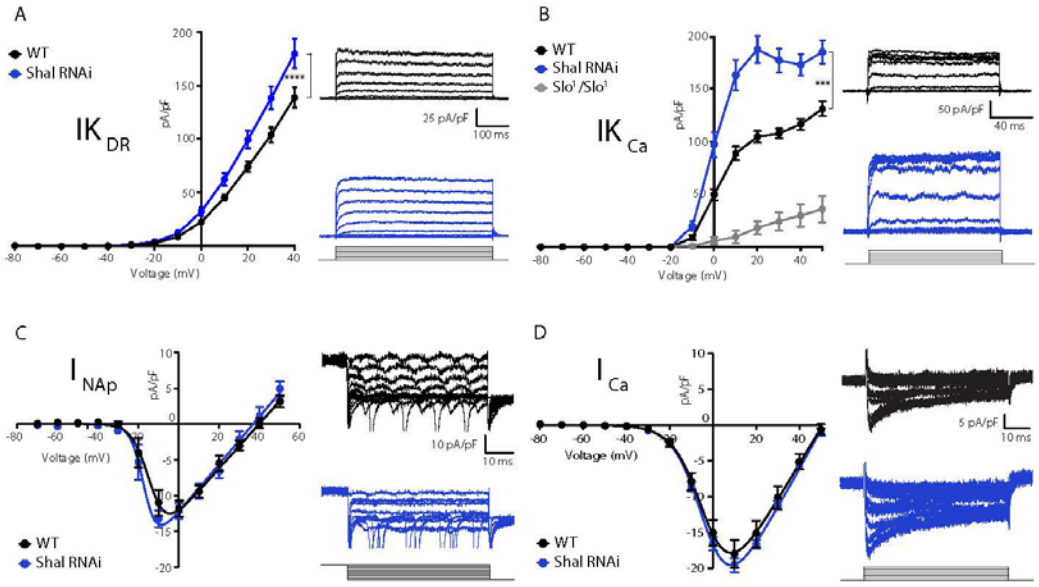

Figure 2. 4 : Homeostatic Potassium Current Rebalancing Stabilizes MN1 Excitability in the Absence of Shal-dependent IK_A.

(A, B) I-V plots and representative traces of voltage-dependent delayed rectifier (IK_{DR}, A) and Ca^{2+}-dependent (IK_{Ca}, B) potassium currents in WT (black; n = 7 and n = 9 for IK_{DR} and IK_{Ca}, respectively) and *Shal-RNAi* (blue; n = 12 and n = 8 for K_{DR} and K_{Ca}, respectively) MN1. The specificity of the IK_{Ca} current protocol was confirmed in *slo*^{1} mutants (B, grey; n = 4), which exhibited minimal Ca^{2+}-dependent potassium currents. (C, D) I-V plots and representative traces of persistent sodium currents (I_{NaP}, C, WT: n = 9; *Shal-RNAi*: n = 9) and voltage dependent calcium currents (I_{Ca}, D; WT, n = 8; *Shal-RNAi*, n = 6) in WT (black) and *Shal-RNAi* (blue) MN1. Mean ± S.E.M.; *p < 0.05; **p < 0.005; ***p < 0.0005. N.S., not significant; two-way RM-ANOVA with Bonferoni post-hoc tests (I-V plots).

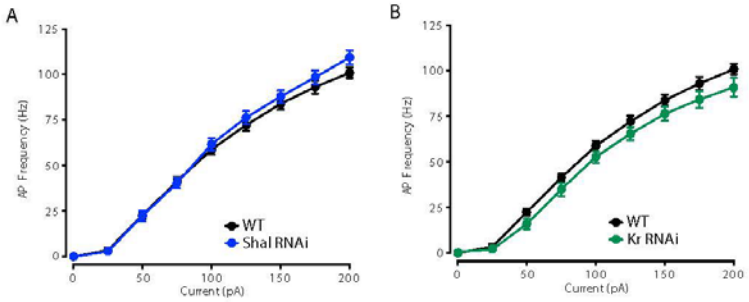

Figure 2. 5: Kr Does Not Contribute to Setting MN1 Baseline Firing Rate.

(A) F-I curves of WT (black, n=10) and *Shal-RNAi* (blue, n=15). (B) F-I curves of WT (black, n=10) and *Kr-RNAi* (green, n=8). Mean ± S.E.M.; two-way RM-ANOVA and Bonferroni's multiple comparisons test.

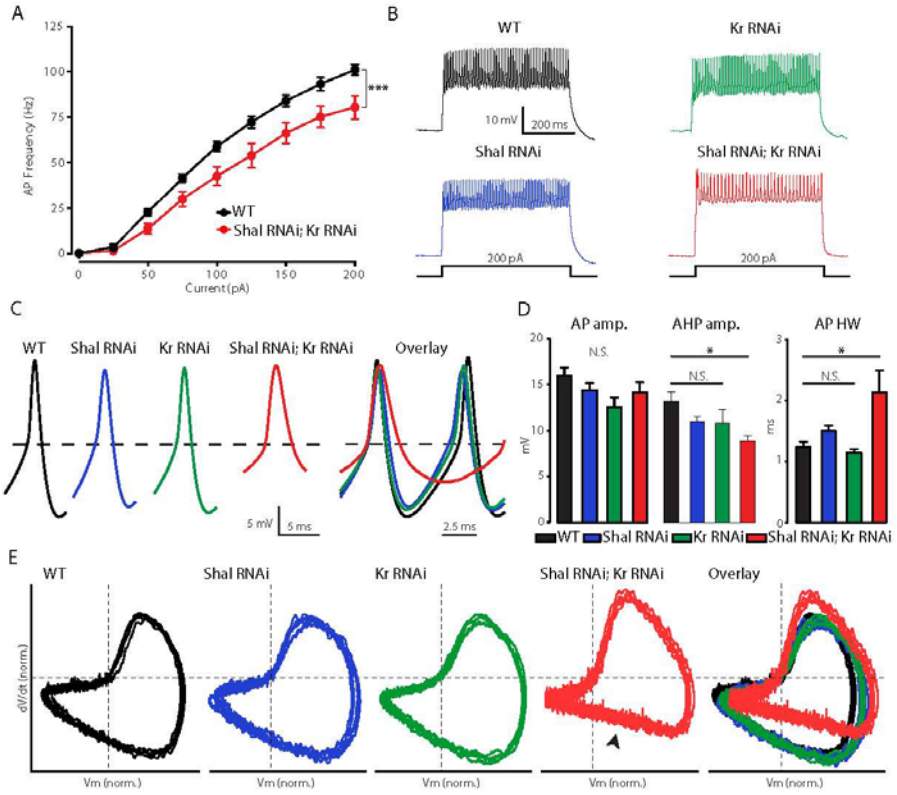

Figure 2. 6: Krüppel is Necessary for Firing Rate Homeostasis and Preservation of AP Waveform.

(A) F-I curves of WT (black; n = 10) and double *Shal-RNAi; Kr-RNAi* (red; n = 16). (B) Representative voltage traces from WT (black), *Shal-RNAi* (blue), *Kr-RNAi* (green) and double *Shal-RNAi; Kr-RNAi* (red) at 200 pA current injections. (C) Left: Example action potential waveforms for WT (black), *Shal-RNAi* (blue), *Kr-RNAi* (green) and double *Shal-RNAi; Kr-RNAi* (red). Right: Action potential overlays. (D) Action potential waveform quantification. (E) Phase plane plots of normalized example action potential waveforms for each genotype (left four panels) and overlays (far right panel). Each plot contains 5 sequential action potentials from a representative cell to illustrate AP to AP consistency. Mean ± S.E.M.; *p < 0.05; **p < 0.005; ***p < 0.0005. N.S., not significant; two-way RM-ANOVA (F-I curves), one-way ANOVA with Bonferoni post-hoc tests (AP waveform comparisons).

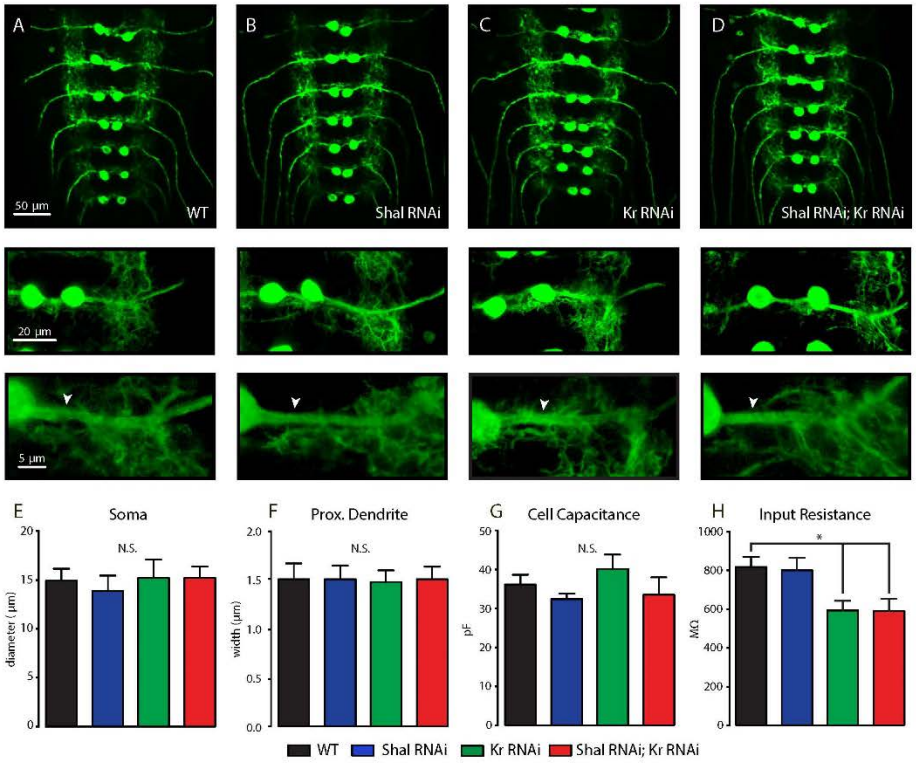

Figure 2. 7: Normal Motoneuron Morphology.

(A-D) Confocal max projections of MN1-Ib motorneurons (*MN1-GAL4 > UAS-CD8:GFP*) in WT (A), *Shal-RNAi* (B), *Krüppel* (*Kr)-RNAi*, C) and combined *Shal* and *Krüppel-RNAi* (*Shal-RNAi; Kr-RNAi*, D). Representative MN1-Ibs shown at higher magnification in inserts to reveal single neuron morphology. Arrows indicate MN1-Ib primary dendrite. (E, F) Quantification of somatic diameter (E) and proximal dendrite width (F) in WT (back), *Shal-RNAi* (blue), *Krüppel-RNAi* (Kr, green) and combined *Shal* and *Krüppel-RNAi* (*Shal-RNAi; Kr-RNAi*, red). (G, H) Whole-cell capacitance (G) and input resistance (H) in WT (back), *Shal-RNAi* (blue), *Krüppel-RNAi* (Kr, green) and combined *Shal-RNAi* and *Krüppel-RNAi* (*Shal-RNAi*; *Kr-RNAi*, red). Mean ± S.E.M.; *p < 0.05; **p < 0.005; ***p < 0.0005. N.S., not significant; one-way ANOVA with Bonferoni post-hoc tests.

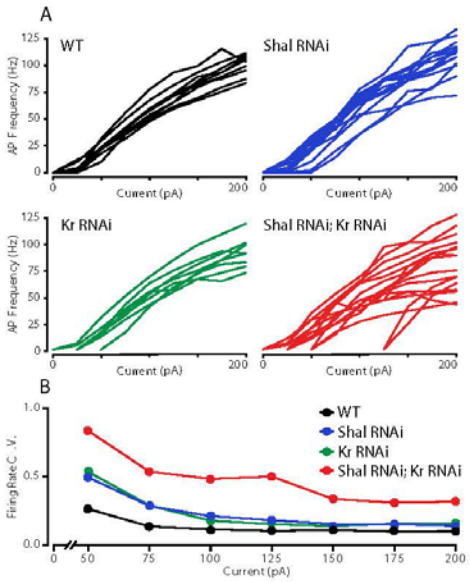

Figure 2. 8: Krüppel Constrains Cell-to-Cell Firing Rate Variance.

(A) Individual motorneuron F-I curves for WT (black), *Shal-RNAi* (blue), *Kr-RNAi* (green) and double *Shal-RNAi; Kr-RNAi* (red) groups. (B) The coefficient of variation across cells is calculated for each genotype at each current injection step and plotted. Data at 25pA are not shown since a large fraction of cells in each genotype failed to fire an action potential.

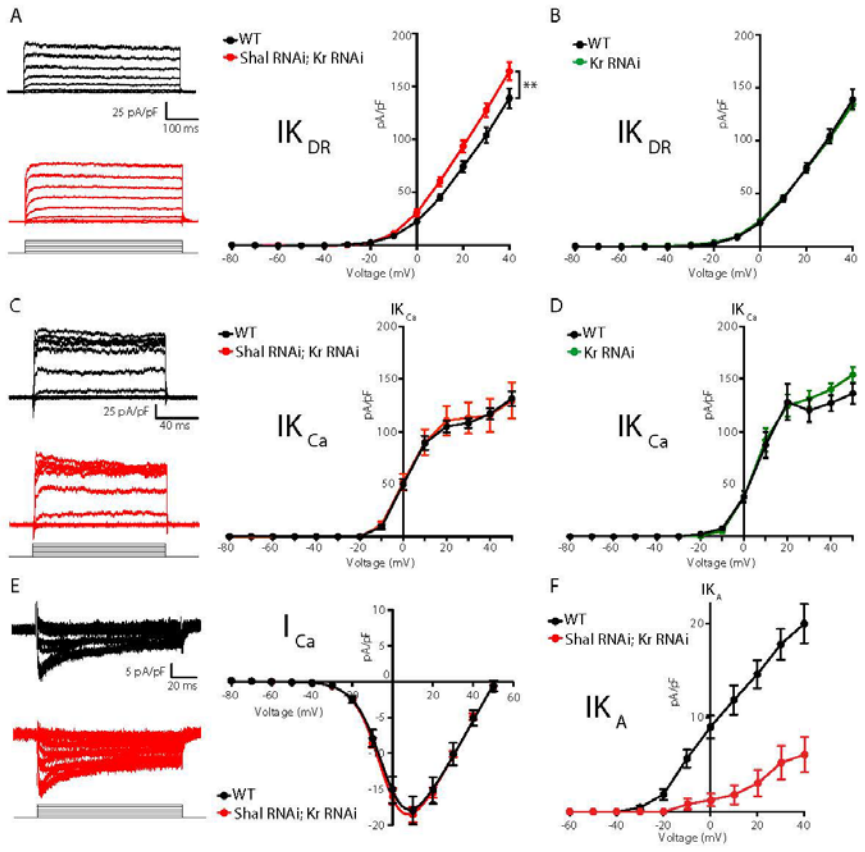

Figure 2. 9: Krüppel Controls IK_{Ca} but not IK_{DR} During Firing Rate Homeostasis.

(A) IK_{DR} I-V plots (right) and representative traces (left) in WT (black, n=7) and *Shal-RNAi; Kr-RNAi* (red, n=19) MN1. (B) I-V plots of WT (black, n = 7) and *Kr-RNAi* (green, n = 14) MN1. (C) IK_{Ca} I-V plots (right) and representative traces (left) in WT (black) and *Shal-RNAi; Kr-RNAi* (red) MN1. (D) I-V plots of WT (black, n = 7) and *Kr-RNAi* (green, n = 9) MN1. (E) I-V plots (right) and representative traces (left) of voltage dependent calcium currents (I_{Ca}) in WT (black; n = 8) and double *Shal-RNAi; Kr-RNAi* (red; n = 6) MN1. (F) I-V plots of MN1 IK_A currents in WT (black, n = 20) and double *Shal-RNAi, Kr-RNAi* (red, n = 10). Mean ± S.E.M.; *p < 0.05; **p < 0.005; ***p < 0.0005; two-way RM-ANOVA with Sidak post-hoc tests. Mean ± S.E.M.; *p < 0.05; **p < 0.005; ***p < 0.0005. N.S., not significant; two-way RMANOVA (I-V plots), one-way ANOVA with Bonferoni post-hoc tests.

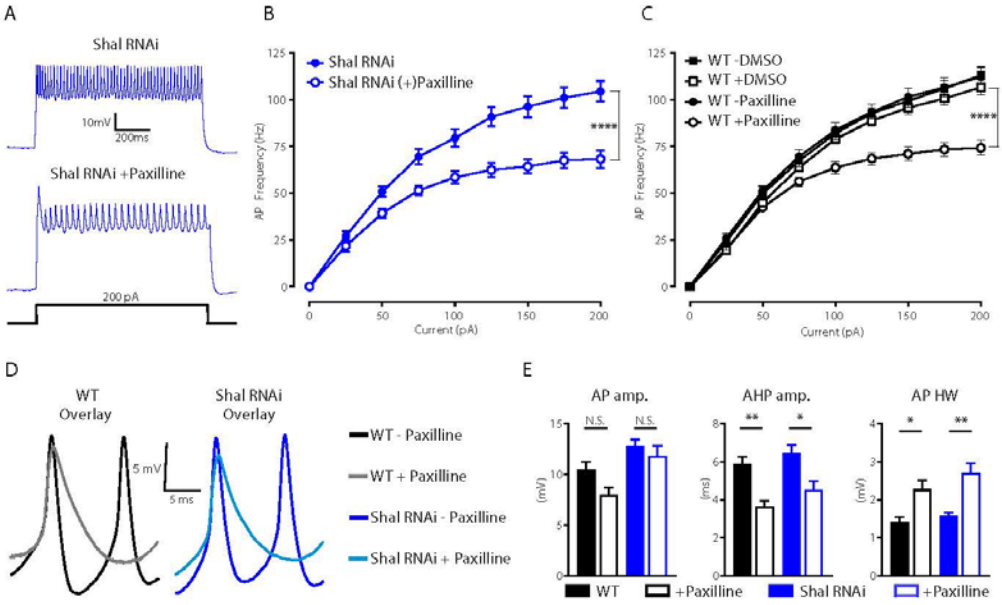

Figure 2. 10: IK_{Ca} is Necessary to Maintaining WT Firing Rates.

(A) Representative voltage traces from *Shal-RNAi* and *Shal-RNAi* + Paxilline at 200pA step current injection. (B) F-I curves of *Shal-RNAi* at baseline (filled circles) and *Shal-RNAi* + Paxilline (open circles), paired recordings, n = 8. (C) F-I curves of WT at baseline (filled circles) and WT + Paxilline (open circles), paired recordings, n = 10; WT at baseline (filled squares) and WT + DMSO (open squares), paired recordings, n = 6. Paxilline was dissolved in DMSO. (D) Example action potential waveforms for WT +/- Paxilline overlayed (black, grey) and *Shal-RNAi* +/- Paxilline overlayed (dark blue, light blue). (E) Action potential waveform quantification. Mean ± S.E.M.; *p ≤ 0.05; **p < 0.01; ***p < 0.0001 ****p ≤ 0.0001. N.S., not significant; two-way RM-ANOVA (F-I curves), one-way ANOVA (AP waveform comparisons) with Tukey post-hoc tests.

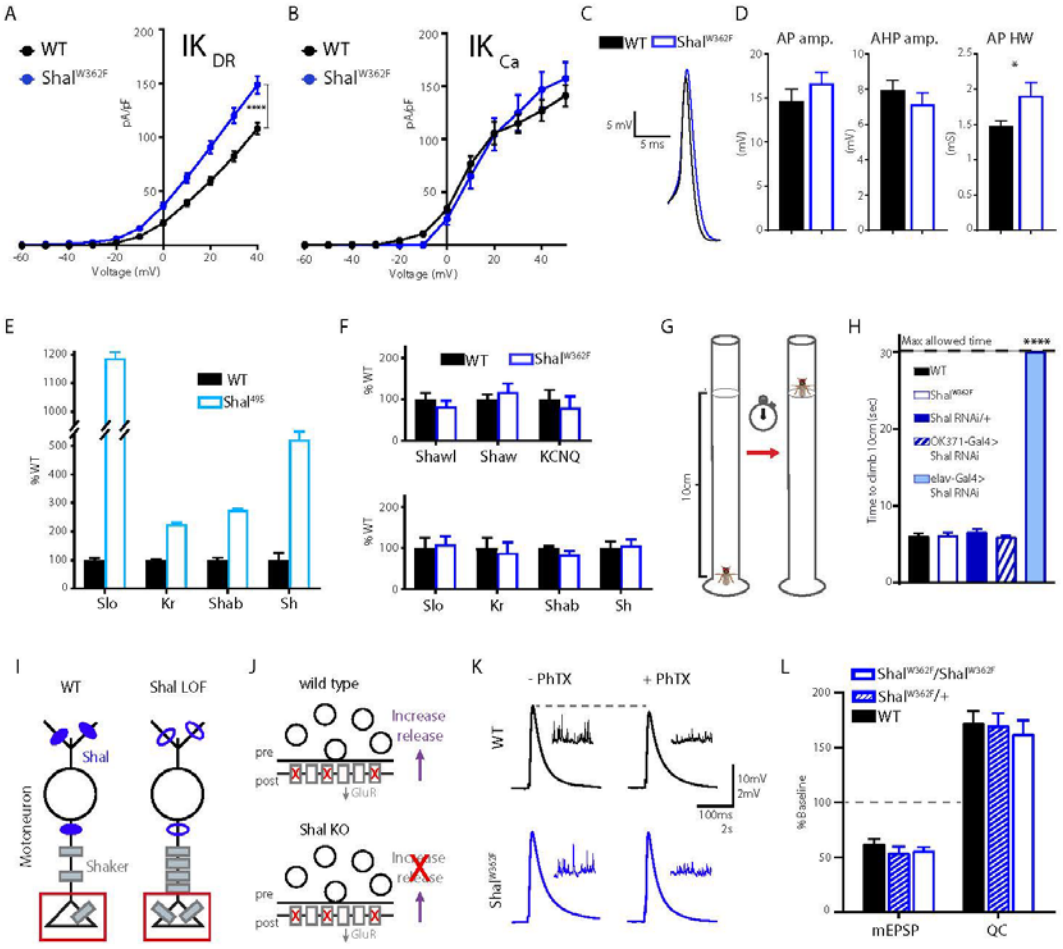

Figure 2. 11: Shal activity block engages distinct homeostatic rebalancing mechanism.

(A) IK_{DR} I-V plots (left) and representative traces (right) in WT (black, n=7) and *Shal*^{W362F} (blue, n=13) motoneurons. **(B)** IK_{Ca} I-V plots (left) and representative traces (right) in WT (black; n = 12) and *Shal*^{W362F} (blue; n=10) motoneurons. **(C)** Example action potential waveforms for WT (black) and *Shal*^{495} (blue) overlaid. **(D)** Action potential waveform quantification. **(E)** Quantitative PCR from WT (black) and *Shal*^{495} (blue) whole third instar larval brains (≥3 biological replicates, each). **(F)** Quantitative PCR from WT (black) and *Shal*^{W362F} (blue) whole third instar larval brains (≥3 biological replicates, each). **(G)** Cartoon representation of negative geotaxis assay. A single animal was placed in a 20 cm tall clean glass tube. The fly was startled by tapping and time to climb to 10 cm high mark was recorded. **(H)** Results of climbing assay. WT n=10, *Shal*^{W362F} n=10, *Shal-RNAi/+* n=10, *Shal-RNAi/OK371* n=10, *elav-Gal4;Shal-RNAi* n=10, *elav-Gal4;Shal-RNAi;Kr-RNAi* n=10. **(I)** Cartoon diagramming how loss of Shal induces compensatory upregulation of Shaker in motoneuron axons and nerve terminals. **(J)** Diagrams illustrating the consequences of ion channel rebalancing on presynaptic homeostatic potentiation (PHP). Top: reduced postsynaptic receptor sensitivity triggers compensatory upregulation of presynaptic neurotransmitter release during PHP. Bottom: Shal knockout animals fail to express PHP. **(K)** Sample traces showing representative EPSP and mEPSP amplitudes in the absence and presence of PhTX for WT (black) and *Shal*^{W362F} (blue). **(L)** Reduction in mEPSP amplitudes and

increase in quantal content (QC) following incubation in PhTX expressed as percent change relative to baseline for each genotype in absence of PhTX. WT baseline n=9, +PhTX n=12; *Shal*^{W362F}/+ baseline n=6, +PhTX n=6; *Shal*^{W362F}/ *Shal*^{W362F} baseline n=9, +PhTX n=10. Mean ± S.E.M.; *p < 0.05; **p < 0.005; ***p < 0.0005, ****p<0.0001. N.S., not significant; two-way RM-ANOVA with Bonferoni post-hoc tests (I-V plots); Student's t test (AP waveform comparisons); one-way ANOVA (climbing assay) with Tukey post-hoc tests.

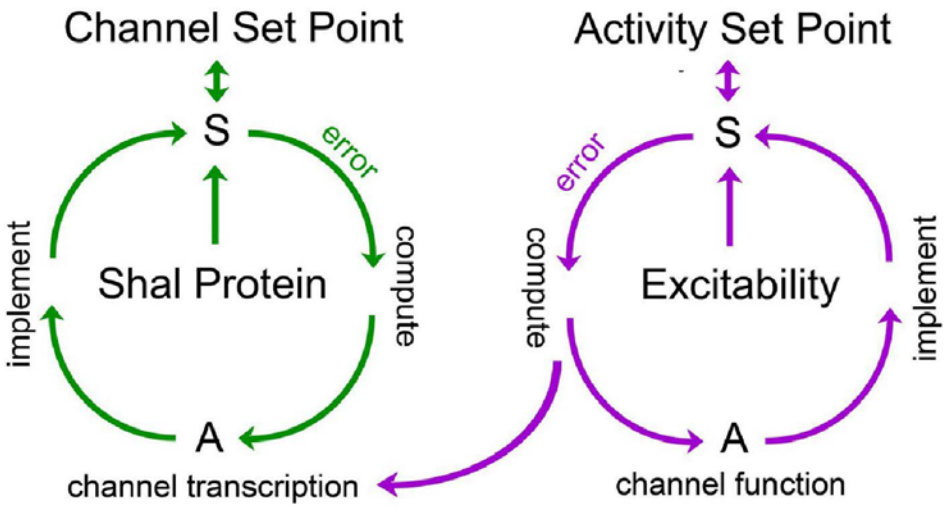

Figure 2. 12: Model for FRH in *Drosophila* motoneurons.

A set point is operationally defined as the level of a variable that is retargeted by a homeostatic signaling system. We propose the existence of a set point for abundance of the Shal protein and a separate set point for neuronal activity. Each set point is connected to a dedicated sensor (S) that monitors either protein levels or neuronal activity. If the sensor detects deviation from the set point, an error signal is produced. The sign and magnitude of the error is computed, over time, and drives changes in actuators (A) that implement negative feedback and restoration of the set point. Actuators in the Shal proteostasis feedback system (green) include the transcription factor Krüppel and downstream transcriptional changes in ion channels that include, but are not be limited to, Shaker and *slo*. Actuators for the activity-dependent homeostat (purple) remain unknown in *Drosophila*, but could include changes in ion channel transcription in other systems. We propose that the activity-dependent homeostat (purple) could be connected to the mechanisms of ion channel homeostasis. In this manner, activity-dependent homeostatic signaling could act primarily on the ion channel proteostatic program. If actuators of the activity-dependent proteostat include changes in ion channel gene expression, then channel proteostasis mechanisms could be secondarlily engaged. This might suggest the existence of repressors that couple channel and activity-dependent homeostatic systems, though there remains no experimental evidence to date.

3. Notch and Nerfin-1: a Molecular Switch for Firing Rate Homeostasis

Introduction

The presumed function of the homeostatic regulation of neuronal activity is to constrain activity within a range that maintains the overall stability of neural circuits. However, neurons can undergo different forms of short and long-term plasticity in response to external and internal stimuli, such as learning-related plasticity and circadian firing rhythms. Current homeostatic theory does not address why these forms of plasticity, which are often associated with changes in activity, do not trigger a homeostatic response. In spite of the ongoing plasticity in the brain, neurons are generally able to maintain their appropriate functions over the lifetime of an organism. Understanding how neurons are endowed with both plasticity and with a homeostatic self-corrective capacity requires an understanding of the homeostatic signaling pathways that specifically respond to deleterious perturbation.

To review, one form of homeostatic plasticity that stabilizes neuronal excitability is Firing Rate Homeostasis (FRH). Loss of the potassium channel Shal triggers a transcriptional rebalancing response that results in the upregulation of a subset of other ion channels, restoring firing rates to wild-type levels. The transcription factor Krüppel is the only known homeostatic controller of firing rates[43,153]. Krüppel, canonically known for its role in embryonic development, is reacativated in the context of the loss of Shal and is specifically required for compensatory BK channel upregulation[43,153]. In the absence of Krüppel, firing rates no longer return to wild-type levels after Shal knockdown[153]. The response of Krüppel is specific to the loss of Shal, not occurring in the background of other channel mutants that are predicted to change neuronal activity[43]. Krüppel is part of a proteostatic signaling system that stabilizes neuronal firing rates, as it is selectively re-activated after elimination of Shal protein and is not re-activated after elimination of Shal activity[153]. This is the first example of a dedicated signaling system that links

loss of an ion channel to homeostatic changes in other channels. The remaining components of this proteostatic signaling system have yet to be discovered.

Here, we present the first evidence that changes in the transcriptional repressor Nerfin-1 (human ortholog INSIM1) and the canonical Notch signaling pathway are necessary for the expression of Firing Rate Homeostasis. After loss of Shal, Nerfin-1 expression is reduced, and overexpression of Nerfin-1 prevents neurons from maintaining normal firing properties. Nerfin-1 is a known repressor of the Notch pathway. In the absence of the Notch pathway components Presenilin, Notch receptor, or Suppressor of Hairless, firing rates no longer return to wild-type levels after Shal loss. We demonstrate that Notch is required for the changes in expression of remaining ion channels following Shal knockdown. These findings are consistent with a model in which loss of Nerfin-1 de-represses Notch signaling in the post-embryonic system, allowing for transcriptional rebalancing of ion channels that compensate for Shal protein loss. While Nerfin-1 and Notch are well-known regulators of neuronal differentiation[76,78,89,91,92], their role in homeostatic plasticity has not previously been reported. We discuss how this signaling system may allow neurons to be resilient to ion channel loss while retaining the capacity to sustain normal changes in activity.

Results

Firing Rate Homeostasis (FRH) following loss of Shal

We have previously established a system in which to study firing rate homeostasis by documenting the response of single, genetically identified motoneurons to loss of an ion channel. In brief, the *GAL4-UAS* system[154] for transgene expression in *Drosophila melanogaster* is used to knock down the expression of the potassium channel Shal with the motoneuron 1 (MN1) driver in third instar larvae (Figure 3.1A). This voltage-gated channel normally serves to

dampen firing rates[153]. Acute pharmacological block of Shal activity causes a hyperexcitable phenotype[153]. However, RNAi-mediated knockdown of Shal results in normal firing properties, in spite of persistent loss of the Shal-mediated A-type potassium current[153] (Figure 3.1B,C; 3.2). The maintenance of normal membrane excitability is due to compensatory alterations in other voltage-gated conductances[153]. We term this phenomenon Firing Rate Homeostasis (FRH).

Nerfin-1 is a candidate FRH regulator

We sought to identify candidate molecular signaling pathways governing FRH. Gene expression profiling through the use of microarray has demonstrated that chronic loss of Shal protein induces a transcriptional response[43]. This work led to the discovery of the first dedicated homeostatic effector molecule, Krüppel, which was the most highly upregulated transcription factor in Shal null mutant motoneurons[43,153]. We used a similar approach to search for additional regulators of FRH. We performed gene expression profiling by using a modified patch-sequencing (patch-seq) protocol[2,3]. In brief, we manually isolated motoneurons using a patch pipette and then performed RNA sequencing to test for expression differences between wild type motoneurons and those in which Shal was knocked down by RNAi (see methods for details). In comparing our patch-seq data set with the previously published microarray results, we found a striking similarity in the transcription factors that had the greatest changes in expression following the loss of Shal (Figure 3.3). In both sets, we noted that the most downregulated transcription factor in Shal-lacking mutant motoneurons was Nerfin-1 (INSIM1)[43]. This result suggested that Nerfin-1 may be involved in the homeostatic response to loss of Shal.

Nerfin-1 drives changes in neuronal firing

We hypothesized that Nerfin-1 may also regulate firing rates, with the prediction that overexpression of Nerfin-1 will block FRH. Consistent with our hypothesis, when we overexpressed Nerfin-1 together with *Shal RNAi* in motoneurons, firing rates were dramatically reduced (Figure 3.4A,B). Overexpression of Nerfin-1 alone was sufficient to drive this change in

firing (Figure 3.4C). These results indicate that the level of Nerfin-1 expression is important for maintenance of normal neuronal firing rates.

The variability in firing rates across neurons is similar between wild type and *Shal RNAi* conditions[153]. However, when homeostatic compensation is disrupted by knockdown of Krüppel together with Shal, variance increases[153]. This observation suggests that loss of Krüppel does not simply cause a neuron to establish a different set point firing rate, in which case a neuron would accurately target the new set point firing rate with low variability across cells. Instead, loss of Krüppel causes a loss of homeostatic control. We hypothesized that overexpression of Nerfin-1, in preventing maintenance of target excitability, also results in greater variability. To test this, we quantified the coefficient of variation for the AP frequency in response to each current step injected across all neurons sampled for each condition (Figure 3.4D-G). Nerfin-1 overexpression resulted in increased variability relative to wild type controls, suggesting that neurons are not able to accurately target a set point firing rate.

We also noted a diversity of phenotypes for the firing patterns of neurons that were not limited to average AP firing rate (Figure 3.4H,I). In some instances, neurons simply fired slower at a constant rate. However, in other cases, fast firing was followed by action potential failures. Failures ranged from one or two APs missing during the entire current step duration to multiple, intermittent instances of firing cessation. In a few cases we observed the complete loss of AP firing following the first action potential. We never observed these “abnormal” phenotypes in wild type neurons, which consistently fired APs at regular intervals, showing little spike frequency adaptation. Thus, not only does Nerfin-1 overexpression cause reduced average firing rates, it also causes a loss of accurate targeting of a set point firing rate and results in a range of phenotypes of varying severity.

Nerfin-1 alters AP trajectory

We have previously demonstrated that the action potential (AP) waveform is homeostatically maintained after loss of Shal[153]. While AP waveforms are indistinguishable between wild type and *Shal RNAi* neurons, knockdown of Krüppel together with Shal causes a significant alteration of the AP waveform. We tested whether Nerfin-1 also contributes to shaping the AP waveform. Nerfin-1 overexpression in motoneurons resulted in a doubling of AP half-width (Figure 3.5A,B). To investigate this further, we performed a phase-plane analysis of action potential trajectory. In phase plane plots, the first time derivative of the membrane potential is plotted against the membrane potential. Nerfin-1 overexpression resulted in a dramatic decrease in maximum instantaneous rate of voltage change over time (Figure 3.5C,D). Additionally, Nerfin-1 drove a reduction in minimum instantaneous rate of voltage change over time, and a depolarizing shift in the AP threshold, peak, and AHP (Figure 3.5C,E,F,G,H). These results suggest that Nerfin-1 overexpression is sufficient to alter ionic conductances contributing to AP firing, potentially interfering with homeostatic mechanisms that maintain the normal AP waveform. Thus, Nerfin-1 may drive changes in ion channel expression, resulting in changes in both action potential waveform and firing rates.

Notch is necessary for FRH

In *Drosophila* CNS, Nerfin-1 maintains neuronal cell fate by promoting the expression of neuronal genes and repressing proliferation and stemness genes, including the Notch pathway[89-91]. Because Nerfin-1 expression is dramatically reduced in Shal mutants (Figure 3.3)[43], we hypothesized the downregulation of Nerfin-1 may act as a 'switch' to permit FRH to occur following loss of Shal by de-repressing Notch. We tested whether Notch plays a role in controlling neuronal firing rates. RNAi-mediated knockdown of Notch had no effect on motoneuron intrinsic excitability, suggesting this signaling system is not involved in setting baseline firing rates (Figure 3.6A,B). However, knocking down Notch together with Shal resulted in significantly slower average firing rates, similar to overexpression of Nerfin-1 (Figure 3.6A,C).

Knocking down Notch using a second RNAi line phenocopied this effect, suggesting the interaction was not due to off-target effects of RNAi (Figure 3.7). Because firing rates following loss of Notch were dysregulated only in the context of Shal knockdown, we inferred that Notch signaling specifically governs the homeostatic stabilization of neuronal intrinsic excitability.

Combined *Notch* and *Shal RNAi* also resulted in increased variability of cell-to-cell firing rates, similarly to the effects of Nerfin overexpression (Figure 3.6D-G). We observed varying degrees of firing rate instability, with phenotypes ranging from regularly spaced action potentials of different frequencies to intermittent action potential failures or profound loss of all firing (Figure 3.6H,I). These results are strikingly similar to the effect of Nerfin overexpression. The abnormal phenotypes were never observed in wild type or *Notch RNAi* alone.

Notch control of AP waveform after Shal loss

We next tested the effect of *Notch RNAi* on action potential waveform. As with firing rates, we observed no effect of Notch knockdown alone on the action potential amplitude, afterhyperpolarization (AHP), or half-width (Figure 3.8A,B). The action potential morphology is similar between wild type and Shal-lacking neurons due to compensatory upregulation of other ionic conductances[153]. However, knocking down Notch together with Shal resulted in action potentials that had a significantly broader half-width (Figure 3.8A,B), similarly to Nerfin-1 overexpression. Thus, Notch knockdown prevented the homeostatic preservation of the action potential waveform after loss of Shal.

Consistent with homeostatic control of the AP waveform, loss of Shal does not have a significant effect on the maximum and minimum instantaneous rate of voltage change over time during the rising and falling phases of the action potential, the action potential peak voltage, or the minimum voltage reached during the AHP (Figure 3.9A-F). The AP threshold is slightly but significantly more hyperpolarized following Shal knockdown. *Notch RNAi* alone did not affect any of these parameters (Figure 3.8C-H). However, knocking down Notch together with Shal

resulted in a large decrease of maximum instantaneous rate of voltage change over time (Figure 3.8D), recapitulating the effect of Nerfin-1 overexpression. These results suggest that loss of Notch in Shal-lacking animals results in altered action potential waveform due to dysregulation of ionic conductances underlying the rising phase of the action potential. Because sodium channels contribute to the rising phase of the action potential, these results also suggest that sodium influx is homeostatically regulated following loss of Shal, and that Notch knockdown interferes with this modulation.

Notch control of passive membrane properties and morphology

Our data is consistent with Notch being a regulator of FRH specifically following loss of Shal. To eliminate alternate possibilities, we performed key controls. First, knocking down Notch alone did not influence the magnitude of the Shal-mediated A-type potassium current (IK_A), nor did knockdown of Notch prevent or change the degree of IK_A reduction following *Shal RNAi* (Figure 3.10). Thus, the difference in firing patterns is not due to altered baseline IK_A or an altered IK_A due to driving multiple RNAi lines.

Second, we examined other electrical properties of neurons. We have previously demonstrated that knockdown of Shal does not cause any major changes to passive electrical properties or neuronal morphology[153]. Here, we found there was no change in the resting membrane potential with *Notch RNAi* alone or with *Shal RNAi* (Figure 3.11A). *Notch RNAi* did not alter input resistance or cell capacitance (Figure 3.11B,C). Combined *Notch* and *Shal RNAi* increased input resistance and reduced cell capacitance (Figure 3.11B,C); however, this observation is not sufficient to explain the firing phenotypes we observed.

We also tested whether there were any changes to neuronal development. Driving knockdown of Shal, Notch, or Notch and Shal together did not prevent neuronal differentiation, expression of MN1, or segmentation and bilateral positioning of the motoneurons. Notch and Shal knockdown together resulted in a slightly reduced somatic volume compared to Notch

alone, consistent with the reduced cell capacitance (Figure 3.12A,B). Together, these results suggest that Notch is necessary for an electrical remodeling of neurons specifically following loss of Shal, and is not generally disrupting neuronal specification, morphology, or passive electrical properties.

Presenilin and Suppressor of Hairless are required for FRH

We hypothesized that the canonical Notch signaling pathway regulates FRH. A prediction is that removal of other key components of the Notch signaling pathway would also interfere with FRH. In the canonical Notch signaling pathway[76], the Notch receptor is membrane-localized. When Notch binds to one of its ligands on the cell surface, the Notch intracellular domain (NICD) is cleaved by the γ-secretase complex, which contains the protease Presenilin. Once cleaved, the NICD travels to the nucleus and heterodimerizes with the DNA-binding transcription factor Suppressor of Hairless (Su(H)), activating gene transcription. We tested the effects of loss of Presenilin and Su(H) on FRH.

RNAi-mediated knockdown of Su(H) alone had minimal impact on motoneuron firing rates (Figure 3.13A,B). In contrast, loss of Su(H) together with *Shal RNAi* substantially reduced AP frequency (Figure 3.13A,C). We also tested a null mutation in *Presenilin* (*Psn*^{143}), which is a deletion and/or splice site mutation within *Psn* resulting in the deletion of amino acids between the first transmembrane domain and the middle of the fourth transmembrane domain (Annette Parks communication to Flybase). Homozygous *Psn*^{143} is lethal at larval stages. While expression of *Psn* is reduced in *Psn*^{143} heterozygotes, there are no associated phenotypes[155]. Heterozygous *Psn*^{143} motoneurons had firing rates close to wild type, but dramatically reduced firing rates in combination with *Shal RNAi* (Figure 3.13D,E,F). Thus, these two components of the Notch signaling pathway phenocopy the reduction in firing rates observed following loss of the Notch receptor and Shal, and the effect of *Nerfin-1* overexpression. It is parsimonious to infer that canonical Notch signaling stabilizes neuronal firing rates.

Notch is required for transcriptional remodeling after Shal loss

We hypothesized that the Notch signaling pathway regulates FRH by controlling transcriptional changes in ion channels. To test this, we performed RNA sequencing on manually isolated motoneurons using patch pipette (patch-seq)[2,3]. Compared to wild-type neurons, cells with Shal knocked down had changes in the expression of many ion channel genes (Figure 3.14). These data were consistent with previous work on transcriptional remodeling in the *Shal*^{495} null mutant background, as assessed by microarray analysis[43]. As previously reported, the expression of numerous ion channels increased after loss of Shal, including *Shab* and *slo*. Notably, the sodium channel gene *para* had the greatest increase in expression in the *Shal RNAi* condition. In contrast, when Shal and Notch were knocked down together, most of the ion channel gene expression differences were eliminated (Figure 3.14). Knockdown of Notch alone did not have profound effects on ion channel gene expression (Figure 3.14). Because of this, when Shal was knocked down in the background of Notch, there were no large changes in ion channel gene expression relative to *Notch RNAi* alone (Figure 3.14). As a result, knockdown of Shal alone had many ion channels that were expressed at levels different from knockdown of Shal and Notch (Figure 3.14). We conclude that knockdown of Notch prevents the transcriptional rebalancing of ion channel genes that normally occurs in response to loss of Shal.

Discussion

A large body of literature catalogues the roles of transcription factors and other genes in establishing neuronal identity during development[156-159]. However, it is virtually unknown how neurons maintain a stable identity and function throughout the lifetime of an animal. Here, we have demonstrated that developmental signaling pathways may be re-engaged by neurons to maintain cell subtype-type specific electrophysiological properties following perturbation. We

have shown that the Notch signaling system is required for stabilization of neuronal firing rates after ion channel disruption. Our data are consistent with a model in which loss of Shal triggers downregulation of Nerfin-1, de-repressing Notch and allowing for Notch signaling to drive conductance rebalancing to restore normal firing rates. We propose the Nerfin-1 and Notch system acts as a molecular switch, changing the cell state in response to perturbation.

Nerfin-1 and Notch have previously been shown to be key players in neuronal differentiation[76,89,91,92]. Nerfin-1 occupies many target genes in developmental signaling and mediators of neuroblast and neuron fate[92]. In particular, Nerfin-1 occupies many Notch pathway genes[92]. In the absence of Nerfin-1, neurons dedifferentiate back to a neuroblast-like fate[89-91]. Nerfin-1 is thought to maintain neuronal cell fate through regulation of the Notch pathway[92]. In the fully differentiated nervous system, Nerfin-1 expression is down-regulated after loss of Shal[43]. Here, we found that over-expression of Nerfin-1 causes dysregulation of firing rates, and that knockdown of Notch prevents homeostatic restoration of normal firing properties following knockdown of Shal. It is tempting to speculate that during FRH, neurons enter into a more plastic, stem cell-like state during which ion channel re-balancing may occur.

How is it is possible for neurons to be capable of various forms of plasticity that alter activity, while also possessing a seemingly contradictory self-correcting capacity that counteracts changes in activity? One possibility is that neurons are equipped with homeostatic signaling systems that are sensitive to specific perturbations, such as the deletion of an ion channel, but do not respond to general changes in activity. It is possible that the transcriptional repressor Nerfin-1 controls such a program, allowing neurons to be dynamic without constantly fluctuating ion channel abundances. In the presence of Nerfin-1, the Notch-dependent homeostatic signaling system is repressed, and normal forms of plasticity can be engaged, allowing for learning and changes in neuronal activity associated with the sleep/wake cycle. However, when a neuron sustains the loss of an ion channel, the neuron enters a state that is

not normal. Nerfin-1 is down-regulated, de-repressing the Notch-dependent homeostatic plasticity program, and allowing for large changes in ion channel gene expression to counteract the loss of Shal.

This work adds to the recent literature highlighting post-developmental functions of Notch. In both mammalian and fly adult nervous systems, Notch signaling has been demonstrated to regulate synaptic plasticity and memory[80,160-168]. Notch signaling has also previously been found to bidirectionally regulate ion channel gene expression. Ectopic activation of Notch signaling can cause differentiation of mammalian chamber cardiac progenitors into specialized conduction-like cells by causing changes in ion channel gene expression[169], and can epigenetically regulate ion channel genes underlying IK_A and IK_{DR} in cardiac myocytes in a cell-type-specific manner[170]. While Notch signaling is typically inactive in the adult myocardium, it is transiently reactivated following cardiac injuries such as myocardial infarction[171-173]. The sufficiency of Notch to drive changes in ion channel gene expression in the mammalian system suggests that its function in FRH may be evolutionarily conserved[169,170]. We speculate that the Notch signaling pathway may be commonly re-engaged in mature electrically excitable cells following pathological insult to drive forms of plasticity involving transcriptional rebalancing of ion channel genes.

We found effects of Nerfin-1 overexpression and dual Notch and Shal knockdown on the AP rising phase, and that knockdown of Notch prevents transcriptional upregulation of the voltage gated sodium channel *para* after loss of Shal. This is evidence that the contribution of sodium current to action potential firing is regulated through homeostatic feedback in response to loss of Shal in a Notch-dependent manner. While we had previously reported no change in persistent sodium current following knockdown of Shal, it is likely that the challenge of space-clamp prevented detection of an increase in sodium influx due to the unusually long neurite of *Drosophila* motoneurons[153]. Prior work has found that *para* expression increases when synaptic

input is blocked and vice-versa when synaptic release is enhanced onto a target neuron in both *Drosophila* and mouse[60,70]. The translational repressor Pumilio regulates expression of *para* and is required for the decrease in *para* under conditions of increased synaptic drive. While the role of Pumilio as a homeostatic signaling molecule has not directly been confirmed by electrophysiological recordings, it is a strong candidate for a modulator of FRH. It is interesting to note the parallel in tuning of sodium as a response to changes in neuronal excitation. Similarly to Notch and Nerfin-1, Pumilio is an important regulator of development, required for establishment of polarity during embryogenesis[174,175]. Together with our data, a theme emerges of canonical embryonic development genes contributing to plasticity of ionic currents in the post-embryonic nervous system.

We find an emerging complexity in homeostatic signaling. We have previously reported that the transcription factor Krüppel is specifically required for the compensatory upregulation of calcium-activated potassium conductance following loss of Shal[153]. Similarly to Notch, Krüppel knockdown together with Shal reduces firing rates, but has no effect on neuronal excitability alone. However, this phenotype is due to a major reduction in the action potential afterhyperpolarization, rather than the main effect being on the action potential rising phase, as we observed in Notch. We had previously proposed that FRH may involve multiple, parallel signaling pathways. These divergent phenotypes provide further evidence of separable signaling components controlling the expression of individual ion channel subtypes. Because neuronal firing properties are emergent from the nonlinear interactions of all of the ionic conductances, 'breaking' only one branch of the homeostat in isolation can result in slower, rather than faster, firing rates, contrary to phenotypic predictions of loss of the activity-dampening Shal in the absence of compensation.

Our work also highlights the challenges of molecularly dissecting ion channel compensation. In the absence of nuclear NICD, Su(H) represses the transcription of target

genes[176,177]. When NICD binds with Su(H), it displaces a co-repressor, de-repressing target gene transcription[178-180]. While we observed a strong interaction between *Su(H)* and *Shal*, *Su(H) RNAi* alone also had a small but significant effect on neuronal firing rates, suggesting that de-repression of genes in the absence of NICD also can contribute to setting neuronal electrical excitability. Similarly, while overexpression of Nerfin-1 together with *Shal RNAi* dysregulates neuronal firing, overexpression of Nerfin-1 alone produces a similar phenotype. Nerfin-1 overexpression phenocopies Notch knockdown with Shal, but with additional effects, suggesting that de-repression of target genes alone is sufficient to impact the ability of neurons to maintain stable firing activity. Furthermore, transcription factors frequently act combinatorially and in a dose-dependent manner. Further work is necessary to fully map the transcription factor regulatory pathways that maintain neuronal excitability set point in the face of variable conditions.

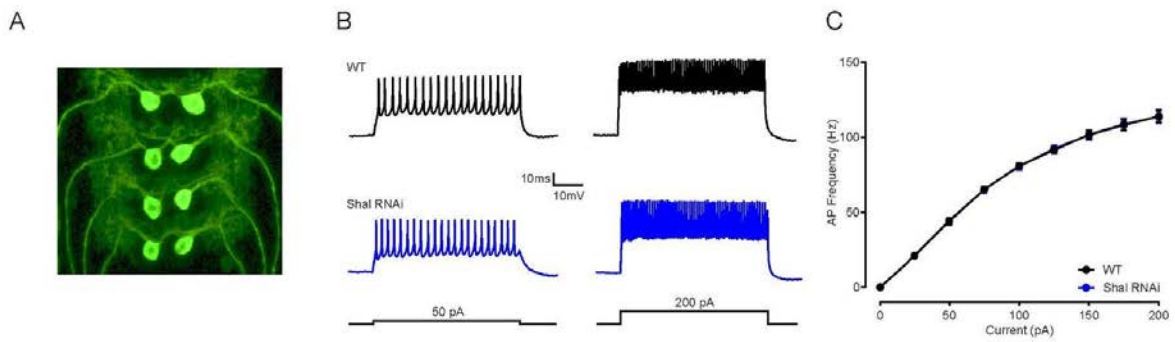

Figure 3. 1: Firing rate homeostasis following loss of Shal

(A) Confocal maximum projection showing GAL4 expression in motoneuron 1 (*MN1-GAL4 > UAS-CD8:GFP*) in ventral nerve cord of *Drosophila* 3rd instar larvae.

(B) Representative voltage traces from WT (black) and *Shal-RNAi* (blue) motoneurons in response to 50 pA (left) and 200 pA (right) current injections.

(C) F-I curves of WT (n = 7) and *Shal-RNAi* (n = 8). Mean ± S.E.M.; p>0.05; two-way RM-ANOVA.

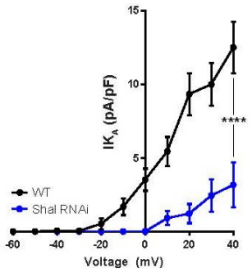

Figure 3. 2: IK_A reduction following Shal knockdown

(A) I-V plots of A-type potassium current in WT (black, n = 17) and *Shal-RNAi* (*MN1-GAL4>Shal-RNAi,* blue, n = 13) motoneurons. Two-way RM-ANOVA with Bonferroni's post-hoc tests, $p<0.0001$. Mean ± S.E.M.

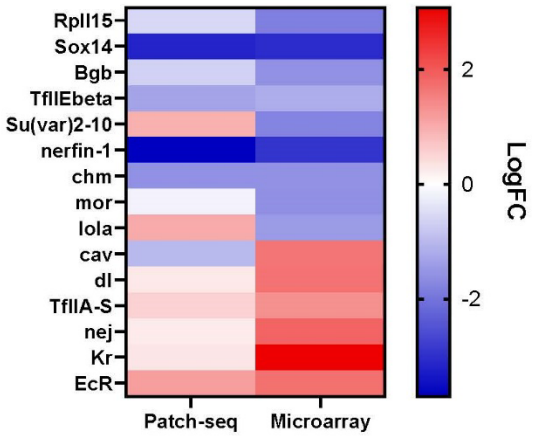

Figure 3. 3: Changes in transcription factor expression following loss of Shal

A comparison of patch-seq (left) and previously published microarray[43] (right) analysis of isolated motoneurons showing differential expression of transcription factors following loss of Shal (vertical axis). In patch-seq experiment, WT and *MN1-GAL4 > Shal-RNAi* motoneurons were manually isolated by patch pipette. In microarray experiment, motoneurons from wild-type and *Shal*^{495} null mutant animals were FACS-isolated[43]. Transcription factors selected for display are subset of the most statistically significant transcription factors differentially regulated in *Shal*^{495} mutant motoneurons based on prior publication[43].

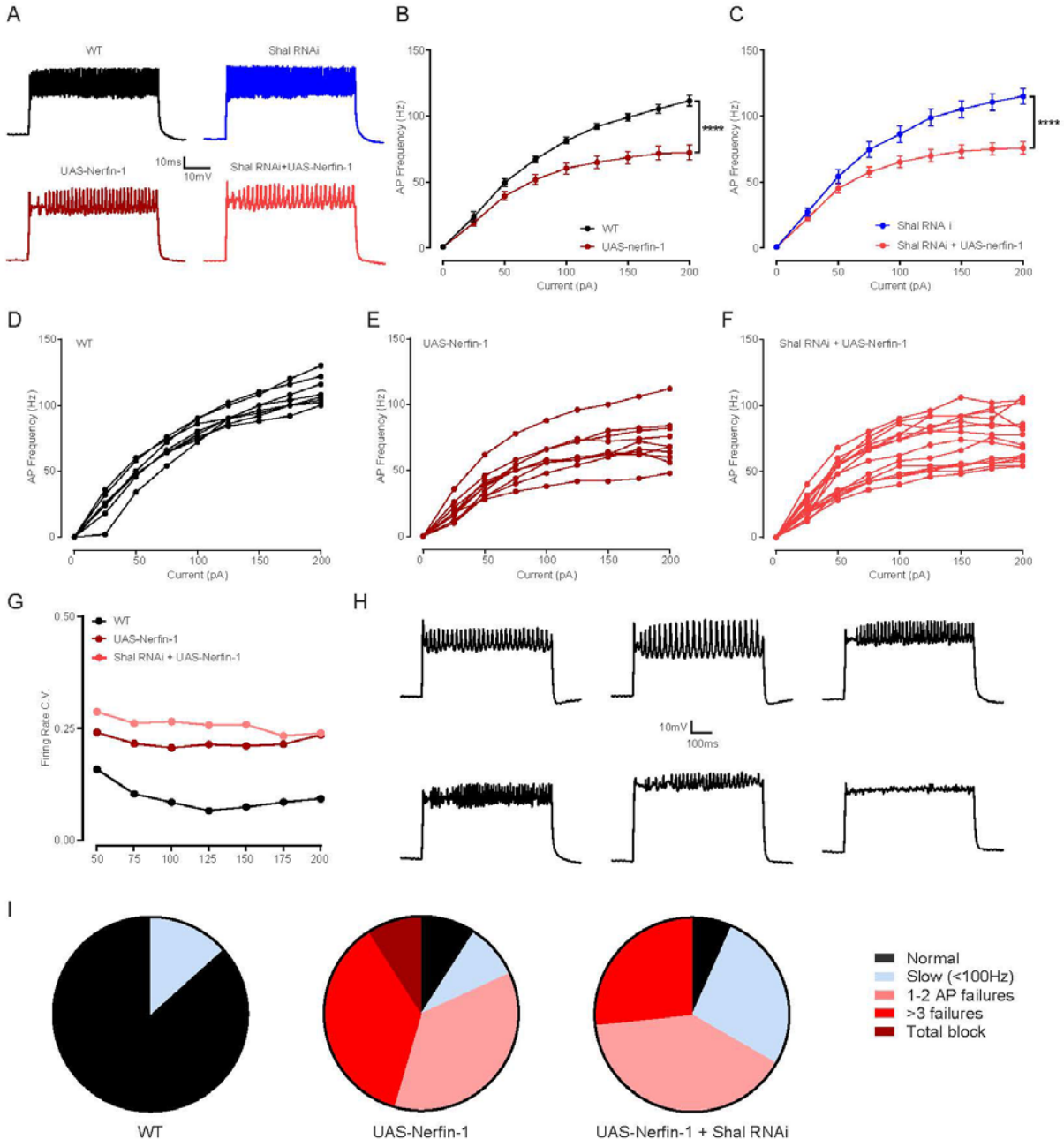

Figure 3. 4: Nerfin-1 is sufficient to drive changes in neuronal firing

(A) Representative voltage traces from WT (black), *Shal-RNAi* (*MN1-GAL4>Shal-RNAi,* blue), Nerfin-1 overexpression (*MN1-GAL4>UAS-Nerfin-1,* dark red), and combined *Shal-RNAi* with Nerfin-1 overexpression (*MN1-GAL4>UAS-Nerfin-1;Shal-RNAi*, bright red) in motoneurons in response to 200 pA current step injection.

(B) F-I curves of WT (n = 8) and Nerfin-1 overexpression (n = 10). Mean ± S.E.M.; p<0.0001 (Two-way RM-ANOVA with Tukey's post-hoc tests).

(C) F-I curves of *Shal-RNAi* (n = 9) and combined *Shal-RNAi* with Nerfin-1 overexpression (n = 15). Mean ± S.E.M.; $p<0.0001$ (Two-way RM-ANOVA with Tukey's post-hoc tests).

(D-F) Individual motoneuron F-I curves for WT (black), Nerfin-1 overexpression (dark red), and combined *Shal-RNAi* with Nerfin-1 overexpression (bright red) groups.

(G) The coefficient of variation for action potential frequency in response to each current injection step across neurons for each condition.

(H) Sample voltage traces from motoneurons overexpressing Nerfin-1 at 200pA current injection.

(I) Proportion of cells exhibiting each firing phenotype from WT (n = 8), Nerfin-1 overexpression (n = 10) and combined *Shal-RNAi* with Nerfin-1 overexpression (n = 15).

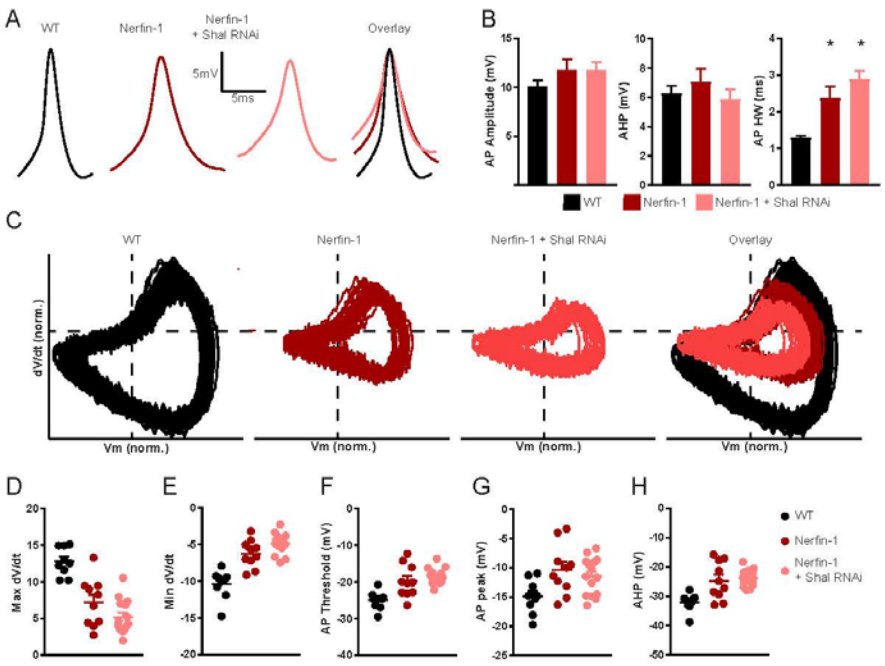

Figure 3. 5: Nerfin-1 is sufficient to drive changes in Action Potential trajectory

(A) Example action potential waveforms for WT (black), Nerfin-1 overexpression (*MN1-GAL4>UAS-Nerfin-1,* dark red), and combined *Shal-RNAi* with Nerfin-1 overexpression (*MN1-GAL4>UAS-Nerfin-1;Shal-RNAi*, bright red) in motoneurons.

(B-D) Quantification of action potential waveform parameters.

(B) Action potential amplitude (One-way ANOVA, $p>0.05$).

(C) Action potential afterhyperpolarization (One-way ANOVA, $p>0.05$).

(D) Action potential half-width (One-way ANOVA with Tukey's post-hoc tests; $p<0.0001$; WT vs. *UAS-Nerfin-1* $p=0.0263$; WT vs. *UAS-Nerfin-1;Shal-RNAi* $p=0.0002$; *UAS-Nerfin-1* vs. *UAS-Nerfin-1;Shal RNAi* $p=0.3932$).

(E) Phase plane plots of normalized example action potential waveforms for each genotype (left three panels) and overlays (far right panel). Each plot contains sequential action potentials from a single representative neuron to illustrate consistency from action potential to action potential.

(F-J) Quantification of AP trajectory parameters.

(F) Maximum instantaneous rate of voltage change over time (One-way ANOVA with Tukey's post-hoc tests; $p<0.0001$; WT vs. *UAS-Nerfin-1* $p=0.0002$; WT vs. *UAS-Nerfin-1;Shal-RNAi* $p<0.0001$; *UAS-Nerfin-1* vs. *UAS-Nerfin-1;Shal-RNAi* $p=0.2313$).

(G) Minimum instantaneous rate of voltage change over time (One-way ANOVA with Tukey's post-hoc tests; p<0.0001; WT vs. *UAS-Nerfin-1* p=0.0003; WT vs. *UAS-Nerfin-1;Shal-RNAi* p<0.0001; *UAS-Nerfin-1* vs. *UAS-Nerfin-1;Shal-RNAi* p=0.3465).

(H) Action potential threshold (One-way ANOVA with Tukey's post-hoc tests; p<0.0001; WT vs. *UAS-Nerfin-1* p=0.0052; WT vs. *UAS-Nerfin-1;Shal-RNAi* p=0.0001; *UAS-Nerfin-1* vs. *UAS-Nerfin-1;Shal-RNAi* p=0.7518).

(I) Action potential peak voltage (One-way ANOVA with Tukey's post-hoc tests; p=0.0073; WT vs. *UAS-Nerfin-1* p=0.0227; WT vs. *UAS-Nerfin-1;Shal-RNAi* p=0.0735; *UAS-Nerfin-1* vs. *UAS-Nerfin-1;Shal-RNAi* p=0.872).

(J) After-hyperpolarization voltage (One-way ANOVA with Tukey's post-hoc tests; p<0.0001; WT vs. *UAS-Nerfin-1* p=0.0049; WT vs. *UAS-Nerfin-1;Shal-RNAi* p=0.0005; *UAS-Nerfin-1* vs. *UAS-Nerfin-1;Shal-RNAi* p=0.9694).

WT (n = 9); Nerfin-1 overexpression (n = 10); *Shal-RNAi* and Nerfin-1 overexpression (n = 15). Graphs show mean ± S.E.M.; *p<0.05.

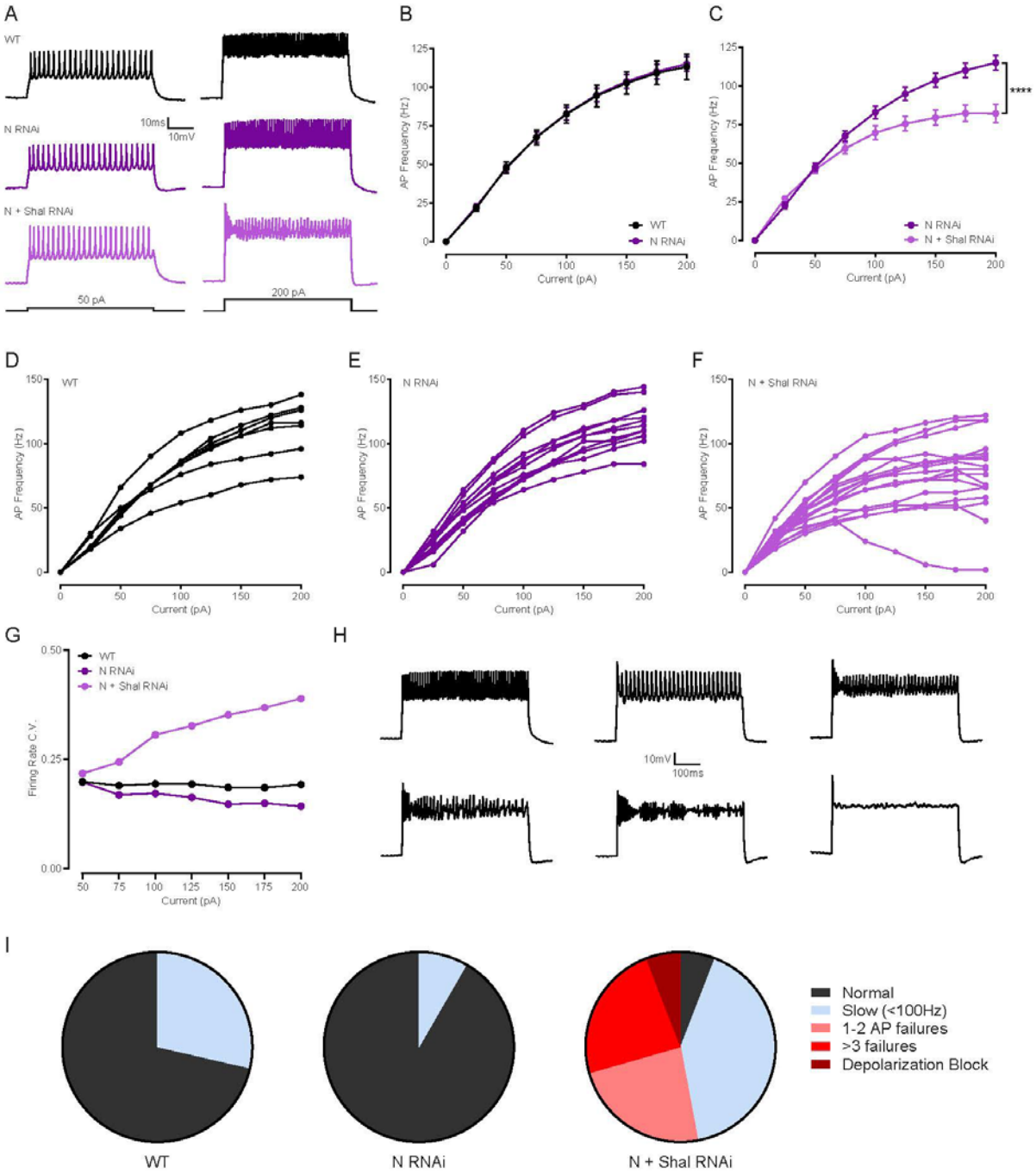

Figure 3. 6: Notch is required for firing rate homeostasis following loss of Shal

(A) Representative voltage traces from WT (black), *Notch-RNAi* (*MN1-GAL4>N-RNAi,* dark purple), and combined *Shal-RNAi* with *Notch-RNAi* (*MN1-GAL4>Shal-RNAi;N-RNAi*, light purple) in motoneurons in response to 50 pA (left) and 200 pA (right) current injections.

(B) F-I curves of WT (n = 7) and *Notch-RNAi* (n = 12). Mean ± S.E.M. p>0.05 (Two-way RM-ANOVA with Tukey's post-hoc tests).

(C) F-I curves of *Notch-RNAi* (n = 12) and combined *Shal-RNAi* with *Notch-RNAi* (n = 17). Mean ± S.E.M.; $p<0.0001$ (Two-way RM-ANOVA with Tukey's post-hoc tests).

(D-F) Individual motoneuron F-I curves for WT (black), *Notch-RNAi* (dark purple), and combined *Shal-RNAi* with *Notch-RNAi* (light purple) groups.

(G) The coefficient of variation for action potential frequency in response to each current injection step across neurons for each condition.

(H) Sample voltage traces from motoneurons expressing dual *Shal-RNAi* and *Notch-RNAi* at 200pA current injection.

(I) Proportion of cells exhibiting each firing phenotype from WT (n = 7), *Notch-RNAi* (n = 12) and combined *Shal-RNAi* with *Notch-RNAi* (n = 17).

Notch RNAi line used in these experiments is JF01053.

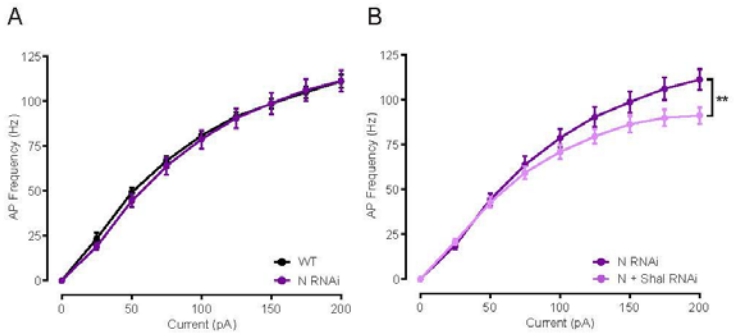

Figure 3. 7: Dysregulation of firing rates following loss of Notch shown with additional RNAi line.

(A) F-I curves of WT (n = 8) and *Notch-RNAi* (n = 11). Two-way RM-ANOVA, $p>0.05$.

(B) F-I curves of WT (n = 11) and *Shal-RNAi;Notch-RNAi* (n = 11). Mean ± S.E.M.; Two-way RM-ANOVA with Sidak's post-hoc tests, $p<0.05$.

Notch RNAi line used in these experiments is JF01043.

Graphs show mean ± S.E.M.

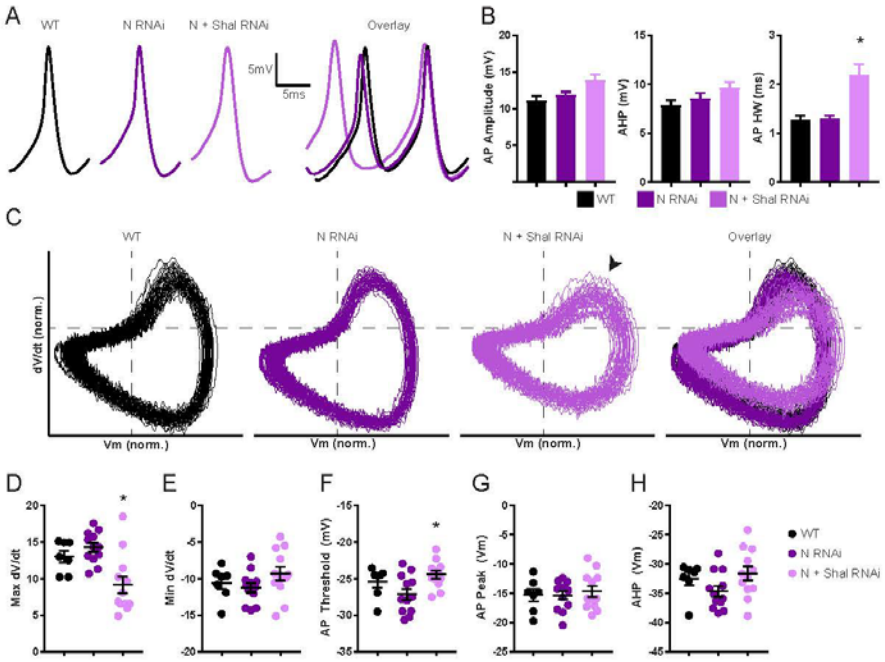

Figure 3. 8: Notch is required to preserve Action Potential trajectory following loss of Shal

(A) Example action potential waveforms for WT (black), *Notch-RNAi* (*MN1-GAL4>N-RNAi,* dark purple), and combined *Shal-RNAi* with *Notch-RNAi* (*MN1-GAL4>Shal-RNAi;N-RNAi*, light purple) in motoneurons.

(B-D) Quantification of action potential waveform parameters.

(B) Action potential amplitude (One-way ANOVA, p=0.0279; WT vs. *Notch-RNAi* p=0.7923; WT vs. *Shal-RNAi;Notch-RNAi* p=0.0470; *Notch-RNAi* vs. *Shal-RNAi;Notch-RNAi* p=0.0986).

(C) Action potential afterhyperpolarization (One-way ANOVA, p=0.1035).

(D) Action potential half-width (One-way ANOVA with Tukey's post-hoc tests; p=0.0012; WT vs. *Notch-RNAi* p=0.9947; WT vs. *Shal-RNAi;Notch-RNAi* p=0.0107; *Notch-RNAi* vs. *Shal-RNAi;Notch-RNAi* p=0.0031).

(E) Phase plane plots of normalized example action potential waveforms for each genotype (left three panels) and overlays (far right panel). Each plot contains sequential action potentials from a single representative neuron to illustrate consistency from action potential to action potential. Arrow indicates impaired action potential rise in *Shal-RNAi;Notch-RNAi* .

(F-J) Quantification of AP trajectory parameters.

(F) Maximum instantaneous rate of voltage change over time (One-way ANOVA with Tukey's post-hoc tests; p=0.0009; WT vs. *Notch-RNAi* p=0.6584; WT vs. *Shal-RNAi;Notch-RNAi* p=0.0325; *Notch-RNAi* vs. *Shal-RNAi;Notch-RNAi* p=0.0008).

(G) Minimum instantaneous rate of voltage change over time (One-way ANOVA p=0.2232).

(H) Action potential threshold (One-way ANOVA with Tukey's post-hoc tests; p=0.0200; WT vs. *Notch-RNAi* p=0.2482; WT vs. *Shal-RNAi;Notch-RNAi* p=0.6308; *Notch-RNAi* vs. *Shal-RNAi;Notch-RNAi* p=0.0158).

(I) Action potential peak voltage (One-way ANOVA p=0.8261).

(J) After-hyperpolarization voltage (One-way ANOVA p=0.1200).

WT (n = 7), *Notch-RNAi* (n = 12) and combined *Shal-RNAi* with *Notch-RNAi* (n = 17). Notch RNAi line used in these experiments is JF01053. Graphs show mean ± S.E.M.; *p<0.05.

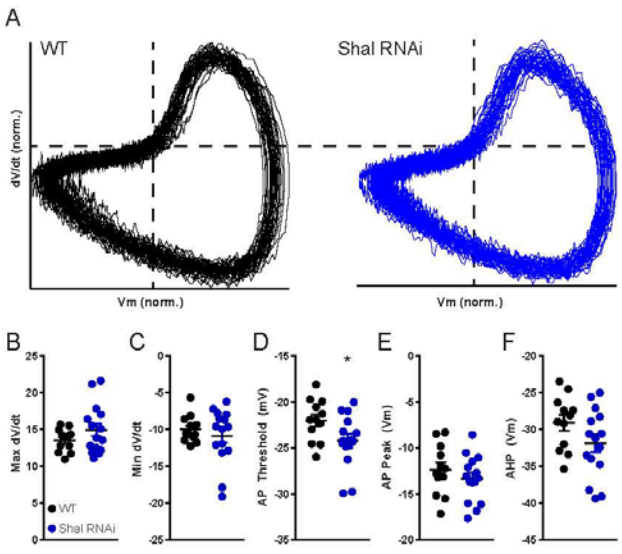

Figure 3. 9: Restoration of AP trajectory following chronic Shal loss

(A) Phase plane plots of normalized example action potential waveforms from WT (black), *Shal-RNAi* (*MN1-GAL4>Shal-RNAi,* blue) motoneurons. Each plot contains sequential action potentials from a single representative neuron to illustrate consistency from action potential to action potential.

(B-F) Quantification of AP trajectory parameters.

(B) Maximum instantaneous rate of voltage change over time (unpaired t-test, p = 0.1939).

(C) Minimum instantaneous rate of voltage change over time (unpaired t-test, p = 0.4692).

(D) Action potential threshold (unpaired t-test, p = 0.0376).

(E) Action potential maximal voltage (unpaired t test, 0.3420).

(F) Action potential afterhyperpolarization minimum voltage (unpaired t test, p = 0.0979).

WT (n = 12) and *Shal-RNAi* (n = 15). Mean ± S.E.M. for all bar graphs. *p<0.05.

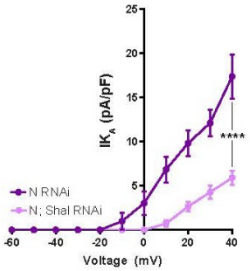

Figure 3. 10: IK_A in *Notch RNAi* background

(A) I-V plots of A-type potassium current in *Notch-RNAi* (*MN1-GAL4>N-RNAi,* dark purple, n = 9) and combined *Notch=RNAi* with *Shal-RNAi* (*MN1-GAL4>N-RNAi;Shal-RNAi,* light purple, n = 15) motoneurons. Two-way RM-ANOVA with Bonferroni's post-hoc tests, $p<0.0001$. Mean ± S.E.M. *$p<0.05$.

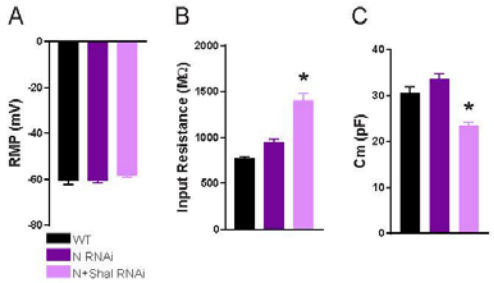

Figure 3. 11: Passive electrical properties following Notch knockdown

(A) Resting membrane potential in WT, Notch knockdown (*MN1-GAL4>N-RNAi*), and dual Notch and Shal knockdown (*MN1-GAL4>N-RNAi;Shal-RNAi*) motoneurons (One-way ANOVA; $p = 0.2538$).

(B) Input resistance of motoneurons (One-way ANOVA with Tukey's post-hoc tests; $p<0.0001$; WT vs. *Notch-RNAi* $p = 0.2655$; WT vs. *Shal-RNAi;Notch-RNAi* $p<0.0001$; *Notch-RNAi* vs. *Shal-RNAi;Notch-RNAi* $p<0.0001$).

(C) Cell capacitance of motoneurons (One-way ANOVA with Tukey's post-hoc tests; $p<0.0001$; WT vs. *Notch-RNAi* $p = 0.1986$; WT vs. *Shal-RNAi;Notch-RNAi* $p<0.0006$; *Notch-RNAi* vs. *Shal-RNAi;Notch-RNAi* $p<0.0001$).

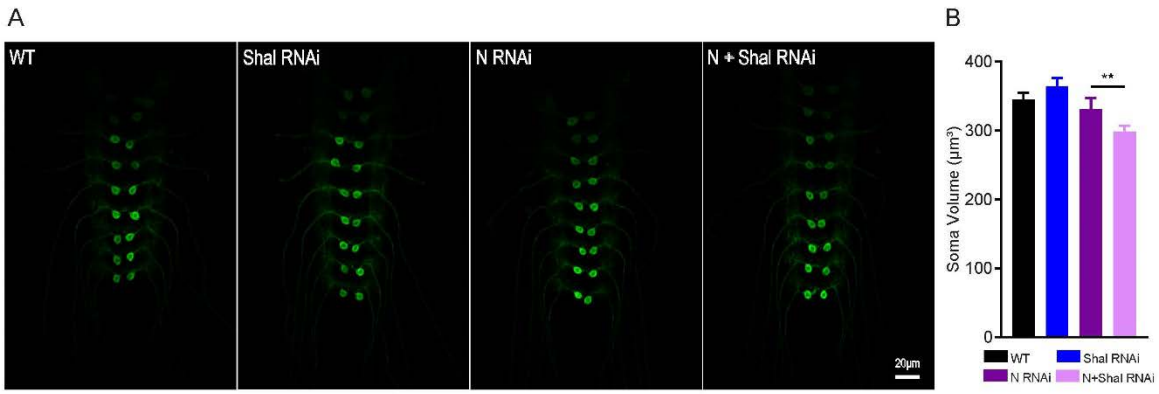

Figure 3. 12: Notch loss does not prevent neuron differentiation and normal morphological development.

(A) Confocal maximum projections of MN1-Ib motoneurons (*MN1-GAL4 > UAS-CD8:GFP*) in wild-type, *Shal RNAi*, *Notch RNAi*, and combined *Shal RNAi* with *Notch RNAi* (*Shal RNAi;N-RNAi)*.

(B) Quantification of soma volume. (One-way ANOVA with Tukey's post-hoc tests; p = 0.0046; WT vs. *Shal-RNAi* p = 0.6795; WT vs. *Notch-RNAi* p = 0.8660; WT vs. *Shal-RNAi;Notch-RNAi* p = 0.0563; *Notch-RNAi* vs. *Shal-RNAi* p = 0.2407; *Shal-RNAi* vs. *Shal-RNAi;Notch-RNAi* p = 0.0027; *Notch-RNAi* vs. *Shal-RNAi;Notch-RNAi* p = 0.2605). Notch RNAi line used in these experiments is JF01053. Graph shows mean ± S.E.M.

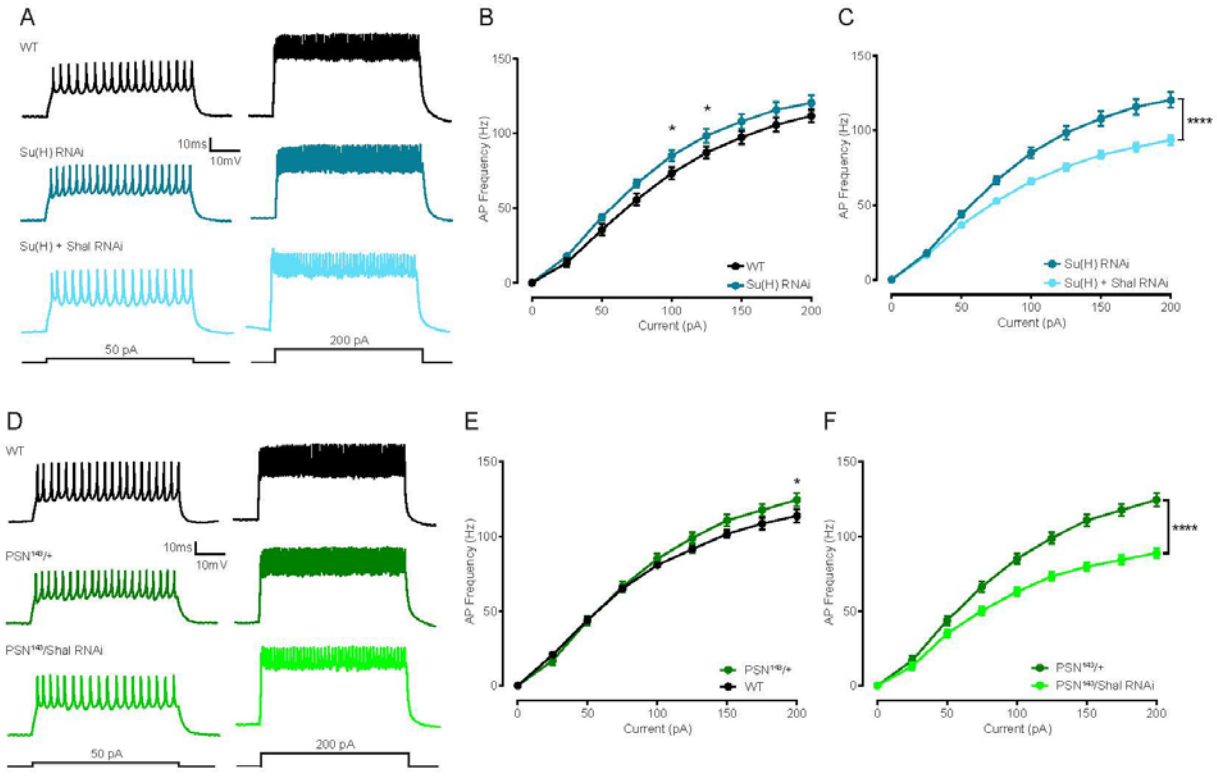

Figure 3. 13: Su(H) and Psn are required for firing rate homeostasis following loss of Shal

(A) Representative voltage traces from WT (black), *Su(H)-RNAi* (*MN1-GAL4>Su(H)-RNAi,* blue), and combined *Shal-RNAi* with *Su(H)-RNAi* (*MN1-GAL4>Shal-RNAi;Su(H)-RNAi*, light blue) in motoneurons in response to 50 pA (left) and 200 pA (right) current injections.

(B) F-I curves of WT (n = 8) and *Su(H)-RNAi* (n = 14). Mean ± S.E.M. p>0.05 (Two-way RM-ANOVA with Tukey's post-hoc tests; p<0.05; for 100 pA current step p=0.0292; for 125 pA current step p=0.0438; p>0.05 at all other steps).

(C) F-I curves of *Su(H)-RNAi* (n = 14) and combined *Shal-RNAi* with *Su(H)-RNAi* (n = 18). Mean ± S.E.M.; p<0.0001 (Two-way RM-ANOVA with Tukey's post-hoc tests).

(D) Representative voltage traces from WT (black), Psn^{143}/+ (dark green), and *Shal-RNAi* in Psn^{143}/+ background (*MN1-GAL4>Shal-RNAi;* Psn^{143}/+, light green) in motoneurons in response to 50 pA (left) and 200 pA (right) current injections.

(E) F-I curves of WT (n = 7) and Psn^{143}/+ (n = 12). Mean ± S.E.M. p>0.05 (Two-way RM-ANOVA with Tukey's post-hoc tests; p<0.05; for 200 pA current step p=0.0468; p>0.05 at all other steps).

(F) F-I curves of *psn*^{143}/+ (n = 12) and *Shal-RNAi* in *Psn*^{143}/+ background (n = 11). Mean ± S.E.M.; p<0.0001 (Two-way RM-ANOVA with Tukey's post-hoc tests).

Graphs show mean ± S.E.M.; *p<0.05; **p<0.005; ***p<0.0005, ****p<0.0001, N.S.=not significant.

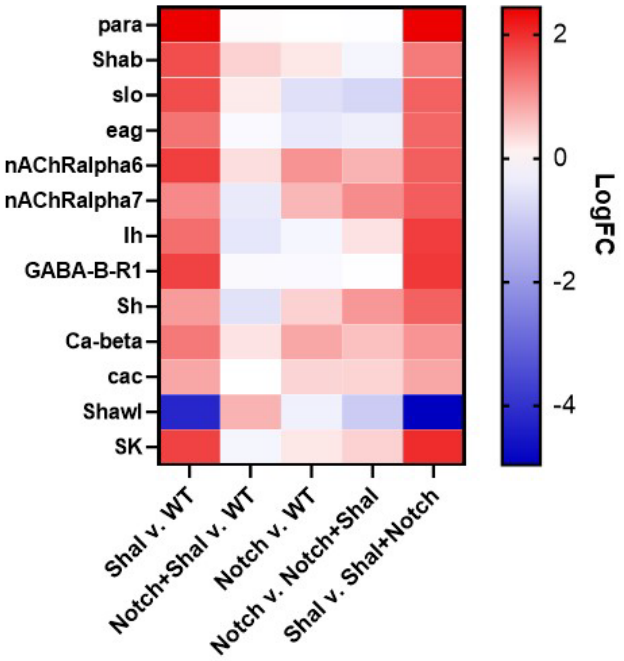

Figure 3. 14: Notch is required for transcriptional remodeling following loss of Shal

Patch-seq analysis of isolated motoneurons showing differential expression of selected ion channel genes (vertical axis). *MN1-GAL4* was used to drive knockdown of Shal, Notch, or both Notch and Shal. From left to right, conditions compared are: *Shal-RNAi* vs. WT, *Shal-RNAi;Notch-RNAi* vs. WT, *Notch-RNAi* vs. WT, *Notch-RNAi* vs. *Shal-RNAi;Notch-RNAi ,* and *Shal-RNAi* vs. *Shal-RNAi;Notch-RNAi,* Notch RNAi line used in these experiments is JF01053.

4. Conclusions

We have demonstrated that FRH can be induced and fully expressed in single neurons. Because individual *Drosophila* motoneurons lack direct proprioceptive feedback in the way that occurs in the mammalian peripheral nervous system, we can conclude that FRH is induced and expressed without a major perturbation to the surrounding neural circuit. We then documented a stereotyped FRH expression mechanism that is specific to the nature of the disruption. A corrective response can be triggered by molecularly distinct disruptions of a single ion channel gene, Shal, restoring firing rates to wild-type levels. When the Shal protein is eliminated, a subset of other ion channels are transcriptionally upregulated, partially through the transcription factor Krüppel. When the Shal conductance is blocked, a different set of conductances increases without a change in ion channel transcripts. This indicates that there are perturbation-specific effects downstream of a single ion channel gene. These different 'solutions' have different effects on the ability of neurons to undergo further plasticity and on animal behavior. Finally, we found evidence for a dedicated homeostatic signaling system within the postembryonic nervous system. The Notch signaling pathway is reactivated post-development and is required for the stabilization of firing rates following loss of Shal. We propose a new model for the homeostatic control of intrinsic excitability that can fully account for our current observations, as well as observations of activity-dependent and activity-independent FRH in other model organisms.

Specificity of pathways

Krüppel is, perhaps, the only published example of a molecular effector specifically modulating homeostatic ion channel compensation. The mRNA-binding factor Pumilio has been described as a regulator of neuronal intrinsic excitability[60,70,139]. Like Pumilio, Krüppel expression changes during a chronic perturbation[42]. However, unlike Pumilio, Krüppel does not set baseline levels of ionic currents or affect intrinsic excitability in the absence of a homeostatic challenge. Krüppel selectively controls the compensatory upregulation of the calcium-activated potassium

current following loss of Shal. The loss of Krüppel causes dysregulation of firing rates only in the background of Shal knockdown, and is not upregulated in the background of the pore-blocked Shal mutant or mutations in other ion channel genes. Likewise, the Notch pathway responds to loss of Shal and specifically causes dysregulation of firing rates after loss of Shal. Notch signaling is not responsible for the upregulation of the calcium-activated potassium current, serving a different role in FRH than Krüppel. These findings demonstrate that there are discoverable molecular components of the homeostatic signaling systems dedicated to the maintenance of stable firing rates. In theory, it should be possible to identify all of the signaling pathways that operate in parallel during FRH by using expression profiling and combinatorial knockdown of channels and signaling factors, as described here.

Distinct protein and activity-sensitive systems

This work challenges the notion that FRH occurs solely through calcium signaling. While the manipulations to Shal were functionally identical, neurons lacking the ion channel protein enacted transcriptional upregulation of one subset of channels, while neurons with the pore-blocked ion channel compensated through non-transcriptional modification of a different conductance. It follows that neurons are equipped with separable proteostatic and activity-sensitive homeostatic signaling systems, each of which enacts a stereotyped but different compensatory response.

It is likely that numerous proteostatic and activity-dependent signaling systems co-exist, involving factors similar to Kr and Notch. If each ion channel is linked to a dedicated proteostatic signaling system and an activity-sensing system that involve different molecular effectors, a network of homeostatic “solutions” based on the combination of channel-specific responses may exist. Mapping these pathways could shed light on the source of the variability in ion channel expression across neurons with similar firing rates from non-isogenic animal populations[109].

Stochasticity versus stereotyped channel expression

The crab stomatogastric nervous system is arguably the only wild model organism that is routinely used to study the robustness of cell-type specific neuronal activity. Prior experimental studies in this system have found that identified neurons in different animals can achieve identical firing patterns using different underlying ionic current densities. This variability of conductances has often been interpreted as evidence that neurons have an activity set point, which they maintain through stochastic sampling of ion channels to express. Our new data speaks to these studies.

While it remains true that many combinations of conductances can be used by neurons to achieve target firing patterns, we propose that the solution space is defined by a large set of 'rules' or discrete biochemical signaling pathways. The aforementioned crabs are harvested from the ocean, and thus are of unknown genetic composition and unknown life history. These animals likely encounter and compensate for a variety of perturbations prior to their capture and study, including exposure to channel-blocking pollutants, temperature fluctuations, and aging. The many combinations of conductances observed in neurons of wild-caught animals could reflect distinct 'solutions' to specific perturbations. Therefore, it is not certain that the differences among cells in the stomatogastric ganglion represent different solutions to a single type of perturbation. Our data suggest single solutions to single perturbations.

Evolutionary conservation of FRH mechanisms

Channel compensation for disrupted homologs of Shal has been documented in the worm[41], fly[42,43], crab[29,38], and rodent[39,40]. Similarly to our results, the Shal homolog Kv4.2 null mouse cortical pyramidal neurons perfectly restore firing rates through the upregulation of delayed rectifier current densities[40], and the Shaker homolog Kv1.4 is upregulated in Kv4.2 null mouse ventricular myocytes[39]. These similarities suggest that there may be evolutionary conservation of mechanism for FRH, underscoring the value of *Drosophila* as a gene-discovery system for dissecting the molecular pathways underlying FRH in higher organisms.

Future challenges

The many levels of regulation through which FRH can operate highlight the challenge of researching its mechanisms. Changes in ion channel gene expression in response to perturbation are well-documented to occur at the transcriptional level[42,43,153,181]. Regulation of intrinsic excitability has also been shown to involve post-transcriptional mechanisms[38], translational control[60,70], and post-translational modification such as phosphorylation[34,59]. Compensation can even occur through changes in ion channel localization[46].

Two recent studies compellingly demonstrated that nonsense-mediated decay triggers transcriptional upregulation of sequence-similar genes to compensate following a genetic mutation[182,183]. The extent to which this may contribute to conductance rebalancing following mutations in ion channel genes and how this response may intersect with activity-sensitive components of the homeostatic system has not yet been tested.

Activity sensors other than calcium-binding proteins have also not been explored, though it is theoretically possible that channel function could be monitored by sensors for other species of ions. For example, E. coli has a potassium binding protein that is induced in response to osmotic stress[184]. This protein acts as a sensor of cytoplasmic potassium concentration, and is required for normal growth at a range of elevated potassium concentrations. It is possible that animals have evolved a similar potassium sensor to monitor potassium channel activity. There is also evidence that changes in intracellular sodium levels due to Nav1.7 deletion trigger changes in gene expression in mouse neurons[185]. Perhaps sodium can act as a second messenger in homeostatic signaling systems.

There are many additional possibilities for how FRH could be enacted. Potassium channels genes from Antarctic and tropical octopus undergo mRNA editing to change gating kinetics, proposed to be a mechanism of temperature adaptation[186]. Whether mRNA editing is also engaged to modify channel function in a homeostatic context has yet to be investigated.

Studies demonstrating post-transcriptional control have stopped short of determining whether the channel compensation occurs through increased translation or increased insertion of ion channels into the neuronal membrane from an intracellular store, or if co-regulation of different ionic conductances involves co-translation or co-assembly of the proteins prior to insertion into the membrane[38]. An additional untested hypothesis is that altered rates of ion channel degradation rather than insertion could account for changes in ionic current density following a homeostatic challenge.

Homeostasis and human health

Discovering mechanisms of homeostatic control of neuronal excitability is pressing, as dysregulation of electrical activity is a hallmark of many human brain disorders such as epilepsy. Epilepsy is the fourth most common neurological disorder. It is estimated that one out of 26 individuals will develop epilepsy in their lifetime[187]. However, approximately 30% of individuals are refractory to therapeutic treatment[188]. Epileptiform activity is also a co-morbidity associated with Alzheimer's Disease and Autism Spectrum Disorder[189,190]. Approximately 10-22% of Alzheimer's disease patients have at least one unprovoked seizure[191]. In individuals affected by Autism, up to 30% have associated epilepsy as part of their clinical diagnosis[192]. Mutations in potassium channel genes also underlie neurological disorders such as spinocerebellar ataxias, in which altered neural activity is likely a contributor to disease pathophysiology[193,194]. Altered neural circuit activity has routinely been hypothesized to be causally related to additional disorders including schizophrenia, anxiety, and depression. How does the human nervous system respond to ion channel mutations and activity perturbations, and how might homeostatic mechanisms participate in disease?

Paralleling the studies on variability of combinatorial ion channel gene expression across animals, there is evidence of large variation in channel genes across humans. An exome sequencing study of 237 ion channel genes in humans compared variant profiles of unaffected individuals to those with the most common neuronal excitability disorder, sporadic idiopathic

epilepsy[112]. Rather than finding a clear genetic predictor of epilepsy, this study uncovered tremendous variation in ion channel genes in both cases and controls. No individuals were completely free of small nucleotide polymorphisms (SNPs), and no two ion channel sequence profiles (channotypes) among the sampled individuals were identical. Most surprisingly, this study found Mendelian disease gene SNP variants in both cases and controls, with the majority of SNPs shared between both groups. Two thirds of controls harbored a missense mutation in at least one known familial human epilepsy gene. Most strikingly, one individual in the control population was found to have an SCN1A mutation that is thought to cause severe myoclonic epilepsy of infancy[195,196].

This study is foundational for several reasons. First, if each person's channotype is unique, human neurons must be using different combinations of conductances to achieve appropriate firing properties, rather than following a single 'wild-type' prescription. Second, since variants of both suspected epilepsy genes and known Mendelian disease genes can be found in healthy individuals, ion channel compensation must occur in the human brain. Third, the variable penetrance of channelopathy-associated alleles suggests there are differences in the resilience of individuals to disease-causing mutations. This effect has been observed for other conditions in a larger-scale sequencing study, in which adults with mutations for severe Mendelian genetic childhood disorders showed no clinical manifestation of the diseases[197].

What might explain the differences in resilience of humans to ion channel gene mutations conferring disease risk? One possibility is that there are limits to the extent of homeostatic compensation. Klassen et al. 2011 found that individuals with epilepsy usually have more than one mutation in known human epilepsy genes. Perhaps neurons can compensate following the disruption of one, but not two key ionic conductances. However, this does not explain the remaining overlap between cases and controls. It is also possible that there is a limit to the degree to which certain species of ion channels can be compensated for, as evidenced by incomplete restoration of firing properties after channel compensation[46]. There is some cell-

type specificity to compensation, and compensation may be suboptimal in some neuronal subtypes[46]. A third possibility is that the variability observed may be due to variation in the genetic background of individuals, “buffering” the effects of deleterious mutations. This could include both protective genetic variants that enhance the compensatory capacity of the system, as well as deleterious mutations in components of homeostatic signaling pathways that prevent the neurons from appropriately re-balancing ionic conductances. If the latter is true, it suggests a new approach to medicine could be taken.

Most epilepsy drugs target voltage-gated sodium channels or the GABAergic system, though with off-target effects, and precise mechanisms of action not well understood. While new pharmacological treatments have made progress in reducing side effects, the efficacy has not improved over time, with responder rates maintaining at approximately 40%. We propose that by studying resilient individuals and understanding genetic mechanisms of compensation, we can uncover new therapeutic targets. By using how nature has already “solved” the problem of conductance disruption in the past, we could tune the knobs of the ion channel homeostat in vulnerable individuals. Perhaps the future of medicine lies in personalizing channel disease treatments using an integrated approach of genomic profiles of mutated channel genes and assessment of homeostatic compensatory pathways.

5. Methods

Fly Stocks and Genetics

In all experiments, the w1118 strain was used as the wild-type control. All fly stocks were maintained at 22-25°C and experimental fly crosses were raised at 25°C. w1118, *UASmCD8:GFP, OK371-GAL4, elav-GAL4, Slo*^{1}, *Shal*^{495}, *Notch RNAi* (JF01053 and JF01043), *Su(H) RNAi* (HM05110), *Psn*^{143} fly stocks were obtained from Bloomington Drosophila Stock Center. The *Shal-RNAi* line (*KK100264*) was from the Vienna Drosophila RNAi Center (VDRC)

and the *Kr-RNAi* line (JF02630) were from the Transgenic RNAi Project (TRiP) at Harvard Medical School. Motor neuron 1-specific RNAi gene knockdown was achieved by crossing the appropriate *UAS-RNAi* lines with a previously-reported *MN1-Ib-GAL4* driver line[113], a gift from Yuh-Nung Jan. The *UAS-Nerfin-1* line was a gift from the Chris Doe lab.The *Shal*^{W362F} mutant was engineered using the 'scarless' CRISPR-Cas9 gene editing method[118,198], substituting phenylalanine for tryptophan at amino acid 362 at the endogenous *Shal* locus.

Whole Cell Patch Clamp Electrophysiology

Whole-cell recordings were obtained from MN1-GFP motor neurons (*MN1-Ib-GAL4, UASmCD8:GFP*) in third-instar larvae. Larvae were prepared for electrophyiological recordings using standard larval fillet preps on a sylgard-coated recording chamber. External recording solution was perfused at 2-3 mL/min and contained (in mM): 135 NaCl, 5 KCl, 4 MgCl2, 5 HEPES, 1.5 CaCl2, pH 7.1, 295 mOsm. The glial sheath surrounding the ventral nerve cord was gently dissolved by local pipette application of 2% protease (Type XIV, *Streptomyces griseus*, Sigma) and the preparation was perfused with recording solution for 10 min to wash away residual protease. 1-naphthylacetyl spermine trihydrochloride (NASP, 25 µM, Sigma) was washed on to the preparation to prevent muscle contraction during the recording. Whole-cell recordings were obtained using standard thick-walled borosilicate glass electrodes (4-6 MΩ, King Precision Glass) filled with appropriate internal solution for each experiment (see below). Whole cell patch clamp recordings were obtained with an Axon 700B (current clamp) or Axon 200B (voltage clamp) amplifiers (Molecular Devices), digitized at 20 kHz with a Digidata 1440A and recorded using Clampex 10.3. Recordings with series resistance greater than 15 MΩ and/or resting membrane potential more depolarized than -55mV and/or input resistance less than 400MΩ were discarded and excluded from analysis. All recordings were made at room temperature (20-22°C). All salts or other reagents used for electrophysiology were obtained from Sigma, unless noted otherwise.

Current clamp recordings

Whole cell patch clamp recordings were made using an intracellular solution containing (in mM): 140 Kmethanesulfonate, 5 KCl, 10 HEPES, 5 NaCl, 5 EGTA, 2 MgATP and 0.2 NaGTP, pH 7.35, 280-290 mOsm. Constant current was injected into cells to adjust Vm to between -50 and -55 mV. Cells requiring more than ±15 pA to set Vm were discarded from analysis. MN1 excitability was assessed by 500 ms square pulse current injections (-50 - +200 pA, 25 pA/step). Frequency vs current (F-I) plots were constructed by calculating the firing rate for each current step and plotting verses current step amplitude. Input resistance was determined from negative current steps. Action potential amplitude was calculated as the difference from action potential threshold to peak. Phase plane analyses were conducted by plotting the first time derivative of the membrane potential and determining values for maximum dV/dt, minimum dV/dt, and Vm values at which dV/dt = 0 (corresponding to the action potential peak and the minimum voltage reached during the action potential afterhyperpolarization).

Voltage clamp recordings

General: All recorded currents were normalized to whole-cell capacitance, and current-voltage (I-V) plots were constructed by plotting measured current amplitudes verses respective voltage steps. The junction potential was measured for each internal solution and corrected in final I-V plots. Leak currents were subtracted offline.

Voltage Dependent Potassium Currents (IK): IK currents were recorded with the same internal solution used for current clamp recordings. Tetrodotoxin (TTX, 1 µM), CdCl2 (300 µM) were added to the external solution to block voltage-activated sodium and calcium channels, respectively. Cells were held at −70 mV after obtaining stable whole-cell configuration, and series resistance and capacitance were compensated (>85% predict./corr., 10 µS lag). A-type potassium currents (IK_A) were isolated by current subtraction following a two-phase voltage step

protocol: 1) voltage steps from -90 to +40 mV (10 mV/step, 500 ms duration, 0.1 Hz inter-step interval), followed by 2) a 250 ms voltage pre-pulse to -30 mV to inactivate A-type potassium channels, followed by voltage steps from -90 to +40 mV (10 mV/step, 500 ms duration, 0.1 Hz inter-step interval). Delayed rectifier potassium currents (IK_{DR}) were measured with a 250 ms voltage pre-pulse to -30 mV to inactivate A-type potassium channels, followed by a voltage step protocol from -90 to +50 mV (10 mV/step, 500 ms duration, 0.1 Hz inter-step interval).

Calcium-dependent Potassium Currents (IK_{Ca}): IK_{Ca} currents were recorded with the same internal solution used for current clamp recordings. Tetrodotoxin (1 µM) was added to the external solution to block voltage-activated sodium channels. K_{Ca} currents were isolated by subtraction of the current traces recorded with a voltage step protocol from -90 to +50 mV (10 mV/step, 100 ms duration, 0.1 Hz inter-step interval) before and after CdCl2 (300 µM) application.

Calcium Currents (I_{Ca}): External recording solutions were optimized for I_{Ca} recordings, and contained (in mM): 100 NaCl, 5 KCl, 4 MgCl2, 30 tetraethylamonium chloride (TEA-Cl), 2 4aminopyridine (4-AP), 5 HEPES, 1.5 CaCl2, 1.5 BaCl2, 0.001 TTX; pH7.1, 295 mOsm. The intracellular solution contained (in mM): 125 Cs-methanesulfonate, 10 TEA-Cl, 5 4-AP, 10 HEPES, 4 NaCl, 5 EGTA, 2 MgATP, 0.2 MgGTP; pH 7.35, 285 mOsm. I_{Ca} currents were recorded using a pre-pulse to -90 mV (1 s) followed by voltage steps from −90 to +50 mV (10 mV/step, 120 ms duration, 0.1 Hz inter-step interval). Ca2+ (1.5 mM, CaCl2) and Ba2+ (1.5 mM, BaCl2) were used as charge carriers to enhance macroscopic currents.

Persistent Sodium Currents (I_{NaP}): I_{NaP} was measured according to previously described protocols (Lin et. al., 2009; Mee et. al., 2004). The external recording solution, optimized for I_{Na} recordings, contained (in mM): 100 NaCl, 5 KCl, 50 TEA-Cl, 10 4-AP, 10 HEPES, 10 glucose, 0.5 CaCl2, 0.3 CdCl2 and 0.001 TTX; pH 7.1, 295 mOsm. The intracellular solution contained (in mM): 125 Cs-methanesulfonate, 10 TEA-Cl, 5 4-AP, 10 HEPES, 4 NaCl, 5 EGTA, 2 MgATP, 0.2 MgGTP; pH 7.35, 285 mOsm. I_{NaP} currents were isolated with a pre-pulse voltage step

protocol containing a conditioning step to +50 mV (50 ms) to inactivate fast transient I_{Na} current spikes, followed by voltage steps from -70 to +50 mV (5 mV/step, 50 ms duration, 0.1 Hz inter-step interval) I_{NaP}. Persistent sodium currents were measured as the steady-state current at the end of each voltage step.

Muscle Recordings

Sharp electrode recordings were made from muscle six in abdominal segments two and three in third instar wandering larvae with an Axoclamp 900A amplifier (Molecular Devices), as described previously (Frank et al., 2006; Muller et al., 2012). Recordings were collected in HL3 saline containing (in mM): NaCl (70), KCl (5), MgCl2 (10), NaHCO3 (10), sucrose (115), trehalose (5), HEPES (5), and CaCl2 (0.3). Philanthotoxin-433 (PhTX; Sigma-Aldrich) was prepared as a stock solution (4mM in DMSO) and diluted in HL3 saline to 16.6 µM. Semi-intact preparations with the CNS fat, and gut left intact were incubated in PhTX for ten minutes (Frank et al., 2006). Following the incubation, the larval preparations were rinsed and the dissection was completed as previously described (Davis et al., 1998). The motoneuron cut axon was stimulated as previously described (Davis et al., 1998). Cells depolarized more than -60mV were excluded from analysis. Quantal content was calculated by dividing mean EPSP by mean mEPSP.

Data Analysis

Data were analyzed using custom procedures written in Igor Pro (Wavemetrics) and MiniAnalysis 6.0.0.7 (Synaptosoft). Statistical analysis was performed in Prism ($\alpha = 0.05$) and statistical tests used for each data set are indicated in figure legends.

Quantitative RT-PCR

Primer probes for real-time PCR detection of *Kr*, *slo*, *Shab*, *Shaker*, *KCNQ*, *Shaw*, *Shawl*, and Ribosomal protein L32 (RpL32) were designed and developed by Applied Biosystems. RNA

was isolated from the CNS of ≥15 third instar larvae per genotype (5 brains for each of at least 3 biological replicates) using RNeasy Plus Micro Kit (Qiagen). A DNase digestion was performed to remove potential DNA contamination (TURBO DNA-free, Ambion). RNA was reverse-transcribed into cDNA (SuperScript III First-Strand synthesis system, Invitrogen). A no reverse transcriptase (RT) control was included for each sample. Purified cDNA was used as a template in PCR reaction with three 10µl technical replicates for each condition (TaqMan Fast Universal PCR Master Mix, no AmpErase UNG, Applied Biosystems). Additionally, a 10µl no RT reaction was included for each sample. The Applied Biosystems 7900HT Fast Real-Time PCR System was used for all PCRs. Cycle Threshold (CT) was determined by automated threshold analysis using SDS2.4 software (Applied Biosystems, Foster City, CA). Relative gene expression levels between WT and mutant animals was determined using the ΔΔCT method. In brief, ΔCT values for experimental animals were subtracted from WT ΔCT values to obtain the ΔΔCT. Using the equation 2^(-ΔΔCT)x100, the percent expression of each gene in the experimental condition relative to the control condition was calculated. Each experimental sample was compared to each wild type sample.

Patch-seq

Individual motoneurons were visualized by driving the expression of membrane-bound GFP (*MN1-Ib-GAL4, UASmCD8:GFP*) in third-instar larvae. To obtain the cytoplasmic content of the cell, whole-cell tight-seal patch-clamp was used. Whole-cell configuration was established with leak currents less than 100pA. The cytoplasmic content of the cell was gently sucked by applying negative pressure to the patch-pipette. The individual motoneuron was then pulled from the tissue while visually confirming the GFP fluorescent signal at the tip of the pipette. Immediately after, the pipette tip was immersed in a test tube containing the Cell Lysis Buffer and RNAse inhibitor medium and the pipette tip was broken by gently touching the tube wall.

The content of the pipette tip was ejected by applying positive pressure. Each reaction contained 4-8 pooled motoneurons.

The Low Input RNA: cDNA Synthesis, Amplification and Library Generation kit from NEB (New England Biolabs Inc.) was used to isolate, reverse-transcribe the RNA and prepare the libraries for sequencing. Following the reverse transcription and template switching, the cDNA was amplified by PCR. Amplified cDNA was cleaned up by using SPRI beads. The quality and quantity of the amplified cDNA were assessed by Bioanalyzer (Agilent Technologies Inc.). After fragmentation and adaptor ligation, adaptor-ligated DNA was enriched with i7 primer and universal primer by PCR-amplification. Amplified libraries were quality checked by Bioanalyzer with High Sensitivity DNA chips (Agilent Technologies Inc.) and the quantity was measured by Qubit fluorometer (ThermoFisher Scientific). Barcoded libraries were sequenced using an Illumina HiSeq 4000 at 100bp paired-end reads in the CAT genomic facility at UCSF.

Raw reads were first processed with flexbar version 3.5.0 (https://github.com/seqan/flexbar) to remove adapters specific to the NEBNext library prep, using parameters as described in https://github.com/nebiolabs/nebnext-single-cell-rna-seq. The reads were then processed with HTStream v.1.1.0 (https://ibest.github.io/HTStream/) to perform data QA/QC, remove Illumina adapter contamination, PCR duplicates, and low-quality bases/sequences.

The trimmed reads were aligned to the *Drosophila melonogaster* genome v.BDGP6.22 (http://ensembl.org/Drosophila_melanogaster/Info/Annotation) with annotation release version 98 using the aligner STAR v. 2.7.0e[199] to generate raw counts per gene. On average, 93.7% of the trimmed reads aligned to the *Drosophila* genome, and 80% of the trimmed reads uniquely aligned to an annotated *Drosophila* gene.

Differential expression analyses were conducted using limma-voom in R (limma version 3.40.6, edgeR version 3.26.7, R 3.6.1). Prior to analysis, genes with fewer than 5 counts per million reads in all samples were filtered, leaving 8598 genes.

Negative Geotaxis Assay

All animals were raised at 25C. Animals were collected within 24 hours of eclosion and singly housed. On day 4 of life, animals were transferred to a glass cylinder with a marking 10 cm from the bottom. Animals were tapped to the bottom of the cylinder and the time to climb to the 10 cm marking was recorded. Three trials were performed for each animal and these times were averaged.

6. References

1 Hernath, F., Schlett, K. & Szucs, A. Alternative classifications of neurons based on physiological properties and synaptic responses, a computational study. *Sci Rep* **9**, 13096, doi:10.1038/s41598-019-49197-8 (2019).

2 Fuzik, J. *et al.* Integration of electrophysiological recordings with single-cell RNA-seq data identifies neuronal subtypes. *Nat Biotechnol* **34**, 175-183, doi:10.1038/nbt.3443 (2016).

3 Cadwell, C. R. *et al.* Electrophysiological, transcriptomic and morphologic profiling of single neurons using Patch-seq. *Nat Biotechnol* **34**, 199-203, doi:10.1038/nbt.3445 (2016).

4 Connors, B. W. & Gutnick, M. J. Intrinsic firing patterns of diverse neocortical neurons. *Trends Neurosci* **13**, 99-104, doi:10.1016/0166-2236(90)90185-d (1990).

5 Tripathy, S. J., Burton, S. D., Geramita, M., Gerkin, R. C. & Urban, N. N. Brain-wide analysis of electrophysiological diversity yields novel categorization of mammalian neuron types. *J Neurophysiol* **113**, 3474-3489, doi:10.1152/jn.00237.2015 (2015).

6 Markram, H. *et al.* Interneurons of the neocortical inhibitory system. *Nat Rev Neurosci* **5**, 793-807, doi:10.1038/nrn1519 (2004).

7 Halabisky, B., Shen, F., Huguenard, J. R. & Prince, D. A. Electrophysiological classification of somatostatin-positive interneurons in mouse sensorimotor cortex. *J Neurophysiol* **96**, 834-845, doi:10.1152/jn.01079.2005 (2006).

8 Jasnow, A. M., Ressler, K. J., Hammack, S. E., Chhatwal, J. P. & Rainnie, D. G. Distinct subtypes of cholecystokinin (CCK)-containing interneurons of the basolateral amygdala identified using a CCK promoter-specific lentivirus. *J Neurophysiol* **101**, 1494-1506, doi:10.1152/jn.91149.2008 (2009).

9 Karagiannis, A. *et al.* Classification of NPY-expressing neocortical interneurons. *J Neurosci* **29**, 3642-3659, doi:10.1523/JNEUROSCI.0058-09.2009 (2009).

10 Sills, J. B., Connors, B. W. & Burwell, R. D. Electrophysiological and morphological properties of neurons in layer 5 of the rat postrhinal cortex. *Hippocampus* **22**, 1912-1922, doi:10.1002/hipo.22026 (2012).

11 Choi, J. C., Park, D. & Griffith, L. C. Electrophysiological and morphological characterization of identified motor neurons in the Drosophila third instar larva central nervous system. *J Neurophysiol* **91**, 2353-2365, doi:10.1152/jn.01115.2003 (2004).

12 Bean, B. P. The action potential in mammalian central neurons. *Nat Rev Neurosci* **8**, 451-465, doi:10.1038/nrn2148 (2007).

13 Jan, L. Y. & Jan, Y. N. Voltage-sensitive ion channels. *Cell* **56**, 13-25, doi:10.1016/0092-8674(89)90979-3 (1989).

14 Bezanilla, F. Ion channels: from conductance to structure. *Neuron* **60**, 456-468, doi:10.1016/j.neuron.2008.10.035 (2008).

15 Hodgkin, A. L. & Huxley, A. F. A quantitative description of membrane current and its application to conduction and excitation in nerve. *J Physiol* **117**, 500-544, doi:10.1113/jphysiol.1952.sp004764 (1952).

16 Papazian, D. M., Schwarz, T. L., Tempel, B. L., Jan, Y. N. & Jan, L. Y. Cloning of genomic and complementary DNA from Shaker, a putative potassium channel gene from Drosophila. *Science* **237**, 749-753, doi:10.1126/science.2441470 (1987).

17 Tempel, B. L., Papazian, D. M., Schwarz, T. L., Jan, Y. N. & Jan, L. Y. Sequence of a probable potassium channel component encoded at Shaker locus of Drosophila. *Science* **237**, 770-775, doi:10.1126/science.2441471 (1987).

18 Taylor, A. L., Goaillard, J. M. & Marder, E. How multiple conductances determine electrophysiological properties in a multicompartment model. *J Neurosci* **29**, 5573-5586, doi:10.1523/JNEUROSCI.4438-08.2009 (2009).

19 Zheng, Y. *et al.* Deep Sequencing of Somatosensory Neurons Reveals Molecular Determinants of Intrinsic Physiological Properties. *Neuron* **103**, 598-616 e597, doi:10.1016/j.neuron.2019.05.039 (2019).

20 Foster, W. R., Ungar, L. H. & Schwaber, J. S. Significance of conductances in Hodgkin-Huxley models. *J Neurophysiol* **70**, 2502-2518, doi:10.1152/jn.1993.70.6.2502 (1993).

21 Bhalla, U. S. & Bower, J. M. Exploring parameter space in detailed single neuron models: simulations of the mitral and granule cells of the olfactory bulb. *J Neurophysiol* **69**, 1948-1965, doi:10.1152/jn.1993.69.6.1948 (1993).

22 Goldman, M. S., Golowasch, J., Marder, E. & Abbott, L. F. Global structure, robustness, and modulation of neuronal models. *J Neurosci* **21**, 5229-5238 (2001).

23 Prinz, A. A., Billimoria, C. P. & Marder, E. Alternative to hand-tuning conductance-based models: construction and analysis of databases of model neurons. *J Neurophysiol* **90**, 3998-4015, doi:10.1152/jn.00641.2003 (2003).

24 Olypher, A. V. & Calabrese, R. L. Using constraints on neuronal activity to reveal compensatory changes in neuronal parameters. *J Neurophysiol* **98**, 3749-3758, doi:10.1152/jn.00842.2007 (2007).

25 Sobie, E. A. Parameter sensitivity analysis in electrophysiological models using multivariable regression. *Biophys J* **96**, 1264-1274, doi:10.1016/j.bpj.2008.10.056 (2009).

26 Schulz, D. J., Goaillard, J. M. & Marder, E. Variable channel expression in identified single and electrically coupled neurons in different animals. *Nat Neurosci* **9**, 356-362, doi:10.1038/nn1639 (2006).

27 Schulz, D. J., Goaillard, J. M. & Marder, E. E. Quantitative expression profiling of identified neurons reveals cell-specific constraints on highly variable levels of gene expression. *Proc Natl Acad Sci U S A* **104**, 13187-13191, doi:10.1073/pnas.0705827104 (2007).

28 Golowasch, J., Goldman, M. S., Abbott, L. F. & Marder, E. Failure of averaging in the construction of a conductance-based neuron model. *J Neurophysiol* **87**, 1129-1131, doi:10.1152/jn.00412.2001 (2002).

29 MacLean, J. N. *et al.* Activity-independent coregulation of IA and Ih in rhythmically active neurons. *J Neurophysiol* **94**, 3601-3617, doi:10.1152/jn.00281.2005 (2005).

30 Swensen, A. M. & Bean, B. P. Robustness of burst firing in dissociated purkinje neurons with acute or long-term reductions in sodium conductance. *J Neurosci* **25**, 3509-3520, doi:10.1523/JNEUROSCI.3929-04.2005 (2005).

31 Khorkova, O. & Golowasch, J. Neuromodulators, not activity, control coordinated expression of ionic currents. *J Neurosci* **27**, 8709-8718, doi:10.1523/JNEUROSCI.1274-07.2007 (2007).

32 Temporal, S. *et al.* Neuromodulation independently determines correlated channel expression and conductance levels in motor neurons of the stomatogastric ganglion. *J Neurophysiol* **107**, 718-727, doi:10.1152/jn.00622.2011 (2012).

33 Zhao, S. & Golowasch, J. Ionic current correlations underlie the global tuning of large numbers of neuronal activity attributes. *J Neurosci* **32**, 13380-13388, doi:10.1523/JNEUROSCI.6500-11.2012 (2012).

34 Ransdell, J. L., Nair, S. S. & Schulz, D. J. Rapid homeostatic plasticity of intrinsic excitability in a central pattern generator network stabilizes functional neural network output. *J Neurosci* **32**, 9649-9658, doi:10.1523/JNEUROSCI.1945-12.2012 (2012).

35 Santin, J. M. & Schulz, D. J. Membrane Voltage Is a Direct Feedback Signal That Influences Correlated Ion Channel Expression in Neurons. *Curr Biol* **29**, 1683-1688 e1682, doi:10.1016/j.cub.2019.04.008 (2019).

36 Liu, Z., Golowasch, J., Marder, E. & Abbott, L. F. A model neuron with activity-dependent conductances regulated by multiple calcium sensors. *J Neurosci* **18**, 2309-2320 (1998).

37 Golowasch, J., Abbott, L. F. & Marder, E. Activity-dependent regulation of potassium currents in an identified neuron of the stomatogastric ganglion of the crab Cancer borealis. *J Neurosci* **19**, RC33 (1999).

38 MacLean, J. N., Zhang, Y., Johnson, B. R. & Harris-Warrick, R. M. Activity-independent homeostasis in rhythmically active neurons. *Neuron* **37**, 109-120, doi:10.1016/s0896-6273(02)01104-2 (2003).

39 Guo, W. *et al.* Targeted deletion of Kv4.2 eliminates I(to,f) and results in electrical and molecular remodeling, with no evidence of ventricular hypertrophy or myocardial dysfunction. *Circ Res* **97**, 1342-1350, doi:10.1161/01.RES.0000196559.63223.aa (2005).

40 Nerbonne, J. M., Gerber, B. R., Norris, A. & Burkhalter, A. Electrical remodelling maintains firing properties in cortical pyramidal neurons lacking KCND2-encoded A-type K+ currents. *J Physiol* **586**, 1565-1579, doi:10.1113/jphysiol.2007.146597 (2008).

41 Fawcett, G. L. *et al.* Mutant analysis of the Shal (Kv4) voltage-gated fast transient K+ channel in Caenorhabditis elegans. *J Biol Chem* **281**, 30725-30735, doi:10.1074/jbc.M605814200 (2006).

42 Bergquist, S., Dickman, D. K. & Davis, G. W. A hierarchy of cell intrinsic and target-derived homeostatic signaling. *Neuron* **66**, 220-234, doi:10.1016/j.neuron.2010.03.023 (2010).

43 Parrish, J. Z. *et al.* Kruppel mediates the selective rebalancing of ion channel expression. *Neuron* **82**, 537-544, doi:10.1016/j.neuron.2014.03.015 (2014).

44 Pratt, K. G. & Aizenman, C. D. Homeostatic regulation of intrinsic excitability and synaptic transmission in a developing visual circuit. *J Neurosci* **27**, 8268-8277, doi:10.1523/JNEUROSCI.1738-07.2007 (2007).

45 Khaliq, Z. M., Gouwens, N. W. & Raman, I. M. The contribution of resurgent sodium current to high-frequency firing in Purkinje neurons: an experimental and modeling study. *J Neurosci* **23**, 4899-4912 (2003).

46 Van Wart, A. & Matthews, G. Impaired firing and cell-specific compensation in neurons lacking nav1.6 sodium channels. *J Neurosci* **26**, 7172-7180, doi:10.1523/JNEUROSCI.1101-06.2006 (2006).

47 Swensen, A. M. & Bean, B. P. Ionic mechanisms of burst firing in dissociated Purkinje neurons. *J Neurosci* **23**, 9650-9663 (2003).

48 O'Leary, T. Homeostasis, failure of homeostasis and degenerate ion channel regulation. *Current Opinion in Physiology* **2**, 129-138, doi:https://doi.org/10.1016/j.cophys.2018.01.006 (2018).

49 Kimm, T., Khaliq, Z. M. & Bean, B. P. Differential Regulation of Action Potential Shape and Burst-Frequency Firing by BK and Kv2 Channels in Substantia Nigra Dopaminergic Neurons. *J Neurosci* **35**, 16404-16417, doi:10.1523/JNEUROSCI.5291-14.2015 (2015).

50 Stocker, M., Krause, M. & Pedarzani, P. An apamin-sensitive Ca2+-activated K+ current in hippocampal pyramidal neurons. *Proc Natl Acad Sci U S A* **96**, 4662-4667, doi:10.1073/pnas.96.8.4662 (1999).

51 Kadas, D., Ryglewski, S. & Duch, C. Transient BK outward current enhances motoneurone firing rates during Drosophila larval locomotion. *J Physiol* **593**, 4871-4888, doi:10.1113/JP271323 (2015).

52 Hawryluk, J. M. *et al.* KCNQ channels determine serotonergic modulation of ventral surface chemoreceptors and respiratory drive. *J Neurosci* **32**, 16943-16952, doi:10.1523/JNEUROSCI.3043-12.2012 (2012).

53 Burdakov, D. & Ashcroft, F. M. Cholecystokinin tunes firing of an electrically distinct subset of arcuate nucleus neurons by activating A-Type potassium channels. *J Neurosci* **22**, 6380-6387, doi:20026685 (2002).

54 Goldman, A. M. *et al.* Arrhythmia in heart and brain: KCNQ1 mutations link epilepsy and sudden unexplained death. *Sci Transl Med* **1**, 2ra6, doi:10.1126/scitranslmed.3000289 (2009).

55 George, A. L., Jr. Inherited Channelopathies Associated with Epilepsy. *Epilepsy Curr* **4**, 65-70, doi:10.1111/j.1535-7597.2004.42010.x (2004).

56 Turrigiano, G., Abbott, L. F. & Marder, E. Activity-dependent changes in the intrinsic properties of cultured neurons. *Science* **264**, 974-977, doi:10.1126/science.8178157 (1994).

57 Turrigiano, G., LeMasson, G. & Marder, E. Selective regulation of current densities underlies spontaneous changes in the activity of cultured neurons. *J Neurosci* **15**, 3640-3652 (1995).

58 Baines, R. A., Uhler, J. P., Thompson, A., Sweeney, S. T. & Bate, M. Altered electrical properties in Drosophila neurons developing without synaptic transmission. *J Neurosci* **21**, 1523-1531 (2001).

59 Baines, R. A. Postsynaptic protein kinase A reduces neuronal excitability in response to increased synaptic excitation in the Drosophila CNS. *J Neurosci* **23**, 8664-8672 (2003).

60 Mee, C. J., Pym, E. C., Moffat, K. G. & Baines, R. A. Regulation of neuronal excitability through pumilio-dependent control of a sodium channel gene. *J Neurosci* **24**, 8695-8703, doi:10.1523/JNEUROSCI.2282-04.2004 (2004).

61 Desai, N. S., Rutherford, L. C. & Turrigiano, G. G. Plasticity in the intrinsic excitability of cortical pyramidal neurons. *Nat Neurosci* **2**, 515-520, doi:10.1038/9165 (1999).

62 Marder, E. & Prinz, A. A. Modeling stability in neuron and network function: the role of activity in homeostasis. *Bioessays* **24**, 1145-1154, doi:10.1002/bies.10185 (2002).

63 O'Leary, T., Williams, A. H., Franci, A. & Marder, E. Cell types, network homeostasis, and pathological compensation from a biologically plausible ion channel expression model. *Neuron* **82**, 809-821, doi:10.1016/j.neuron.2014.04.002 (2014).

64 Hengen, K. B., Lambo, M. E., Van Hooser, S. D., Katz, D. B. & Turrigiano, G. G. Firing rate homeostasis in visual cortex of freely behaving rodents. *Neuron* **80**, 335-342, doi:10.1016/j.neuron.2013.08.038 (2013).

65 Hengen, K. B., Torrado Pacheco, A., McGregor, J. N., Van Hooser, S. D. & Turrigiano, G. G. Neuronal Firing Rate Homeostasis Is Inhibited by Sleep and Promoted by Wake. *Cell* **165**, 180-191, doi:10.1016/j.cell.2016.01.046 (2016).

66 LeMasson, G., Marder, E. & Abbott, L. F. Activity-dependent regulation of conductances in model neurons. *Science* **259**, 1915-1917, doi:10.1126/science.8456317 (1993).

67 Rees, C. M. *et al.* The Ca(2+) transient as a feedback sensor controlling cardiomyocyte ionic conductances in mouse populations. *Elife* **7**, doi:10.7554/eLife.36717 (2018).

68 Ping, Y. & Tsunoda, S. Inactivity-induced increase in nAChRs upregulates Shal K(+) channels to stabilize synaptic potentials. *Nat Neurosci* **15**, 90-97, doi:10.1038/nn.2969 (2011).

69 Muraro, N. I. *et al.* Pumilio binds para mRNA and requires Nanos and Brat to regulate sodium current in Drosophila motoneurons. *J Neurosci* **28**, 2099-2109, doi:10.1523/JNEUROSCI.5092-07.2008 (2008).

70 Driscoll, H. E., Muraro, N. I., He, M. & Baines, R. A. Pumilio-2 regulates translation of Nav1.6 to mediate homeostasis of membrane excitability. *J Neurosci* **33**, 9644-9654, doi:10.1523/JNEUROSCI.0921-13.2013 (2013).

71 Wharton, K. A., Johansen, K. M., Xu, T. & Artavanis-Tsakonas, S. Nucleotide sequence from the neurogenic locus notch implies a gene product that shares homology with proteins containing EGF-like repeats. *Cell* **43**, 567-581, doi:10.1016/0092-8674(85)90229-6 (1985).

72 Kidd, S., Kelley, M. R. & Young, M. W. Sequence of the notch locus of Drosophila melanogaster: relationship of the encoded protein to mammalian clotting and growth factors. *Mol Cell Biol* **6**, 3094-3108, doi:10.1128/mcb.6.9.3094 (1986).

73 Morgan, T. H. Sex Limited Inheritance in Drosophila. *Science* **32**, 120-122, doi:10.1126/science.32.812.120 (1910).

74 Bellen, H. J., Tong, C. & Tsuda, H. 100 years of Drosophila research and its impact on vertebrate neuroscience: a history lesson for the future. *Nat Rev Neurosci* **11**, 514-522, doi:10.1038/nrn2839 (2010).

75 Poulson, D. F. Chromosomal Deficiencies and the Embryonic Development of Drosophila Melanogaster. *Proc Natl Acad Sci U S A* **23**, 133-137, doi:10.1073/pnas.23.3.133 (1937).

76 Bray, S. J. Notch signalling: a simple pathway becomes complex. *Nat Rev Mol Cell Biol* **7**, 678-689, doi:10.1038/nrm2009 (2006).

77 Lewis, J. Notch signalling and the control of cell fate choices in vertebrates. *Semin Cell Dev Biol* **9**, 583-589, doi:10.1006/scdb.1998.0266 (1998).

78 Bray, S. J. Notch signalling in context. *Nat Rev Mol Cell Biol* **17**, 722-735, doi:10.1038/nrm.2016.94 (2016).

79 Lowell, S., Benchoua, A., Heavey, B. & Smith, A. G. Notch promotes neural lineage entry by pluripotent embryonic stem cells. *PLoS Biol* **4**, e121, doi:10.1371/journal.pbio.0040121 (2006).

80 Petruccelli, E. *et al.* Alcohol Activates Scabrous-Notch to Influence Associated Memories. *Neuron* **100**, 1209-1223 e1204, doi:10.1016/j.neuron.2018.10.005 (2018).

81 Kopan, R. & Ilagan, M. X. The canonical Notch signaling pathway: unfolding the activation mechanism. *Cell* **137**, 216-233, doi:10.1016/j.cell.2009.03.045 (2009).

82 Roca, C. & Adams, R. H. Regulation of vascular morphogenesis by Notch signaling. *Genes Dev* **21**, 2511-2524, doi:10.1101/gad.1589207 (2007).

83 Kelleher, R. J., 3rd & Shen, J. Presenilin-1 mutations and Alzheimer's disease. *Proc Natl Acad Sci U S A* **114**, 629-631, doi:10.1073/pnas.1619574114 (2017).

84 Homem, C. C. & Knoblich, J. A. Drosophila neuroblasts: a model for stem cell biology. *Development* **139**, 4297-4310, doi:10.1242/dev.080515 (2012).

85 Bowman, S. K. *et al.* The tumor suppressors Brat and Numb regulate transit-amplifying neuroblast lineages in Drosophila. *Dev Cell* **14**, 535-546, doi:10.1016/j.devcel.2008.03.004 (2008).

86 Lee, C. Y., Wilkinson, B. D., Siegrist, S. E., Wharton, R. P. & Doe, C. Q. Brat is a Miranda cargo protein that promotes neuronal differentiation and inhibits neuroblast self-renewal. *Dev Cell* **10**, 441-449, doi:10.1016/j.devcel.2006.01.017 (2006).

87 Choksi, S. P. *et al.* Prospero acts as a binary switch between self-renewal and differentiation in Drosophila neural stem cells. *Dev Cell* **11**, 775-789, doi:10.1016/j.devcel.2006.09.015 (2006).

88 Betschinger, J., Mechtler, K. & Knoblich, J. A. Asymmetric segregation of the tumor suppressor brat regulates self-renewal in Drosophila neural stem cells. *Cell* **124**, 1241-1253, doi:10.1016/j.cell.2006.01.038 (2006).

89 Froldi, F. *et al.* The transcription factor Nerfin-1 prevents reversion of neurons into neural stem cells. *Genes Dev* **29**, 129-143, doi:10.1101/gad.250282.114 (2015).

90 Southall, T. D., Davidson, C. M., Miller, C., Carr, A. & Brand, A. H. Dedifferentiation of neurons precedes tumor formation in Lola mutants. *Dev Cell* **28**, 685-696, doi:10.1016/j.devcel.2014.01.030 (2014).

91 Xu, J. *et al.* Prevention of medulla neuron dedifferentiation by Nerfin-1 requires inhibition of Notch activity. *Development* **144**, 1510-1517, doi:10.1242/dev.141341 (2017).

92 Vissers, J. H. A. *et al.* The Scalloped and Nerfin-1 Transcription Factors Cooperate to Maintain Neuronal Cell Fate. *Cell Rep* **25**, 1561-1576 e1567, doi:10.1016/j.celrep.2018.10.038 (2018).

93 Friedmann-Morvinski, D. & Verma, I. M. Dedifferentiation and reprogramming: origins of cancer stem cells. *EMBO Rep* **15**, 244-253, doi:10.1002/embr.201338254 (2014).

94 Nusslein-Volhard, C. & Wieschaus, E. Mutations affecting segment number and polarity in Drosophila. *Nature* **287**, 795-801, doi:10.1038/287795a0 (1980).

95 Borg, J., Patrinos, G. P., Felice, A. E. & Philipsen, S. Erythroid phenotypes associated with KLF1 mutations. *Haematologica* **96**, 635-638, doi:10.3324/haematol.2011.043265 (2011).

96 Oishi, Y. *et al.* Kruppel-like transcription factor KLF5 is a key regulator of adipocyte differentiation. *Cell Metab* **1**, 27-39, doi:10.1016/j.cmet.2004.11.005 (2005).

97 Narla, G. *et al.* KLF6, a candidate tumor suppressor gene mutated in prostate cancer. *Science* **294**, 2563-2566, doi:10.1126/science.1066326 (2001).

98 Takahashi, K. & Yamanaka, S. Induction of pluripotent stem cells from mouse embryonic and adult fibroblast cultures by defined factors. *Cell* **126**, 663-676, doi:10.1016/j.cell.2006.07.024 (2006).

99 Davis, G. W. Homeostatic signaling and the stabilization of neural function. *Neuron* **80**, 718-728, doi:10.1016/j.neuron.2013.09.044 (2013).

100 Haedo, R. J. & Golowasch, J. Ionic mechanism underlying recovery of rhythmic activity in adult isolated neurons. *J Neurophysiol* **96**, 1860-1876, doi:10.1152/jn.00385.2006 (2006).

101 Gonzalez-Islas, C., Chub, N., Garcia-Bereguiain, M. A. & Wenner, P. GABAergic synaptic scaling in embryonic motoneurons is mediated by a shift in the chloride reversal potential. *J Neurosci* **30**, 13016-13020, doi:10.1523/JNEUROSCI.1659-10.2010 (2010).

102 Andrasfalvy, B. K., Makara, J. K., Johnston, D. & Magee, J. C. Altered synaptic and non-synaptic properties of CA1 pyramidal neurons in Kv4.2 knockout mice. *J Physiol* **586**, 3881-3892, doi:10.1113/jphysiol.2008.154336 (2008).

103 Marrus, S. B. & Nerbonne, J. M. Mechanisms linking short- and long-term electrical remodeling in the heart...is it a stretch? *Channels (Austin)* **2**, 117-124, doi:10.4161/chan.2.2.6104 (2008).

104 Michael, G., Xiao, L., Qi, X. Y., Dobrev, D. & Nattel, S. Remodelling of cardiac repolarization: how homeostatic responses can lead to arrhythmogenesis. *Cardiovasc Res* **81**, 491-499, doi:10.1093/cvr/cvn266 (2009).

105 Joseph, A. & Turrigiano, G. G. All for One But Not One for All: Excitatory Synaptic Scaling and Intrinsic Excitability Are Coregulated by CaMKIV, Whereas Inhibitory Synaptic Scaling Is Under Independent Control. *J Neurosci* **37**, 6778-6785, doi:10.1523/JNEUROSCI.0618-17.2017 (2017).

106 Goold, C. P. & Nicoll, R. A. Single-cell optogenetic excitation drives homeostatic synaptic depression. *Neuron* **68**, 512-528, doi:10.1016/j.neuron.2010.09.020 (2010).

107 El-Brolosy, M. A. & Stainier, D. Y. R. Genetic compensation: A phenomenon in search of mechanisms. *PLoS Genet* **13**, e1006780, doi:10.1371/journal.pgen.1006780 (2017).

108 Marder, E. & Goaillard, J. M. Variability, compensation and homeostasis in neuron and network function. *Nat Rev Neurosci* **7**, 563-574, doi:10.1038/nrn1949 (2006).

109 Golowasch, J. Ionic Current Variability and Functional Stability in the Nervous System. *Bioscience* **64**, 570-580, doi:10.1093/biosci/biu070 (2014).

110 Carrasquillo, Y. & Nerbonne, J. M. IA channels: diverse regulatory mechanisms. *Neuroscientist* **20**, 104-111, doi:10.1177/1073858413504003 (2014).

111 Ben-Shalom, R. *et al.* Opposing Effects on NaV1.2 Function Underlie Differences Between SCN2A Variants Observed in Individuals With Autism Spectrum Disorder or Infantile Seizures. *Biol Psychiatry* **82**, 224-232, doi:10.1016/j.biopsych.2017.01.009 (2017).

112 Klassen, T. *et al.* Exome sequencing of ion channel genes reveals complex profiles confounding personal risk assessment in epilepsy. *Cell* **145**, 1036-1048, doi:10.1016/j.cell.2011.05.025 (2011).

113 Kim, M. D., Wen, Y. & Jan, Y. N. Patterning and organization of motor neuron dendrites in the Drosophila larva. *Dev Biol* **336**, 213-221, doi:10.1016/j.ydbio.2009.09.041 (2009).

114 Rudy, B. Diversity and ubiquity of K channels. *Neuroscience* **25**, 729-749, doi:10.1016/0306-4522(88)90033-4 (1988).

115 Kirsch, G. E. & Drewe, J. A. Gating-dependent mechanism of 4-aminopyridine block in two related potassium channels. *J Gen Physiol* **102**, 797-816, doi:10.1085/jgp.102.5.797 (1993).

116 Ford, K. J. & Davis, G. W. Archaerhodopsin voltage imaging: synaptic calcium and BK channels stabilize action potential repolarization at the Drosophila neuromuscular junction. *J Neurosci* **34**, 14517-14525, doi:10.1523/JNEUROSCI.2203-14.2014 (2014).

117 Jackson, A. C. & Bean, B. P. State-dependent enhancement of subthreshold A-type potassium current by 4-aminopyridine in tuberomammillary nucleus neurons. *J Neurosci* **27**, 10785-10796, doi:10.1523/JNEUROSCI.0935-07.2007 (2007).

118 Gratz, S. J., Rubinstein, C. D., Harrison, M. M., Wildonger, J. & O'Connor-Giles, K. M. CRISPR-Cas9 Genome Editing in Drosophila. *Curr Protoc Mol Biol* **111**, 31 32 31-31 32 20, doi:10.1002/0471142727.mb3102s111 (2015).

119 Barry, D. M., Xu, H., Schuessler, R. B. & Nerbonne, J. M. Functional knockout of the transient outward current, long-QT syndrome, and cardiac remodeling in mice expressing a dominant-negative Kv4 alpha subunit. *Circ Res* **83**, 560-567, doi:10.1161/01.res.83.5.560 (1998).

120 Ping, Y. *et al.* Shal/K(v)4 channels are required for maintaining excitability during repetitive firing and normal locomotion in Drosophila. *PLoS One* **6**, e16043, doi:10.1371/journal.pone.0016043 (2011).

121 French, C. R., Sah, P., Buckett, K. J. & Gage, P. W. A voltage-dependent persistent sodium current in mammalian hippocampal neurons. *J Gen Physiol* **95**, 1139-1157, doi:10.1085/jgp.95.6.1139 (1990).

122 Lin, W. H., Wright, D. E., Muraro, N. I. & Baines, R. A. Alternative splicing in the voltage-gated sodium channel DmNav regulates activation, inactivation, and persistent current. *J Neurophysiol* **102**, 1994-2006, doi:10.1152/jn.00613.2009 (2009).

123 Butler, A., Tsunoda, S., McCobb, D. P., Wei, A. & Salkoff, L. mSlo, a complex mouse gene encoding "maxi" calcium-activated potassium channels. *Science* **261**, 221-224, doi:10.1126/science.7687074 (1993).

124 Elkins, T., Ganetzky, B. & Wu, C. F. A Drosophila mutation that eliminates a calcium-dependent potassium current. *Proc Natl Acad Sci U S A* **83**, 8415-8419, doi:10.1073/pnas.83.21.8415 (1986).

125 Komatsu, A., Singh, S., Rathe, P. & Wu, C. F. Mutational and gene dosage analysis of calcium-activated potassium channels in Drosophila: correlation of micro- and macroscopic currents. *Neuron* **4**, 313-321, doi:10.1016/0896-6273(90)90105-o (1990).

126 Singh, S. & Wu, C. F. Complete separation of four potassium currents in Drosophila. *Neuron* **2**, 1325-1329, doi:10.1016/0896-6273(89)90070-6 (1989).

127 Cavaliere, S. & Hodge, J. J. Drosophila KCNQ channel displays evolutionarily conserved electrophysiology and pharmacology with mammalian KCNQ channels. *PLoS One* **6**, e23898, doi:10.1371/journal.pone.0023898 (2011).

128 Wang, H. S. *et al.* KCNQ2 and KCNQ3 potassium channel subunits: molecular correlates of the M-channel. *Science* **282**, 1890-1893, doi:10.1126/science.282.5395.1890 (1998).

129 Isshiki, T., Pearson, B., Holbrook, S. & Doe, C. Q. Drosophila neuroblasts sequentially express transcription factors which specify the temporal identity of their neuronal progeny. *Cell* **106**, 511-521, doi:10.1016/s0092-8674(01)00465-2 (2001).

130 McConnell, B. B. & Yang, V. W. Mammalian Kruppel-like factors in health and diseases. *Physiol Rev* **90**, 1337-1381, doi:10.1152/physrev.00058.2009 (2010).

131 Younger, M. A., Muller, M., Tong, A., Pym, E. C. & Davis, G. W. A presynaptic ENaC channel drives homeostatic plasticity. *Neuron* **79**, 1183-1196, doi:10.1016/j.neuron.2013.06.048 (2013).

132 Orr, B. O. *et al.* Composition and Control of a Deg/ENaC Channel during Presynaptic Homeostatic Plasticity. *Cell Rep* **20**, 1855-1866, doi:10.1016/j.celrep.2017.07.074 (2017).

133 Frank, C. A., Kennedy, M. J., Goold, C. P., Marek, K. W. & Davis, G. W. Mechanisms underlying the rapid induction and sustained expression of synaptic homeostasis. *Neuron* **52**, 663-677, doi:10.1016/j.neuron.2006.09.029 (2006).

134 Schaefer, J. E., Worrell, J. W. & Levine, R. B. Role of intrinsic properties in Drosophila motoneuron recruitment during fictive crawling. *J Neurophysiol* **104**, 1257-1266, doi:10.1152/jn.00298.2010 (2010).

135 Baines, R. A. & Bate, M. Electrophysiological development of central neurons in the Drosophila embryo. *J Neurosci* **18**, 4673-4683 (1998).

136 Davis, G. W. Homeostatic control of neural activity: from phenomenology to molecular design. *Annu Rev Neurosci* **29**, 307-323, doi:10.1146/annurev.neuro.28.061604.135751 (2006).

137 Zhang, Y., Khorkova, O., Rodriguez, R. & Golowasch, J. Activity and neuromodulatory input contribute to the recovery of rhythmic output after decentralization in a central pattern generator. *J Neurophysiol* **101**, 372-386, doi:10.1152/jn.01290.2007 (2009).

138 Srinivasan, S., Lance, K. & Levine, R. B. Contribution of EAG to excitability and potassium currents in Drosophila larval motoneurons. *J Neurophysiol* **107**, 2660-2671, doi:10.1152/jn.00201.2011 (2012).

139 Lin, W. H. & Baines, R. A. Regulation of membrane excitability: a convergence on voltage-gated sodium conductance. *Mol Neurobiol* **51**, 57-67, doi:10.1007/s12035-014-8674-0 (2015).

140 Frolov, R. V., Bagati, A., Casino, B. & Singh, S. Potassium channels in Drosophila: historical breakthroughs, significance, and perspectives. *J Neurogenet* **26**, 275-290, doi:10.3109/01677063.2012.744990 (2012).

141 Kim, E. Z., Vienne, J., Rosbash, M. & Griffith, L. C. Nonreciprocal homeostatic compensation in Drosophila potassium channel mutants. *J Neurophysiol* **117**, 2125-2136, doi:10.1152/jn.00002.2017 (2017).

142 Kawasaki, F., Felling, R. & Ordway, R. W. A temperature-sensitive paralytic mutant defines a primary synaptic calcium channel in Drosophila. *J Neurosci* **20**, 4885-4889 (2000).

143 Stern, M. & Ganetzky, B. Altered synaptic transmission in Drosophila hyperkinetic mutants. *J Neurogenet* **5**, 215-228, doi:10.3109/01677068909066209 (1989).

144 Brandman, O. & Meyer, T. Feedback loops shape cellular signals in space and time. *Science* **322**, 390-395, doi:10.1126/science.1160617 (2008).

145 Contet, C., Goulding, S. P., Kuljis, D. A. & Barth, A. L. BK Channels in the Central Nervous System. *Int Rev Neurobiol* **128**, 281-342, doi:10.1016/bs.irn.2016.04.001 (2016).

146 Tobin, A. E., Cruz-Bermudez, N. D., Marder, E. & Schulz, D. J. Correlations in ion channel mRNA in rhythmically active neurons. *PLoS One* **4**, e6742, doi:10.1371/journal.pone.0006742 (2009).

147 Temporal, S., Lett, K. M. & Schulz, D. J. Activity-dependent feedback regulates correlated ion channel mRNA levels in single identified motor neurons. *Curr Biol* **24**, 1899-1904, doi:10.1016/j.cub.2014.06.067 (2014).

148 Lorenz, S., Heils, A., Kasper, J. M. & Sander, T. Allelic association of a truncation mutation of the KCNMB3 gene with idiopathic generalized epilepsy. *Am J Med Genet B Neuropsychiatr Genet* **144B**, 10-13, doi:10.1002/ajmg.b.30369 (2007).

149 Du, W. *et al.* Calcium-sensitive potassium channelopathy in human epilepsy and paroxysmal movement disorder. *Nat Genet* **37**, 733-738, doi:10.1038/ng1585 (2005).

150 Beecham, G. W. *et al.* Genome-wide association study implicates a chromosome 12 risk locus for late-onset Alzheimer disease. *Am J Hum Genet* **84**, 35-43, doi:10.1016/j.ajhg.2008.12.008 (2009).

151 Burns, L. C. *et al.* Replication study of genome-wide associated SNPs with late-onset Alzheimer's disease. *Am J Med Genet B Neuropsychiatr Genet* **156B**, 507-512, doi:10.1002/ajmg.b.31194 (2011).

152 Beecham, G. W. *et al.* Genome-wide association meta-analysis of neuropathologic features of Alzheimer's disease and related dementias. *PLoS Genet* **10**, e1004606, doi:10.1371/journal.pgen.1004606 (2014).

153 Kulik, Y., Jones, R., Moughamian, A. J., Whippen, J. & Davis, G. W. Dual separable feedback systems govern firing rate homeostasis. *Elife* **8**, doi:10.7554/eLife.45717 (2019).

154 Brand, A. H. & Perrimon, N. Targeted gene expression as a means of altering cell fates and generating dominant phenotypes. *Development* **118**, 401-415 (1993).

155 Mahoney, M. B. *et al.* Presenilin-based genetic screens in Drosophila melanogaster identify novel notch pathway modifiers. *Genetics* **172**, 2309-2324, doi:10.1534/genetics.104.035170 (2006).

156 Lanuza, G. M., Gosgnach, S., Pierani, A., Jessell, T. M. & Goulding, M. Genetic identification of spinal interneurons that coordinate left-right locomotor activity necessary for walking movements. *Neuron* **42**, 375-386, doi:10.1016/s0896-6273(04)00249-1 (2004).

157 Lewis, K. E. & Eisen, J. S. From cells to circuits: development of the zebrafish spinal cord. *Prog Neurobiol* **69**, 419-449, doi:10.1016/s0301-0082(03)00052-2 (2003).

158 Millen, K. J., Millonig, J. H. & Hatten, M. E. Roof plate and dorsal spinal cord dl1 interneuron development in the dreher mutant mouse. *Dev Biol* **270**, 382-392, doi:10.1016/j.ydbio.2004.03.008 (2004).

159 Wonders, C. P. & Anderson, S. A. The origin and specification of cortical interneurons. *Nat Rev Neurosci* **7**, 687-696, doi:10.1038/nrn1954 (2006).

160 Alberi, L. *et al.* Activity-induced Notch signaling in neurons requires Arc/Arg3.1 and is essential for synaptic plasticity in hippocampal networks. *Neuron* **69**, 437-444, doi:10.1016/j.neuron.2011.01.004 (2011).

161 Costa, R. M., Honjo, T. & Silva, A. J. Learning and memory deficits in Notch mutant mice. *Curr Biol* **13**, 1348-1354, doi:10.1016/s0960-9822(03)00492-5 (2003).

162 Ge, X. *et al.* Notch signaling in Drosophila long-term memory formation. *Proc Natl Acad Sci U S A* **101**, 10172-10176, doi:10.1073/pnas.0403497101 (2004).

163 Kidd, S., Struhl, G. & Lieber, T. Notch is required in adult Drosophila sensory neurons for morphological and functional plasticity of the olfactory circuit. *PLoS Genet* **11**, e1005244, doi:10.1371/journal.pgen.1005244 (2015).

164 Matsuno, M., Horiuchi, J., Tully, T. & Saitoe, M. The Drosophila cell adhesion molecule klingon is required for long-term memory formation and is regulated by Notch. *Proc Natl Acad Sci U S A* **106**, 310-315, doi:10.1073/pnas.0807665106 (2009).

165 Presente, A., Boyles, R. S., Serway, C. N., de Belle, J. S. & Andres, A. J. Notch is required for long-term memory in Drosophila. *Proc Natl Acad Sci U S A* **101**, 1764-1768, doi:10.1073/pnas.0308259100 (2004).

166 Song, Q. *et al.* Suppressor of Hairless is required for long-term memory formation in Drosophila. *J Neurogenet* **23**, 405-411, doi:10.3109/01677060903096133 (2009).

167 Zhang, J., Little, C. J., Tremmel, D. M., Yin, J. C. & Wesley, C. S. Notch-inducible hyperphosphorylated CREB and its ultradian oscillation in long-term memory formation. *J Neurosci* **33**, 12825-12834, doi:10.1523/JNEUROSCI.0783-13.2013 (2013).

168 Pavlopoulos, E., Anezaki, M. & Skoulakis, E. M. Neuralized is expressed in the alpha/beta lobes of adult Drosophila mushroom bodies and facilitates olfactory long-term memory formation. *Proc Natl Acad Sci U S A* **105**, 14674-14679, doi:10.1073/pnas.0801605105 (2008).

169 Rentschler, S. *et al.* Myocardial Notch signaling reprograms cardiomyocytes to a conduction-like phenotype. *Circulation* **126**, 1058-1066, doi:10.1161/CIRCULATIONAHA.112.103390 (2012).

170 Khandekar, A. *et al.* Notch-Mediated Epigenetic Regulation of Voltage-Gated Potassium Currents. *Circ Res* **119**, 1324-1338, doi:10.1161/CIRCRESAHA.116.309877 (2016).

171 Gude, N. A. *et al.* Activation of Notch-mediated protective signaling in the myocardium. *Circ Res* **102**, 1025-1035, doi:10.1161/CIRCRESAHA.107.164749 (2008).

172 Croquelois, A. *et al.* Control of the adaptive response of the heart to stress via the Notch1 receptor pathway. *J Exp Med* **205**, 3173-3185, doi:10.1084/jem.20081427 (2008).

173 Nemir, M. *et al.* The Notch pathway controls fibrotic and regenerative repair in the adult heart. *Eur Heart J* **35**, 2174-2185, doi:10.1093/eurheartj/ehs269 (2014).

174 Murata, Y. & Wharton, R. P. Binding of pumilio to maternal hunchback mRNA is required for posterior patterning in Drosophila embryos. *Cell* **80**, 747-756, doi:10.1016/0092-8674(95)90353-4 (1995).

175 Gamberi, C., Peterson, D. S., He, L. & Gottlieb, E. An anterior function for the Drosophila posterior determinant Pumilio. *Development* **129**, 2699-2710 (2002).

176 Dou, S. *et al.* The recombination signal sequence-binding protein RBP-2N functions as a transcriptional repressor. *Mol Cell Biol* **14**, 3310-3319, doi:10.1128/mcb.14.5.3310 (1994).

177 Kao, H. Y. *et al.* A histone deacetylase corepressor complex regulates the Notch signal transduction pathway. *Genes Dev* **12**, 2269-2277, doi:10.1101/gad.12.15.2269 (1998).

178 Morel, V. & Schweisguth, F. Repression by suppressor of hairless and activation by Notch are required to define a single row of single-minded expressing cells in the Drosophila embryo. *Genes Dev* **14**, 377-388 (2000).

179 Klein, T., Seugnet, L., Haenlin, M. & Martinez Arias, A. Two different activities of Suppressor of Hairless during wing development in Drosophila. *Development* **127**, 3553-3566 (2000).

180 Furriols, M. & Bray, S. A model Notch response element detects Suppressor of Hairless-dependent molecular switch. *Curr Biol* **11**, 60-64, doi:10.1016/s0960-9822(00)00044-0 (2001).

181 Lee, K. Y. *et al.* N-methyl-D-aspartate receptors mediate activity-dependent down-regulation of potassium channel genes during the expression of homeostatic intrinsic plasticity. *Mol Brain* **8**, 4, doi:10.1186/s13041-015-0094-1 (2015).

182 El-Brolosy, M. A. *et al.* Genetic compensation triggered by mutant mRNA degradation. *Nature* **568**, 193-197, doi:10.1038/s41586-019-1064-z (2019).

183 Ma, Z. *et al.* PTC-bearing mRNA elicits a genetic compensation response via Upf3a and COMPASS components. *Nature* **568**, 259-263, doi:10.1038/s41586-019-1057-y (2019).

184 Ashraf, K. U. *et al.* The Potassium Binding Protein Kbp Is a Cytoplasmic Potassium Sensor. *Structure* **24**, 741-749, doi:10.1016/j.str.2016.03.017 (2016).

185 Minett, M. S. *et al.* Endogenous opioids contribute to insensitivity to pain in humans and mice lacking sodium channel Nav1.7. *Nat Commun* **6**, 8967, doi:10.1038/ncomms9967 (2015).

186 Garrett, S. & Rosenthal, J. J. RNA editing underlies temperature adaptation in K+ channels from polar octopuses. *Science* **335**, 848-851, doi:10.1126/science.1212795 (2012).

187 Hesdorffer, D. C. *et al.* Estimating risk for developing epilepsy: a population-based study in Rochester, Minnesota. *Neurology* **76**, 23-27, doi:10.1212/WNL.0b013e318204a36a (2011).

188 Dalic, L. & Cook, M. J. Managing drug-resistant epilepsy: challenges and solutions. *Neuropsychiatr Dis Treat* **12**, 2605-2616, doi:10.2147/NDT.S84852 (2016).

189 Luz-Escamilla, L. & Morales-Gonzalez, J. A. Association between Interictal Epileptiform Discharges and Autistic Spectrum Disorder. *Brain Sci* **9**, doi:10.3390/brainsci9080185 (2019).

190 Vossel, K. A., Tartaglia, M. C., Nygaard, H. B., Zeman, A. Z. & Miller, B. L. Epileptic activity in Alzheimer's disease: causes and clinical relevance. *Lancet Neurol* **16**, 311-322, doi:10.1016/S1474-4422(17)30044-3 (2017).

191 Mendez, M. & Lim, G. Seizures in elderly patients with dementia: epidemiology and management. *Drugs Aging* **20**, 791-803, doi:10.2165/00002512-200320110-00001 (2003).

192 Jeste, S. S. & Tuchman, R. Autism Spectrum Disorder and Epilepsy: Two Sides of the Same Coin? *J Child Neurol* **30**, 1963-1971, doi:10.1177/0883073815601501 (2015).

193 Waters, M. F. *et al.* Mutations in voltage-gated potassium channel KCNC3 cause degenerative and developmental central nervous system phenotypes. *Nat Genet* **38**, 447-451, doi:10.1038/ng1758 (2006).

194 Nelson, R. Potassium channels have a key role in neurodegeneration. *Lancet Neurol* **5**, 298-299, doi:10.1016/s1474-4422(06)70399-4 (2006).

195 Claes, L. *et al.* De novo SCN1A mutations are a major cause of severe myoclonic epilepsy of infancy. *Hum Mutat* **21**, 615-621, doi:10.1002/humu.10217 (2003).

196 Claes, L. *et al.* De novo mutations in the sodium-channel gene SCN1A cause severe myoclonic epilepsy of infancy. *Am J Hum Genet* **68**, 1327-1332, doi:10.1086/320609 (2001).

197 Chen, R. *et al.* Analysis of 589,306 genomes identifies individuals resilient to severe Mendelian childhood diseases. *Nat Biotechnol* **34**, 531-538, doi:10.1038/nbt.3514 (2016).

198 Gratz, S. J., Harrison, M. M., Wildonger, J. & O'Connor-Giles, K. M. Precise Genome Editing of Drosophila with CRISPR RNA-Guided Cas9. *Methods Mol Biol* **1311**, 335-348, doi:10.1007/978-1-4939-2687-9_22 (2015).

199 Dobin, A. *et al.* STAR: ultrafast universal RNA-seq aligner. *Bioinformatics* **29**, 15-21, doi:10.1093/bioinformatics/bts635 (2013).

Publishing Agreement

It is the policy of the University to encourage the distribution of all theses, dissertations, and manuscripts. Copies of all UCSF theses, dissertations, and manuscripts will be routed to the library via the Graduate Division. The library will make all theses, dissertations, and manuscripts accessible to the public and will preserve these to the best of their abilities, in perpetuity.

I hereby grant permission to the Graduate Division of the University of California, San Francisco to release copies of my thesis, dissertation, or manuscript to the Campus Library to provide access and preservation, in whole or in part, in perpetuity.

Author Signature 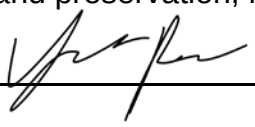 Date 12/13/2019